Louisiana State University
LSU Scholarly Repository

LSU Doctoral Dissertations | Graduate School

2014

Robust Preconditioners for the High-Contrast Elliptic Partial Differential Equations

Zuhal Unlu
Louisiana State University and Agricultural and Mechanical College

Follow this and additional works at: https://repository.lsu.edu/gradschool_dissertations

 Part of the Applied Mathematics Commons

Recommended Citation

Unlu, Zuhal, "Robust Preconditioners for the High-Contrast Elliptic Partial Differential Equations" (2014). *LSU Doctoral Dissertations*. 1635.
https://repository.lsu.edu/gradschool_dissertations/1635

This Dissertation is brought to you for free and open access by the Graduate School at LSU Scholarly Repository. It has been accepted for inclusion in LSU Doctoral Dissertations by an authorized graduate school editor of LSU Scholarly Repository. For more information, please contactgradetd@lsu.edu.

ROBUST PRECONDITIONERS FOR THE HIGH-CONTRAST ELLIPTIC PARTIAL DIFFERENTIAL EQUATIONS

A Dissertation

Submitted to the Graduate Faculty of the
Louisiana State University and
Agricultural and Mechanical College
in partial fulfillment of the
requirements for the degree of
Doctor of Philosophy

in

The Department of Mathematics

by
Zuhal Unlu
B.S., Middle East Technical University, 2007
M.S., Louisiana State University, 2009
August 2014

Dedicated to my husband Emre, my parents Ali and Gulseren, and my sisters Ilknur, Yasemin and Ayse.

Acknowledgments

I would like to express my deepest gratitude to my advisor, Dr. Burak Aksoylu for patiently guiding me through this rigorous academic process. My association with him has been the most fortunate and cherished experience of my entire academic journey. His encouragement, optimism and involvement have been a constant source of inspiration for me and have made me believe in myself. Without his continuous support, this dissertation would not have been possible.

I would like to express my sincere gratitude to my committee co-chair, Dr. Robert Lipton for his constant support and encouragement. I have immensely benefited from my discussions with him. I am also deeply indebted to my other committee members, Dr. Shawn Walker, Dr. Richard Litherland and Dr. Jerome Hoffman for their insightful comments and guidance.

My parents, Gulseren and Ali Yeter, have been my inspirations. I am extremely fortunate to have their unconditional love, support and sacrifice. I would like to express my gratitude to my sisters, Ilknur, Yasemin, Ayse and my brother-in-law Furuzan for their support and friendship over the years. Their faith in me has given me strength to surpass every hurdle in my life.

I would like to thank my dear husband Emre Unlu for his endless love, encouragement and understanding. I am grateful for having him as a friend, colleague and also a great husband. His love and his support mean more to me than I can ever put into words. I appreciate everything that he has done for me.

Table of Contents

List of Tables

List of Figures

Abstract

In this thesis, we discuss a robust preconditioner (the AGKS preconditioner) for solving linear systems arising from approximations of partial differential equations (PDEs) with high-contrast coefficients. The problems considered here include the standard second and higher order elliptic PDEs such as high-contrast diffusion equation, Stokes' equation and biharmonic-plate equation. The goal of this study is the development of robust and parallelizable preconditioners that can easily be integrated to treat large configurations. The construction of the preconditioner consists of two phases. The first one is an algebraic phase which partitions the degrees of freedom into high and low permeability regions which may be of arbitrary geometry. This yields a corresponding block partitioning of the stiffness matrix allowing us to use a formula for the action of its inverse involving the inverses of both the high permeability block and its Schur complement in the original matrix. Singular perturbation analysis plays a big role to analyze the structure of the required subblock inverses in the high contrast case which shows that for high enough contrast each of the subblock inverses can be approximated well by solving only systems with constant coefficients. The second phase involves an efficient multigrid approximation of this exact inverse. After applying singular perturbation theory to each of the sub-blocks, we obtain that inverses of each of the sub-blocks with high contrast entries can be approximated efficiently using geometric multigrid methods, and that this approximation is robust with respect to both the contrast and the mesh size. The result is a multigrid method for high contrast problems which is provably optimal to both contrast and mesh size. We demonstrate the advantageous properties of the AGKS preconditioner using experiments on model high-contrast problems. We examine its performance against multigrid method under varying discretizations of diffusion equation, Stokes equation and biharmonic-plate equation. Thus, we show that we accomplished a desirable preconditioning design goal by using the same family of preconditioners to solve the elliptic family of PDEs with varying discretizations.

Chapter 1

Introduction

1.1 Background

Systems of linear equations arise from discretization of partial differential equations and other problems. In many cases, the sparse matrices in these systems are symmetric and positive definite, or positive semi definite. Often, they are M-matrix. Producing a solution for these equations efficiently on a fine mesh is a challenging task, and the conditioning of an operator equation plays a big role in this task. Conditioning, represented by condition number, is a measure that indicates the stability of the equation with respect to perturbations on the input data. A large sensitivity to such perturbations causes the equation to be unstable and this is referred as ill-conditioning. The mechanism, usually in the form of numerical methods, designed to correct ill-conditioning of the underlying equation is called preconditioning.

To solve these large systems of linear equations $Kx = b$, we can apply iterative methods. These iterative methods start with an approximate solution x_0, and then modify the approximation x_i at each iteration step i until convergence is reached. However, for ill-conditioned systems, which occurs in many applications, even though the iterative methods are theoretically founded, they have not been too successful with such problems and suffer from slow convergence. To speed up the convergence of iterative methods, preconditioning enters into the equation, especially for Krylov subspace methods. The idea of preconditioning technique is that instead of solving the system directly, we can solve the following preconditioned system $B^{-1}Kx = B^{-1}b$. Here the preconditioner B should be a matrix approximating to K, and $Bx = b$ is inexpensive to solve compared to the original system.

Designing efficient preconditioners for solving elliptic PDEs with high contrast coefficients is a challenging task as the resulting stiffness matrix is ill-conditioned. There has been intense research activity, specifically in the setting of multiscale solvers [2, 41, 42, 80], and any significant achievement in this area is vital to a wide set of real-world applications, such as reservoir and underground water flow simulation, composite plate bending, slab subduction and many others.

Classical preconditioners, such as Jacobi, Gauss Seidel, SOR, and SSOR are effective for a number of simple problems. However, they do not have the efficiency required by current applications. Their main drawback is not being numerically optimal, i.e. the computational work is not linear with respect to the number of unknowns. The development of multigrid methods, which have been shown to be very efficient for elliptic-type problems, and for which various adaptations have been brought,in the 1960s provided a solution to this problem. Multigrid theory is based on the use of a hierarchy of grids or discretizations, to solve a coarse problem, in order to obtain a global correction to the solution. The convergence theory for the geometric multigrid algorithm shows convergence with an $\mathcal{O}(N)$ computational complexity implying that the geometric multigrid algorithm is highly optimal. However, the increase in complexity of the problem grids slowed down the development of such methods, and lead to a different adaptation: algebraic multigrid. The algebraic multigrid (AMG) methods is a generalization of the multigrid idea to handle problems whose solution with geometric multigrid is unfeasible, for example discretized problems on unstructured grids. Unlike geometric multigrid, AMG does not assume any underlying geometry. An important feature of this is that they can be used as a black box algorithm, i.e. the only input for the coarsening procedures is the coefficient matrix. One such preconditioner was proposed by K.Stüben and his collaborators [78]. It can be used for any symmetric positive semi definite system, and sometime it converges even for unsymmetrical systems. However, the main drawback is that there is no straightforward theoretical justification of this method. While multigrid methods are not ideal as general purpose solvers for indefinite or general

sparse linear systems of equations, they can be used as preconditioners in conjunction with Krylov accelerators, to yield efficient iterative solvers. Krylov subspace methods belong to a class of iterative solvers called projection methods. They extract approximate solutions to the linear system from the subspace $span\{\tilde{r}^0, \mathcal{A}\tilde{r}^0, \ldots \mathcal{A}^k\tilde{r}^0\}$, where $\tilde{r}^0 = \mathcal{B}^{-1}r^0$ is the initial residual for an initial guess x_0. The approximate solution lies in the affine space $x_0 + span\{\tilde{r}^0, \mathcal{A}\tilde{r}^0, \ldots \mathcal{A}^k\tilde{r}^0\}$.

1.2 Robust multigrid preconditioner

The ill-conditioning of the stiffness matrices in high-contrast elliptic PDEs is due to the contrast in the entries which caused by the presence of both low ($\mathcal{O}(1)$) and high ($\mathcal{O}(m)$) magnitude PDE coefficients. This disproportionate coupling leads to small ($\mathcal{O}(m^{-1})$) eigenvalues in the diagonally scaled stiffness matrix. In a high-contrast elliptic PDE, the solver issues, in particular the loss of robustness, are largely due those small eigenvalues. The treatment of the coupling between the degrees of freedom (DOF) associated to low and high PDE coefficient is a delicate task. It would be ideal to decouple the problem without complications. Hence, the *design philosophy* of the AGKS preconditioner is based on *decoupling*. This enables us to create blocks in the system matrix associated to low and high magnitude DOF that are entirely of $\mathcal{O}(1)$ and $\mathcal{O}(m)$, respectively. The AGKS preconditioner's *decoupling* role becomes more and more conspicuous as $m \to \infty$ and that is why the effectiveness of the preconditioner increases for m in the asymptotic regime. Once the decoupling is in place, the AGKS preconditioner employs multigrid(MG) because it can effectively handle both blocks.

The purpose of this dissertation is two-phased. First, it is to design, analyze, and test new efficient preconditioners for algebraic problems arising from the conventional discretization (for instance, finite volume method) of a diffusion type equation with high-contrast coefficients. Second, it is to extend the theory of the preconditioner to a family of discretization methods and family of equations so that the preconditioner for a resulting system can be

used broadly. The dissertation is organized as follows. In Chapter 2 we introduce a multilevel preconditioner for high-contrast diffusion equation. In Chapter 3 we use the properties of saddle point matrix and various solver methods to couple the AGKS preconditioner with a basic preconditioner (the pressure mass matrix) for the solution of high-contrast stokes equation. Finally, in Chapter 4 we extend the preconditioner to a fourth order problem (the biharmonic plate equation), and generalize the use of AGKS preconditioner for family of high contrast elliptic PDEs. In each Chapter, we present the aforementioned singular perturbation analysis and reveal the asymptotic qualitative nature of the solution for the model problem, and we write down the proposed preconditioner as we prove its effectiveness by establishing a spectral bound for the preconditioned system. Moreover, the m- and h-robustness of the AGKS preconditioner is demonstrated and compared with the performance of MG preconditioner by numerical experiments.

1.2.1 Related publications

The following articles resulted from this dissertation:

- B. Aksoylu and Z.Yeter, Robust multigrid preconditioners for cell-centered finite volume discretization of the high-contrast diffusion equation([10])

In this article, we study a conservative 5-point cell-centered finite volume discretization of the high-contrast diffusion equation to construct preconditioners that are robust with respect to the coefficient contrast size and the mesh size simultaneously. We prove and numerically demonstrate the robustness of the AGKS preconditioner. As a side result, we prove a fundamental qualitative property of solution of the high-contrast diffusion equation.

- B. Aksoylu and Z. Unlu, Numerical study of the high-contrast Stokes equation and its robust preconditioning([8])

In this article, we numerically study the Stokes equation with high-contrast viscosity coefficients. We examine the performance of the AGKS preconditioner against multigrid and

provide a comparative study reflecting the effect of the underlying discretization and the aspect ratio of the mesh by utilizing the preconditioned inexact Uzawa and Minres solvers.

- B. Aksoylu and Z. Unlu, Robust preconditioners for the high-contrast Stokes equation([9])

In this study, We address the rigorous justification of the solver methods in [8], and utilize a new solver method, Schur complement reduction (SCR). As the contrast size grows asymptotically, we prove and numerically demonstrate that the inexact p-Uzawa solver converges to the exact one. Finally, we show that our preconditioner is contrast size and mesh size robust under p-Minres when the Schur complement solve is accurate enough.

- B. Aksoylu and Z.Yeter, Robust multigrid preconditioners for the high-contrast biharmonic plate equation([11])

In this article, we focus on the high-contrast biharmonic plate equation with HCT finite element discretizations. We extend the devised singular perturbation analysis from linear finite element discretization to the above discretization to prove the main result. We also present a strategy on how to generalize the proposed preconditioner to cover high-contrast elliptic PDEs of order $2k,\ k > 2$. Moreover, we prove a fundamental qualitative property of solution of the high-contrast biharmonic plate equation.

Chapter 2

The AGKS Preconditioner for the High-contrast Diffusion Equation

2.1 The underlying PDE and the linear system

In this Chapter, we focus on the construction and convergence of a family of algebraic preconditioners for the high-contrast diffusion equation. We consider the preconditioners for the finite volume discretizations of the following high-contrast stationary diffusion equation:

$$\begin{cases} -\nabla \cdot (\alpha \nabla u) &= f \quad \text{in } \Omega \\ u &= 0 \quad \text{on } \partial\Omega \end{cases} \tag{2.1}$$

where $\Omega \subset \mathbb{R}^d,\ d = 2, 3$. The coefficient $\alpha(x)$ may vary over many orders of magnitude in an unstructured way on Ω.

Problems with high-contrast coefficients are ubiquitous in porous media flow applications. Many examples of this kind arise in groundwater flow and oil reservoir simulation; see for example the comprehensive overviews [1, 38, 65, 69]. Consequently, development of efficient solvers for high-contrast heterogeneous media has been an active area of research, specifically in the setting of multiscale solvers [2, 41, 43, 44, 81]. In addition, the fictitious domain method and composite materials are also sources of rough coefficients; see the references in [51].

Important current applications deal with composite materials whose components have nearly constant diffusivity, but vary by several orders of magnitude. In composite material applications, it is quite common to idealize the diffusivity by a piecewise constant function. Likewise, we restrict the diffusion process to a *binary regime* (see Figure 2.1) in which the

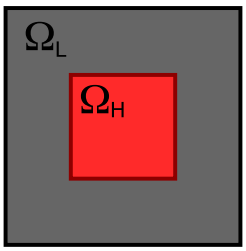

Figure 2.1: The domain $\Omega = \overline{\Omega}_H \cup \Omega_L$ where Ω_H and Ω_L are high and low diffusivity regions, respectively.

coefficient α is a piecewise constant function with the following values:

$$\alpha(x) = \begin{cases} m \gg 1, & x \in \Omega_H, \\ 1, & x \in \Omega_L. \end{cases}$$

Due to the atomistic structure of matter, the physical treatment of diffusion involves regular (C^∞-) diffusivity, Aksoylu and Beyer [4] showed that the idealization of diffusivity by piecewise constant coefficients is meaningful by showing a continuous dependence of the solutions on the diffusivity.

The first algebraic phase of the preconditioner involves partitioning of the DOF in to high-permeability and low-permeability region. Note that algebraically this partitioning can be obtained by examining the magnitude of the diagonal entries of the stiffness matrix for high enough contrast.

Let us denote the linear system arising from the finite volume discretization by:

$$K(m)\ x(m) = b. \tag{2.2}$$

Let Ω be decomposed with respect to diffusivity value as

$$\Omega = \overline{\Omega}_H \cup \Omega_L, \tag{2.3}$$

where Ω_H and Ω_L denote the high and low diffusivity regions, respectively. When m-

dependence is explicitly stated and the discretization system (2.2) is decomposed with respect to (2.3), i.e., the magnitude of the coefficient values, we arrive at the following 2×2 block system:

$$\begin{bmatrix} K_{HH}(m) & K_{HL}(m) \\ K_{LH}(m) & K_{LL}(m) \end{bmatrix} \begin{bmatrix} x_H(m) \\ x_L(m) \end{bmatrix} = \begin{bmatrix} b_H \\ b_L \end{bmatrix}. \tag{2.4}$$

Note that all the subblocks in (2.4) have m-dependence.

The exact inverse of K can be written as:

$$K^{-1}(m) = \begin{bmatrix} I_{HH} & -K_{HH}^{-1}(m)K_{HL}(m) \\ 0 & I_{LL} \end{bmatrix} \begin{bmatrix} K_{HH}^{-1}(m) & 0 \\ 0 & S^{-1}(m) \end{bmatrix} \begin{bmatrix} I_{HH} & 0 \\ -K_{LH}(m)K_{HH}^{-1}(m) & I_{LL} \end{bmatrix} \tag{2.5}$$

where I_{HH} and I_{LL} denote the identity matrices of the appropriate dimension and the $S(m)$ is the Schur complement of $K_{HH}(m)$ in $K(m)$ given by

$$S(m) = K_{LL}(m) - K_{LH}(m)K_{HH}^{-1}(m)K_{HL}(m). \tag{2.6}$$

Let $\mathcal{N}_{HH}$ denote the Neumann matrix corresponding to the pure Neumann problem for the Laplace operator on Ω_H. We write an important decomposition which will be used in the analysis to come:

$$K_{HH}(m) = m\,\mathcal{N}_{HH} + \Delta(m)\ . \tag{2.7}$$

Singular perturbation analysis can be devised to explain the properties of the subblocks in (2.5). However, before that, since the utilized analysis is based on matrix entries, we provide the outline of the cell-centered FV discretization for the 5-point stencil used for the discretization; for more details see [33].

2.2 The cell-centered finite volume discretization

2.2.1 The outline of the discretization scheme

Let $\mathcal{T} = V_{i,j}$ with $i, j = 1, \ldots, n^{1/2}$ be the mesh and the control volume be defined by

$$V_{i,j} = [x_{i-1/2}, x_{i+1/2}] \times [y_{j-1/2}, y_{j+1/2}].$$

The FV scheme is constructed by integrating (2.1) over each control volume $V_{i,j}$, which yields

$$\begin{aligned} - & \int_{y_{j-1/2}}^{y_{j+1/2}} \alpha_{i+1/2,j}\ u_x(x_{i+1/2}, y)\, dy + \int_{y_{j-1/2}}^{y_{j+1/2}} \alpha_{i-1/2,j}\ u_x(x_{i-1/2}, y)\, dy \\ + & \int_{x_{i-1/2}}^{x_{i+1/2}} \alpha_{i,j-1/2}\ u_y(x, y_{j-1/2})\, dx - \int_{x_{i-1/2}}^{x_{i+1/2}} \alpha_{i,j+1/2}\ u_y(x, y_{j+1/2})\, dx \\ = & \int_{V_{i,j}} f(x, y)\, dxdy. \end{aligned}$$

Let $k_{x_i} = x_{i+1/2} - x_{i-1/2}$ and $k_{y_j} = y_{j+1/2} - y_{j-1/2}$ be the x- and y-size of the control volume $V_{i,j}$, respectively. Since a uniform mesh is used, $k_{x_i} = k_x$ and $k_{y_j} = k_y$ for all $i, j = 1, \ldots, n^{1/2}$. Then, the discretization scheme is

$$F_{i+1/2,j} - F_{i-1/2,j} + F_{i,j+1/2} - F_{i,j-1/2} = h_{i,j} f_{i,j},$$

where $h_{i,j} = k_x\, k_y$, and $f_{i,j}$ is the mean value of f over $V_{i,j}$, and where

$$\begin{aligned} F_{i+1/2,j} &= -\frac{k_y}{k_x}\ \overline{h}_{\alpha_i} \left\{ u(x_{i+1}, y_j) - u(x_i, y_j) \right\}, \\ F_{i,j+1/2} &= -\frac{k_x}{k_y}\ \overline{h}_{\alpha_j} \left\{ u(x_i, y_{j+1}) - u(x_i, y_j) \right\}, \end{aligned}$$

and

$$\overline{h}_{\alpha_i} = \frac{2\, \alpha_{i,j}\, \alpha_{i+1,j}}{\alpha_{i,j} + \alpha_{i+1,j}}, \quad \overline{h}_{\alpha_j} = \frac{2\, \alpha_{i,j}\, \alpha_{i,j+1}}{\alpha_{i,j} + \alpha_{i,j+1}}. \tag{2.8}$$

Note that $\overline{h}_{\alpha_i}$ and $\overline{h}_{\alpha_j}$ are the harmonic means of the diffusion coefficients for the adjacent

control volumes in x and y directions respectively. The discretization formula can be written explicitly as follows:

$$\begin{aligned} - \quad & \overline{h}_{\alpha_i} u(x_{i+1}, y_j) - \overline{h}_{\alpha_{i-1}} u(x_{i-1}, y_j) \\ + \quad & (\overline{h}_{\alpha_i} + \overline{h}_{\alpha_{i-1}} + \overline{h}_{\alpha_j} + \overline{h}_{\alpha_{j-1}}) u(x_i, y_j) \\ - \quad & \overline{h}_{\alpha_j} u(x_i, y_{j+1}) - \overline{h}_{\alpha_{j-1}} u(x_i, y_{j-1}) = h_{i,j} f_{i,j}. \end{aligned} \tag{2.9}$$

In our binary diffusivity regime, for notational convenience, we denote the harmonic mean by

$$\overline{h}_m := \frac{2\,m}{m+1}. \tag{2.10}$$

The *harmonic mean* is used to ensure the *continuity of the flux* across the control volume interfaces. As a result, this flavor of finite volume discretization enjoys the desirable property of mass conservation.

One can write the discretization matrix entries *a priori* due to the formula (2.9). Hence, in 2D, we explicitly state each contribution of the off-diagonals to the diagonal entry values in the following:

$$[K(m)]_{pp} = \begin{cases} m + m + m + m, & p \in I_{\Omega_1}, \\ m + m + m + \overline{h}_m, & p \in \Gamma_{\Omega_1} \text{ and non-corner}, \\ m + m + \overline{h}_m + \overline{h}_m, & p \in \Gamma_{\Omega_1} \text{ and corner}, \\ 1 + 1 + 1 + \overline{h}_m, & p \in \Gamma_{\Omega_2}, \\ 1 + 1 + 1 + 1, & p \in I_{\Omega_2} \text{ and strictly interior}, \\ 5, & p \in I_{\Omega_2} \text{ and non-corner boundary}, \\ 6, & p \in I_{\Omega_2} \text{ and corner boundary}. \end{cases} \tag{2.11}$$

2.2.2 1D example of finite volume method for the 5-point stencil

We explicitly provide the discretization matrix utilizing the FV method in (2.9) corresponding to (2.1). The domain is chosen to be $\Omega := (0,1)$ with the highly-diffusive island $\Omega_H := (2/7, 5/7)$. The mesh consists of 7 cells. The cells and cell-centers are denoted by $V_1, \ldots, V_7$ and $x_1, \ldots, x_7$, respectively. See Figure 2.2.

The corresponding submatrices in (2.4) are given below:

$$
\begin{aligned}
K_{HH}(m) &= \begin{bmatrix} 2m & -m & -m \\ -m & m+\overline{h}_m & 0 \\ -m & 0 & m+\overline{h}_m \end{bmatrix}, \\
K_{HL}(m) &= \begin{bmatrix} 0 & 0 & 0 & 0 \\ -\overline{h}_m & 0 & 0 & 0 \\ 0 & -\overline{h}_m & 0 & 0 \end{bmatrix} = K_{LH}^T(m), \\
K_{LL}(m) &= \begin{bmatrix} 1+\overline{h}_m & 0 & -1 & 0 \\ 0 & 1+\overline{h}_m & 0 & -1 \\ -1 & 0 & 3 & 0 \\ 0 & -1 & 0 & 3 \end{bmatrix}.
\end{aligned}
$$

Moreover, from (2.7), we obtain

$$
\mathcal{N}_{HH}(m) = \begin{bmatrix} 2m & -m & -m \\ -m & m & 0 \\ -m & 0 & m \end{bmatrix}, \quad \Delta(m) = \begin{bmatrix} 0 & 0 & 0 \\ 0 & \overline{h}_m & 0 \\ 0 & 0 & \overline{h}_m \end{bmatrix}.
$$

$$
|\underbrace{-x_6 - |-x_4-}_{\alpha=1}|\underbrace{-x_2 - |-x_1 - |-x_3-}_{\alpha=m\gg 1}|\underbrace{-x_5 - |-x_7-}_{\alpha=1}|
$$

Figure 2.2: The finite volume mesh where the cell-centers are denoted by $x_i,\ i = 1, \ldots, 7$.

We readily see that the m-dependence of the matrices $K_{LH}(m), K_{HL}(m)$, $K_{LL}(m)$, and

$\Delta(m)$ is eliminated asymptotically. For instance,

$$\Delta(m) \;=\; \Delta^{\infty} + \mathcal{O}(m^{-1}) = \begin{bmatrix} 0 & 0 & 0 \\ 0 & 2 & 0 \\ 0 & 0 & 2 \end{bmatrix} + \mathcal{O}(m^{-1}).$$

2.3 Spectral analysis of the diagonally scaled finite volume discretization matrix

Roughness of PDE coefficients causes loss of robustness of the preconditioners. This is mainly due to clusters of eigenvalues with varying magnitude. Although diagonal scaling has no effect on the asymptotic behavior of the condition number, it leads to an improved clustering in the spectrum; see Table 2.1.

In this section we will analyze the behavior of the spectrum of the symmetrically scaled discretization matrix

$$A(m) := (\mathrm{diag}K(m))^{-1/2}\, K(m)\, (\mathrm{diag}K(m))^{-1/2}\,. \tag{2.12}$$

In the case of a single highly-diffusive island corresponding to the configuration in Figure 2.1, $A(m)$ contains only one small eigenvalue for which the below main result is established:

$$C_1\; m^{-1} \leq \lambda_{\min}(A(m)) \leq C_2\; m^{-1/2}. \tag{2.13}$$

The analysis also supports multiple highly-diffusive islands. In fact, the number of small eigenvalues of $A(m)$ depends on the number of isolated islands comprising the highly-diffusive region.

Table 2.1: A 2D example showing the condition numbers and eigenvalues of the finite volume discretization matrix $K(m)$ and its diagonally scaled version $A(m)$ in which the eigenvalues are sorted in ascending order.

m	$\kappa(K(m))$	$\lambda_1(K(m))$	$\lambda_{61}(K(m))$	$\lambda_{62}(K(m))$	$\lambda_{64}(K(m))$	$\kappa(A(m))$	$\lambda_1(A(m))$	$\lambda_2(A(m))$	$\lambda_{64}(A(m))$
10^0	2.63×10^1	3.05×10^{-1}	7.70×10^0	7.85×10^0	8.00×10^0	2.55×10^1	7.54×10^{-2}	1.80×10^{-1}	1.925×10^0
10^2	1.25×10^3	3.24×10^{-1}	8.00×10^0	2.04×10^2	4.04×10^2	3.45×10^2	5.78×10^{-3}	1.36×10^{-1}	1.99×10^0
10^4	1.24×10^5	3.24×10^{-1}	8.00×10^0	2.00×10^4	4.00×10^4	3.26×10^4	6.14×10^{-5}	1.35×10^{-1}	2.00×10^0
10^6	1.24×10^7	3.24×10^{-1}	8.00×10^0	2.00×10^6	4.00×10^6	3.26×10^6	6.14×10^{-7}	1.35×10^{-1}	2.00×10^0
10^8	1.24×10^9	3.24×10^{-1}	8.00×10^0	2.00×10^8	4.00×10^8	3.26×10^8	6.14×10^{-9}	1.35×10^{-1}	2.00×10^0
10^{10}	1.24×10^{11}	3.24×10^{-1}	8.00×10^0	2.00×10^{10}	4.00×10^{10}	3.26×10^{10}	6.14×10^{-11}	1.35×10^{-1}	2.00×10^0

The required analysis is quite technical and will be presented in the appendix. In this section, we outline only the steps leading to the main result (2.13). The upper bound in (2.13) is obtained by an application of Courant-Fischer mini-max Theorem; see Lemma 3.

REMARK 1. *Numerically we observe that the smallest eigenvalue is* $\mathcal{O}(m^{-1})$; *see Table 2.1. The perturbation expansion leads to* $\mathcal{O}(m^{-1})$ *estimate with one exceptional case corresponding to the first "Case 1" in §2.8.1.1. Hence,* $\mathcal{O}(m^{-1/2})$ *estimate is an artifact of the perturbation expansion. The same artifact also appears in the FE analysis; see [41, Eq. (5.14)].*

The lower bound proof is more involved; see §2.8.1.2. For that, first we establish the below estimate for $K(m)$:

$$x^T K(m)x \;\geq\; x^T K(1)x \;\geq\; m^{-1}x^T K(m)x. \tag{2.14}$$

Then, we establish a similar estimate for diag $K(m)$:

$$x^T \text{diag } K(m)x \;\geq\; x^T \text{diag } K(1)x \;\geq\; m^{-1}x^T \text{diag } K(m)x. \tag{2.15}$$

Combining (2.14) and (2.15), yields the lower bound estimate for the smallest eigenvalue:

$$C_1\; m^{-1} \leq \lambda_{\min}(A(m)).$$

We illustrate the spectral effects of diagonal scaling by an example in Table 2.1. In the example, $K(m)$ has 3 eigenvalues approaching to ∞ and 61 bounded eigenvalues, whereas, $A(m)$ has only one eigenvalue approaching to zero. The merit of diagonal scaling becomes apparent after studying the spectral behavior of $A(m)$. We observe that the number of the eigenvalues of A of $\mathcal{O}(m^{-1})$ depends only on the number of isolated islands. On the other hand, the number of the eigenvalues of $K(m)$ of $\mathcal{O}(m)$ depends on the number of DOF of the islands, asymptotically. Note that the reduction in the number of m-dependent eigenvalues is a desirable feature for fast convergence of Krylov subspace solvers.

2.4 Singular perturbation analysis on matrix entries

2.4.1 Preliminaries on matrix properties

The discretization formula (2.9) with the harmonic means (2.8) gives rise to the matrix entries given in (2.11). Due to harmonic means, the m-dependence of the matrix entries corresponding to HL and LL couplings is asymptotically eliminated. As a result, the sub-matrices $K_{HL}(m)$ and $K_{LL}(m)$ do not have m-dependence asymptotically:

$$\begin{aligned} K_{HL}(m) &= K_{HL}^{\infty} + \mathcal{O}(m^{-1}), \\ K_{LH}(m) &= K_{HL}^{\infty^T} + \mathcal{O}(m^{-1}), \\ K_{LL}(m) &= K_{LL}^{\infty} + \mathcal{O}(m^{-1}). \end{aligned} \tag{2.16}$$

The analysis mainly relies on this crucial property.

To analyze the m-robustness of preconditioners based on (2.5), we need to analyze the asymptotic behaviour of the block components $K_{HH}(m)^{-1}$, $S(m)^{-1}$, and $K_{LH}(m)K_{HH}(m)^{-1}$ as $m \to \infty$. This is the purpose of Lemma 1 below. To prepare for this, we further decompose DOF associated with $\overline{\Omega}_H$ into a set of interior DOF associated with index I and boundary DOF with index Γ. This leads to the following further block representation of

$$K_{HH}(m) = \begin{bmatrix} K_{II}(m) & K_{I\Gamma}(m) \\ K_{\Gamma I}(m) & K_{\Gamma\Gamma}(m) \end{bmatrix}. \tag{2.17}$$

By using (2.11), we can write a more refined expression for the block $K_{\Gamma\Gamma}(m)$:

$$K_{\Gamma\Gamma}(m) = K_{\Gamma\Gamma}^{(H)}(m) + \overline{h}_m D_{\Gamma\Gamma}^{(L)},$$

with

$$D_{\Gamma\Gamma}^{(L)} := \mathrm{diag}(0, \ldots, 0, 1, \ldots, 1, 2, \ldots, , 2), \tag{2.18}$$

where the number of 0, 1, and 2 entries is equal to the cardinality of interior, non-corner interface, and corner interface cell-centers, respectively. Thus, we can characterize the Neumann matrix $\mathcal{N}_{HH}$ on Ω_H as described in (2.7) as follows:

$$\begin{aligned} K_{HH}(m) &= m\mathcal{N}_{HH} + \Delta(m), && (2.19)\\ \Delta(m) &= \overline{h}_m \begin{bmatrix} 0 & 0 \\ 0 & D_{\Gamma\Gamma}^{(L)} \end{bmatrix}, && (2.20)\\ &= \Delta^{\infty} + \mathcal{O}(m^{-1}), && (2.21) \end{aligned}$$

where $\Delta(m)$ is a diagonal matrix due to (2.18). $\mathcal{N}_{HH}$ is a SPSD matrix with a simple zero eigenvalue and associated constant eigenvector. If n_H denotes the number of DOF in Ω_H, a suitable normalized eigenvector is the constant vector with entries $n_H^{-1/2}$, which we denote by e_H. We further write in block form as $e_H^T = (e_I^T \ , \ e_\Gamma^T)$. Finally we note that the off-diagonal blocks in (2.4) have the decomposition:

$$K_{LH}(m) = \begin{bmatrix} 0 & K_{L\Gamma}(m) \end{bmatrix} = K_{HL}(m)^T. \tag{2.22}$$

As we prepare for the proof of our main Lemma, we need to define the following quantity:

$$\eta(m) := e_H^T K_{HH}(m) e_H. \tag{2.23}$$

$\eta(m) > 0$ because $K_{HH}(m)$ is SPD as a diagonal subblock of $K(m)$. Moreover, combining (2.19) and (2.20), one can reduce the expression in (2.23) to

$$\eta(m) = \overline{h}_m \, e_\Gamma^T D_{\Gamma\Gamma}^{(L)} e_\Gamma. \tag{2.24}$$

In fact, (2.24) can be expressed explicitly by:

$$\eta(m) = \overline{h}_m \ \frac{n_{H,nc} + n_{H,c}}{n_H}, \tag{2.25}$$

where

$$\begin{aligned} n_{H,nc} &:= \#\{\text{non-corner interface cell-centers}\} \\ n_{H,c} &:= \#\{\text{corner interface cell-centers}\}. \end{aligned}$$

Finally, (2.25) delivers the asymptotic convergence expression for $\eta(m)$:

$$\eta(m) = \eta + \mathcal{O}(m^{-1}), \tag{2.26}$$

where $\eta = 2\,\frac{n_{H,nc}+n_{H,c}}{n_H}$.

2.4.2 The main results on the preconditioner

LEMMA 1. *The asymptotic behaviour of the submatrices in* (2.5) *is described by the following:*

(i) $K_{HH}(m)^{-1} = e_H \eta^{-1} e_H^T + \mathcal{O}(m^{-1})$,

(ii) $S(m) = K_{LL}^{\infty} - (K_{L\Gamma}^{\infty} e_\Gamma)\eta^{-1}(e_\Gamma^T K_{\Gamma L}^{\infty}) + \mathcal{O}(m^{-1})$,

(iii) $K_{LH}(m)K_{HH}(m)^{-1} = (K_{L\Gamma}^{\infty} e_\Gamma)\eta^{-1} e_H^T + \mathcal{O}(m^{-1})$.

Proof. Since $\mathcal{N}_{HH}$ is symmetric positive semidefinite we have the eigenvalue decomposition:

$$Z^T \mathcal{N}_{HH} Z = \mathrm{diag}(\lambda_1, \ldots, \lambda_{n_H - 1}, 0), \tag{2.27}$$

where $\{\lambda_i : \ i = 1, \ldots, n_H\}$ is a non-increasing sequence of eigenvalues of $\mathcal{N}_{HH}$ and Z is orthogonal. Since, the eigenvector corresponding to the zero eigenvalue is constant, we can

write $Z = \left[\tilde{Z} \mid e_H\right]$ and so, using (2.19), we have

$$\begin{aligned} & Z^T K_{HH}(m) Z \\ &= \begin{bmatrix} m \text{ diag}(\lambda_1, \ldots, \lambda_{n_{H-1}}) + \tilde{Z}^T \Delta(m) \tilde{Z} & \tilde{Z}^T \Delta(m) e_H \\ e_H^T \Delta(m) \tilde{Z} & e_H^T \Delta(m) e_H \end{bmatrix} \\ &=: \begin{bmatrix} \tilde{\Lambda}(m) & \tilde{\delta}(m) \\ \tilde{\delta}^T(m) & \eta(m) \end{bmatrix}. \end{aligned} \tag{2.28}$$

To find the limiting form of $K_{HH}(m)^{-1}$ note that

$$\begin{aligned} \tilde{\Lambda}(m) &= m \text{ diag}(\lambda_1, \ldots, \lambda_{n_{H-1}}) + \tilde{Z}^T \Delta(m) \tilde{Z} \\ &= m \text{ diag}(\lambda_1, \ldots, \lambda_{n_{H-1}}) \left(\tilde{I} + m^{-1} \text{ diag}(\lambda_1^{-1}, \ldots, \lambda_{n_{H-1}}^{-1}) \tilde{Z}^T \Delta(m) \tilde{Z} \right). \end{aligned}$$

Now, let $C_\lambda := \max_{i<n_H} \lambda_i^{-1}$ and C_Δ be the constant in (2.21), i.e., $\|\Delta(m)\|_2 \leq \|\Delta^\infty\|_2 + C_\Delta m^{-1}$. Then, for sufficiently large m,

$$\|\tilde{\Lambda}(m)^{-1}\|_2 \;\leq\; \frac{m^{-1} C_\lambda}{1 - m^{-1} C_\lambda \|\tilde{Z}^T \Delta(m) \tilde{Z}\|_2} \;\leq\; \frac{m^{-1} C_\lambda}{C_{\tilde{\Lambda}}}$$

where

$$\begin{aligned} C_{\tilde{\Lambda}} &:= 1 - m^{-1} C_\lambda \|\tilde{Z}^T\|_2 \|\Delta^\infty\|_2 \|\tilde{Z}\|_2 - m^{-2} C_\Delta C_\lambda \|\tilde{Z}^T\|_2 \|\tilde{Z}\|_2 \\ &= 1 + \mathcal{O}(m^{-1}). \end{aligned} \tag{2.29}$$

Hence, combining (2.29) and (2.29), we obtain:

$$\tilde{\Lambda}(m)^{-1} = \mathcal{O}(m^{-1}). \tag{2.30}$$

We proceed with the following inversion:

$$\begin{bmatrix} \tilde{\Lambda}(m) & \tilde{\delta}(m) \\ \tilde{\delta}(m)^T & \eta(m) \end{bmatrix}^{-1} = U(m)\ V(m)\ U(m)^T,$$

where

$$\begin{aligned} U(m) &:= \begin{bmatrix} \tilde{I} & -\tilde{\Lambda}(m)^{-1}\tilde{\delta}(m) \\ 0^T & 1 \end{bmatrix}, \\ V(m) &:= \begin{bmatrix} \tilde{\Lambda}(m)^{-1} & 0 \\ 0^T & \Big(\eta(m) - \tilde{\delta}(m)^T\tilde{\Lambda}(m)^{-1}\tilde{\delta}(m)\Big)^{-1} \end{bmatrix}. \end{aligned}$$

Using (2.21), one gets

$$\tilde{\delta}(m) = \tilde{Z}^T\Delta^{\infty}e_H + \mathcal{O}(m^{-1}). \tag{2.31}$$

Then, (2.26), (2.30), and (2.31) imply that

$$\begin{aligned} \eta(m)^{-1} &= \eta^{-1} + \mathcal{O}(m^{-1}), \\ U(m) &= I + \mathcal{O}(m^{-1}), \\ V(m) &= \begin{bmatrix} O & 0 \\ 0^T & \eta^{-1} \end{bmatrix} + \mathcal{O}(m^{-1}). \end{aligned}$$

Combining the above results, we arrive at

$$\begin{bmatrix} \tilde{\Lambda}(m) & \tilde{\delta}(m) \\ \tilde{\delta}(m)^T & \eta(m) \end{bmatrix}^{-1} = \begin{bmatrix} O & 0 \\ 0^T & \eta^{-1} \end{bmatrix} + \mathcal{O}(m^{-1})\ , \tag{2.32}$$

and, by (2.28), we have

$$\begin{aligned} K_{HH}(m)^{-1} &= Z \begin{bmatrix} O & 0 \\ 0^T & \eta^{-1} \end{bmatrix} Z^T \; + \; \mathcal{O}(m^{-1}) \\ &= e_H \left(e_\Gamma^T \; 2\, D_{\Gamma\Gamma}^{(L)} e_\Gamma \right)^{-1} e_H^T \; + \; \mathcal{O}(m^{-1}) \; , \end{aligned}$$

which proves part (i) of the Lemma.

Parts (ii) and (iii) follow from simple substitution, using (2.6) and (2.22). □

We use the following limiting forms in the definition of the proposed preconditioner (2.35):

$$K_{HH}^{\infty^\dagger} := e_H \eta^{-1} e_H^T, \tag{2.33}$$

$$\begin{aligned} Q_{LH}^{\infty} &:= K_{LH}^{\infty} K_{HH}^{\infty^\dagger}, \\ S^{\infty} &:= K_{LL}^{\infty} - K_{LH}^{\infty} K_{HH}^{\infty^\dagger} K_{HL}^{\infty}. \end{aligned} \tag{2.34}$$

Based on the above perturbation analysis we propose the following preconditioner:

$$B_{AGKS}(m) := \begin{bmatrix} I_{HH} & -Q_{LH}^{\infty^T} \\ 0 & I_{LL} \end{bmatrix} \begin{bmatrix} K_{HH}(m)^{-1} & 0 \\ 0 & S^{\infty^{-1}} \end{bmatrix} \begin{bmatrix} I_{HH} & 0 \\ -Q_{LH}^{\infty} & I_{LL} \end{bmatrix}. \tag{2.35}$$

The following theorem shows that AGKS preconditioner is an effective preconditioner for $m \gg 1$.

THEOREM 1. *For m sufficiently large we have*

$$\sigma(B_{AGKS}(m) \; K(m)) \; \subset \; [1 - cm^{-1/2}, 1 + cm^{-1/2}]$$

for some constant c independent of m, and therefore

$$\kappa(B_{AGKS}(m) \; K(m)) \; = \; 1 \; + \; \mathcal{O}(m^{-1/2}).$$

Proof. The m-dependence of $K_{HL}(m), K_{LH}(m)$, and $K_{LL}(m)$ are eliminated asymptotically as in (2.16). Furthermore, m-dependence of $\eta(m)$ is also eliminated as a result of (2.21). Therefore, the proof of this theorem is as following:

Letting $M^{1/2}$ denote the square root of any symmetric positive definite matrix M, we write $B_{AGKS} = L^T L$ with

$$L \;:=\; \begin{bmatrix} K_{HH}^{-1/2} & 0 \\ \\ -S^{\infty^{-1/2}} Q_{LH}^{\infty} & S^{\infty^{-1/2}} \end{bmatrix}.$$

(Note that for notational convenience we do not explicitly state which terms depend on m everywhere in this proof.) A straightforward calculation shows that

$$\sigma(B_{AGKS}K) \;=\; \sigma(LKL^T) \;=\; \sigma(I+R)\;, \tag{2.36}$$

where R is the matrix:

$$\begin{bmatrix} 0 & K_{HH}^{-1/2}(K_{HL} - K_{HH}Q_{LH}^{\infty^T})S^{\infty^{-1/2}} \\ \\ S^{\infty^{-1/2}}(K_{LH} - Q_{LH}^{\infty}K_{HH})K_{HH}^{-1/2} & 0 \end{bmatrix}.$$

As an example of the computation leading to (2.36), note that the bottom right-hand entry of the product LAL^T reads:

$$S^{\infty^{-1/2}} \left[Q_{LH}^{\infty} K_{HH} Q_{LH}^{\infty^T} - Q_{LH}^{\infty} K_{HL} - K_{LH} Q_{LH}^{\infty^T} + K_{LL} \right] S^{\infty^{-1/2}} \;=\; I,$$

since, by definition of Q_{LH}^{∞} and of η, we have $-K_{LH}Q_{LH}^{\infty^T} + K_{LL} = S^{\infty}$ and

$$Q_{LH}^{\infty} K_{HH} Q_{LH}^{\infty^T} - Q_{LH}^{\infty} K_{HL} \;=\; K_{LH}\left(\mathbf{e}_H \eta^{-1} \mathbf{e}_H^T K_{HH} \mathbf{e}_H \eta^{-1} \mathbf{e}_H^T - \mathbf{e}_H \eta^{-1} \mathbf{e}_H^T \right) K_{HL} \;=\; 0\;.$$

To finish the proof we shall show that, for m sufficiently large,

$$K_{HH}^{-1/2} = \mathbf{e}_H \eta^{-1/2} \mathbf{e}_H^T + \mathcal{O}(m^{-1/2}). \tag{2.37}$$

On the assumption that (2.37) holds, we have

$$R_{LH} \;=\; S^{\infty^{-1/2}} K_{LH}(I_{HH} - \mathbf{e}_H \eta^{-1} \mathbf{e}_H^T K_{HH}) \mathbf{e}_H \eta^{-1/2} \mathbf{e}_H^T + \mathcal{O}(m^{-1/2}) \;=\; \mathcal{O}(m^{-1/2}) \tag{2.38}$$

and so the spectral radius $\rho(R)$ of R is $\mathcal{O}(m^{-1/2})$, which together with (2.36) completes the proof.

To prove (2.37), let us write down the eigenvalue decomposition of $K_{HH}(m)$

$$V(m)^T K_{HH}(m) V(m) \;=\; \operatorname{diag}(\mu_1(m), \ldots, \mu_{n_H}(m)) \tag{2.39}$$

where $\{\mu_i(m) : \; i = 1, \ldots, n_H\}$ denotes any non-increasing ordering of the eigenvalues of $K_{HH}(m)$. Since $K_{HH}(m)$ is SPD, we have $\mu_i(m) > 0$ for all $i \leq n_H$. Moreover, the μ_i are continuous functions of m, with

$$m^{-1} \mu_i(m) \;=\; \lambda_i + \mathcal{O}(m^{-1}), \tag{2.40}$$

as $m \to \infty$, where the λ_i are as defined in the proof of Lemma 1 and we have used (2.28). However, we also know from (2.33) that (for m sufficiently large) the largest eigenvalue of $K_{HH}(m)^{-1}$ is given by

$$\mu_{n_H}(m)^{-1} = \eta^{-1} + \mathcal{O}(m^{-1}) \; . \tag{2.41}$$

Therefore, using (2.39), (2.40) and (2.41), we have

$$V(m)^T K_{HH}(m)^{-1/2} V(m) \;=\; \operatorname{diag}(0, \ldots, 0, \; \eta^{-1/2}) \;+\; \mathcal{O}(m^{-1/2}) \; .$$

The required estimate (2.37) follows by noting that the last column of $V(m)$ approaches $\mathbf{e}_H$ with $\mathcal{O}(m^{-1})$ as $m \to \infty$.

□

2.5 Qualitative nature of the solution of the high-contrast diffusion equation and decoupling

We advocate the usage of SPA because it is a very effective tool in gaining qualitative insight about the asymptotic behavior of the solution of the underlying PDE. Through SPA, in Lemma 1, we were able to fully reveal the asymptotic behaviour of the submatrices of K in (2.5). This information leads to a characterization of the limit of the underlying discretized inverse operator and we studied this in more detail in [3]. We now prove that *asymptotically, the solution over the highly-diffusive island goes to a constant vector*. This is probably the most fundamental qualitative feature of the solution of the high-contrast diffusion equation.

LEMMA 2. *Let $x_H(m)$ be the solution in* (2.4) *corresponding the highly-diffusive island and e_H be the constant vector. Then,*

$$x_H(m) = c_H \; e_H \; + \; \mathcal{O}(m^{-1}), \tag{2.42}$$

where c_H is determined by the solution in the lowly-diffusive region.

Proof. We prove the result by providing an explicit quantification of the limiting process based on Lemma 1:

$$\begin{aligned} x_L(m) &= S^{-1}(m) \; \{b_L - K_{LH}(m) K_{HH}^{-1}(m) b_H\} \\ &= S^{\infty^{-1}} \{b_L - K_{LH}^{\infty} K_{HH}^{\infty^{\dagger}} b_H\} + \mathcal{O}(m^{-1}) \\ &=: x_L^{\infty} + \mathcal{O}(m^{-1}), \end{aligned}$$

$$
\begin{aligned}
x_H(m) &= K_{HH}^{-1}(m)\ \{b_H - K_{HL}(m)x_L(m)\} \\
&= K_{HH}^{\infty\dagger}\{b_H - K_{HL}^{\infty}x_L^{\infty}\} + \mathcal{O}(m^{-1}) \\
&=: c_H\ e_H\ +\ \mathcal{O}(m^{-1}).
\end{aligned}
$$

□

SPA helps to reveal a further qualitative property, namely, the decoupling phenomenon. We show how the original algebraic solution strategy decouples into two algebraic problems of different nature and the decoupling is indeed an implication of (2.42). This observation would be very valuable also for designing preconditioners for different classes of PDEs and discretizations. In Chapter 4 we will give a solution behaviour result similar to (2.42) for the high-contrast biharmonic plate equation for HCT and Morley discretizations.

In order to show the decoupling, let us start by noting that S^{∞} in Lemma 1 can also be interpreted as the Schur complement of $c^2\ e_\Gamma^T K_{\Gamma\Gamma}^{(L)} e_\Gamma$ in the matrix

$$
KK_{LL}^{\infty} = \begin{bmatrix} c^2\ e_\Gamma^T K_{\Gamma\Gamma}^{(L)} e_\Gamma & c\ e_\Gamma^T K_{\Gamma L} \\ c\ K_{L\Gamma} e_\Gamma & K_{LL} \end{bmatrix},
$$

for any nonzero value of c. In particular, if we choose $c := n_H^{1/2}$, then $ce_\Gamma = 1_\Gamma$, the vector of all ones on Γ and, using also (2.19), we have

$$
\begin{aligned}
KK_{LL}^{\infty} &:= \begin{bmatrix} 1_\Gamma^T K_{\Gamma\Gamma}^{(L)} 1_\Gamma & 1_\Gamma^T K_{\Gamma L} \\ K_{L\Gamma} 1_\Gamma & K_{LL} \end{bmatrix} \\
&= \begin{bmatrix} 1_H^T K_{HH}(1) 1_H & 1_H^T K_{HL} \\ K_{LH} 1_H & K_{LL} \end{bmatrix}.
\end{aligned} \tag{2.43}
$$

This is the stiffness matrix for a pure Dirichlet problem for the Laplacian on all of Ω with the additional constraint that the solution is constant on Ω_H. See Figure 2.3. Thus, when $m \gg 1$, the original problem *decouples almost entirely into a (regularized) Neumann*

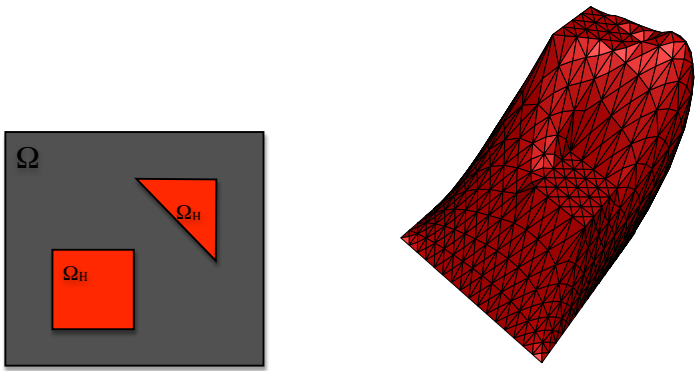

Figure 2.3: $x_{H_i}(m_i) = c_{H_i} + \mathcal{O}(m_i^{-1})$, $i = 1, 2$ where Ω_{H_1} and Ω_{H_2} correspond to square and triangle shaped highly-diffusive islands, respectively with $m_i = 10^6$.

problem (i.e. $K_{HH}(m)$) for the Laplacian on Ω_H (scaled by m) and a Dirichlet problem (i.e. KK^{∞}_{LL}) for the Laplacian on all of Ω, but under the additional constraint that the solution is constant on Ω_H.

Next, we show an additional decoupling. This time the preconditioner decouples into a block diagonal matrix with the help of a deflation method.

2.6 Implementation aspects and the related deflation-method

The fact that $\mathcal{N}_{HH}$ has a simple zero eigenvalue (with the corresponding constant eigenvector e_H) and $\mathcal{N}_{HH}$ is of co-rank 1 imply that $K_{HH}(m)$ has a single eigenvalue of $\mathcal{O}(1)$ and $n_H - 1$ eigenvalues of $\mathcal{O}(m)$. For sufficiently large m, e_H can be taken as an approximate eigenvector corresponding to $\mathcal{N}_{HH}$'s single smallest eigenvalue. Therefore, in the light of (2.5),

$$e^T := [e_H^T, 0^T],$$

becomes an approximate eigenvector corresponding to the smallest eigenvalue of the decoupled matrix:

$$\begin{bmatrix} K_{HH}(m) & 0 \\ 0 & S(m) \end{bmatrix}. \tag{2.44}$$

In order to eliminate the negative effect of the smallest eigenvalue, we utilize a deflation method under the constraint that it gives the decoupling as in (2.44). If such decoupling occurs, it would provide a large computational advantage. We utilize a deflation method, known as *subdomain deflation* [68, 85, 86, 87] constructed by the following K-orthogonal projection onto the subspace orthogonal to e, provides the desired decoupling.

$$\mathcal{P}^T \;:=\; I - e\,\eta(m)^{-1}\,e^T\,K\,. \tag{2.45}$$

We apply AGKS preconditioner within a conjugate gradient algorithm for the deflated system

$$\mathcal{P}Kx^{\perp} \;=\; \mathcal{P}b, \tag{2.46}$$

where $x^{\perp} := \mathcal{P}^T x$ is the projected solution. The component of x in the direction of e is then simply given by

$$x - x^{\perp} \;=\; (I - \mathcal{P}^T)x = \; e\,\eta(m)^{-1}\,e^T\,b\;.$$

When we rewrite (2.35) as

$$B_{AGKS}(m) = L^T\,D(m)\,L,$$

where

$$\begin{aligned} L \;&:=\; \begin{bmatrix} I_{HH} & 0 \\ -Q_{LH}^{\infty} & I_{LL} \end{bmatrix}, \\ D(m) \;&:=\; \begin{bmatrix} K_{HH}(m)^{-1} & 0 \\ 0 & S^{\infty^{-1}} \end{bmatrix}. \end{aligned} \tag{2.47}$$

By observing the following interesting property

$$L\,\mathcal{P} = \mathcal{P}, \tag{2.48}$$

the system in (2.46) after preconditioned by $B_{AGKS}(m)$ turns into:

$$B_{AGKS}(m)\ \left(\mathcal{P}Kx^{\perp}\right) = B_{AGKS}(m)\ (\mathcal{P}b)\,.$$

Then, it reduces to the following block diagonal system:

$$D(m)\ \mathcal{P}\,K\,x^{\perp} = D(m)\ \mathcal{P}\,b.$$

REMARK 2. *The fact that e becomes an approximate eigenvector corresponding to the smallest eigenvalue of the decoupled matrix in* (2.44) *is not necessarily true for the original matrix $K(m)$ because it is not block diagonal. Therefore, utilizing the above deflation method in the direction of e will not necessarily provide any further robustness for the underlying preconditioner if that preconditioner uses off-diagonal blocks of $K(m)$ as well. Multigrid method is one such preconditioner. In fact, numerically we observed that introducing deflation did not improve the multigrid convergence rate at all. If one still wants to improve the convergence rate by the help of deflation, then the approximate eigenvector corresponding to the smallest eigenvalue must be computed in an alternative way rather than the simple usage of e. Consequently, we can say that $B_{AGKS}(m)$, by its design, naturally goes with subdomain deflation. The incorporation of subdomain deflation not only brings robustness with respect to the smallest eigenvalue, but also provides huge computational savings due to reduction to a block diagonal system. This is a significant computational advantage $B_{AGKS}(m)$ offers.*

By exploiting the fact that S^{∞} in (2.34) is only a low-rank perturbation of K^{∞}, we can build robust preconditioners for S^{∞} in (2.35) via standard multigrid preconditioners. Combining (2.33) and (2.34), we arrive at

$$S^{\infty} = K^{\infty}_{LL} - v\eta^{-1}v^{T},$$

where $v := K_{LH}^{\infty} e_H$. If M_{LL} denotes a standard multigrid V-cycle preconditioner for K_{LL}, we can construct an efficient and robust preconditioner $\tilde{S}^{-1}$ for S^{∞} using the Sherman-Morrison-Woodbury formula [40, Eq. (2.1.4)], i.e.

$$\tilde{S}^{-1} \;:=\; M_{LL} \;+\; M_{LL} v \,(1-\eta)^{-1}\, v^T M_{LL}. \tag{2.49}$$

Note also that we can precompute and store $M_{LL}v$ during the setup phase. This means we only need to apply the multigrid V-cycle M_{LL} once per iteration. Therefore, the following practical version of preconditioner (2.35) is used in the implementation:

$$\tilde{B}_{AGKS} := \begin{bmatrix} I_{HH} & -Q_{LH}^{\infty^T} \\ 0 & I_{LL} \end{bmatrix} \begin{bmatrix} M_{HH} & 0 \\ 0 & \tilde{S}^{-1} \end{bmatrix} \begin{bmatrix} I_{HH} & 0 \\ -Q_{LH}^{\infty} & I_{LL} \end{bmatrix}, \tag{2.50}$$

where M_{HH} denotes a multigrid V-cycle preconditioner for $K_{HH}(m)$.

2.7 Numerical experiments

The goal of the numerical experiments is to compare the performance of the two preconditioners: AGKS and CCMG. The domain is unit square with a uniform mesh consisting of $2^{\ell} \times 2^{\ell},\ \ell = 3, \ldots, 6$, cells. The coarsest level mesh contains 8×8 cells with a highly-diffusive single island of size 2×2 cells centered at the point $(3/8, 3/8)$. For the discussion of multiple disconnected islands, refer to [6, Sections 3 and 4].

We denote the norm of the relative residual at iteration t by $rr^{(t)}$:

$$rr^{(t)} := \frac{\|r^{(t)}\|_2}{\|r^{(0)}\|_2},$$

where $r^{(t)}$ denotes the residual at iteration t with a stopping criterion of $rr^{(t)} \leq 10^{-9}$. In the tables, we report the iteration count and the average reduction factor of the residual which is defined as:

$$\left(rr^{(t)}\right)^{1/t}.$$

We enforce an iteration bound of 60. If the method seems to converge slightly beyond this bound, we denote it by 60^{+}. Whereas, the divergence is denoted by ∞. In Tables 2.2–2.10, iteration count and the average reduction factor are reported for combinations of preconditioner, prolongation, and smoother types.

We use Galerkin variational approach to construct the coarser level algebraic systems. There are two types of prolongation operators under consideration; Wesseling-Khalil [92] and bi-linear, given by respectively:

$$P^{(WK)} = \frac{1}{4}\begin{bmatrix} 1 & 1 & & 0 & 0 \\ 1 & 3 & & 2 & 0 \\ & & . & & \\ 0 & 2 & & 3 & 1 \\ 0 & 0 & & 1 & 1 \end{bmatrix}_{2h}^{h}, \quad \text{and} \quad R^{(WK)} = P^{(WK)^*},$$

$$P^{(B)} = \frac{1}{16}\begin{bmatrix} 1 & 3 & & 3 & 1 \\ 3 & 9 & & 9 & 3 \\ & & . & & \\ 3 & 9 & & 9 & 3 \\ 1 & 3 & & 3 & 1 \end{bmatrix}_{2h}^{h}, \quad \text{and} \quad R^{(B)} = P^{(B)^*}.$$

The multigrid preconditioner CCMG is derived from the implementation by Aksoylu, Bond, and Holst [5]. We employ a V(1,1)-cycle with point symmetric Gauss-Seidel (sGS) or ILU smoothers. A direct solver is used for the coarsest level. We construct two different multilevel hierarchies for multigrid preconditioners M_{HH} in (2.50) and M_{LL} in (2.49) for DOF corresponding to Ω_H and Ω_L, respectively. The corresponding prolongation matrices P_{HH} and P_{LL} are extracted from the prolongation matrix for the whole domain Ω in the fashion following (2.4):

Table 2.2: Preconditioner = CCMG - V(1,1)-cycle, prolongation = Wesseling-Khalil, smoother = ILU

$h\backslash m$	10^0	10^1	10^2	10^3	10^4	10^5	10^6	10^7	10^8	10^9
1/8	**10**, 0.025	**29**, 0.472	**30**, 0.500	**35**, 0.528	**36**, 0.559	**40**, 0.593	**44**, 0.622	**52**, 0.669	**52**, 0.669	**58**, 0.697
1/16	**10**, 0.121	**12**, 0.165	**15**, 0.240	**21**, 0.315	**31**, 0.481	**38**, 0.541	**50**, 0.644	**60**$^+$, 0.786	**60**$^+$, 0.770	**60**$^+$, 0.922
1/32	**8**, 0.069	**10**, 0.093	**12**, 0.162	**14**, 0.224	**19**, 0.309	**27**, 0.455	**52**, 0.668	**60**$^+$, 0.829	**60**$^+$, 1.002	**60**$^+$, 1.033
1/64	**8**, 0.064	**10**, 0.099	**13**, 0.160	**14**, 0.201	**19**, 0.311	**29**, 0.462	**47**, 0.638	**60**$^+$, 0.860	**60**$^+$, 1.014	**60**$^+$, 1.033

Table 2.3: Preconditioner = CCMG - V(1,1)-cycle, prolongation = Wesseling-Khalil, smoother = sGS

$h\backslash m$	10^0	10^1	10^2	10^3	10^4	10^5	10^6	10^7	10^8	10^9
1/8	**10**, 0.025	**29**, 0.472	**30**, 0.500	**35**, 0.528	**36**, 0.559	**40**, 0.593	**44**, 0.622	**52**, 0.669	**52**, 0.669	**58**, 0.697
1/16	**12**, 0.166	**14**, 0.222	**19**, 0.310	**26**, 0.409	**38**, 0.535	**52**, 0.649	**60**$^+$, 0.777	**60**$^+$, 0.843	**60**$^+$, 0.938	∞, 1.070
1/32	**14**, 0.195	**15**, 0.217	**18**, 0.294	**25**, 0.432	**39**, 0.552	**58**, 0.698	**60**$^+$, 0.917	∞, 1.002	∞, 1.080	∞, 1.127
1/64	**13**, 0.197	**14**, 0.221	**17**, 0.282	**22**, 0.362	**31**, 0.497	**48**, 0.645	**60**$^+$, 0.793	∞, 0.954	∞, 1.097	∞, 1.120

Table 2.4: Preconditioner = CCMG - V(1,1)-cycle, prolongation = bi-linear, smoother = ILU

$h\backslash m$	10^0	10^1	10^2	10^3	10^4	10^5	10^6	10^7	10^8	10^9
1/8	**10**, 0.025	**29**, 0.472	**30**, 0.500	**35**, 0.528	**36**, 0.559	**40**, 0.593	**44**, 0.622	**52**, 0.669	**52**, 0.669	**58**, 0.697
1/16	**9**, 0.095	**12**, 0.145	**14**, 0.225	**23**, 0.403	**32**, 0.514	**48**, 0.637	**59**, 0.693	$\mathbf{60}^+$, 0.834	$\mathbf{60}^+$, 0.924	∞, 0.990
1/32	**7**, 0.040	**9**, 0.074	**12**, 0.154	$\mathbf{60}^+$, 1.051	∞, 1.001	∞, 1.001	∞, 1.001	∞, 1.001	∞, 1.001	∞, 1.001
1/64	**7**, 0.039	**8**, 0.075	**11**, 0.127	**21**, 0.350	∞, 1.001	∞, 1.001	∞, 1.001	∞, 1.001	∞, 1.001	∞, 1.001

Table 2.5: Preconditioner = CCMG - V(1,1)-cycle, prolongation = bi-linear, smoother = sGS

$h\backslash m$	10^0	10^1	10^2	10^3	10^4	10^5	10^6	10^7	10^8	10^9
1/8	**10**, 0.025	**29**, 0.472	**30**, 0.500	**35**, 0.528	**36**, 0.559	**40**, 0.593	**44**, 0.622	**52**, 0.669	**52**, 0.669	**58**, 0.697
1/16	**11**, 0.122	**13**, 0.194	**18**, 0.293	**24**, 0.414	**38**, 0.564	**58**, 0.692	$\mathbf{60}^+$, 0.827	$\mathbf{60}^+$, 0.931	∞, 0.995	∞, 1.094
1/32	**8**, 0.075	**11**, 0.121	**15**, 0.229	**22**, 0.362	**35**, 0.545	$\mathbf{60}^+$, 0.722	$\mathbf{60}^+$, 0.903	∞, 1.022	∞, 1.085	∞, 1.133
1/64	**8**, 0.068	**10**, 0.115	**14**, 0.216	**19**, 0.334	**27**, 0.449	**44**, 0.600	$\mathbf{60}^+$, 0.773	∞, 0.965	∞, 1.116	∞, 1.168

Table 2.6: Preconditioner = CCMG - W(1,1)-cycle, prolongation = Wesseling-Khalil, smoother = ILU

$h\backslash m$	10^0	10^1	10^2	10^3	10^4	10^5	10^6	10^7	10^8	10^9
1/8	**10**, 0.025	**29**, 0.472	**30**, 0.500	**35**, 0.528	**36**, 0.559	**40**, 0.593	**44**, 0.622	**52**, 0.669	**52**, 0.669	**58**, 0.697
1/16	**10**, 0.121	**12**, 0.166	**15**, 0.245	**21**, 0.315	**31**, 0.481	**38**, 0.541	**50**, 0.644	**60**$^+$, 0.786	**60**$^+$, 0.769	**60**$^+$, 922
1/32	**8**, 0.070	**12**, 0.165	**17**, 0.263	**19**, 0.328	∞, 0.968	∞, 1.110	∞, 1.127	∞, 1.164	∞, 1.169	∞, 1.184
1/64	**8**, 0.064	**12**, 0.137	**16**, 0.267	**18**, 0.305	**20**, 0.345	**32**, 0.520	∞, 1.115	∞, 1.137	∞, 1.190	∞, 1.199

Table 2.7: Preconditioner = AGKS - V(1,1)-cycle, prolongation = Wesseling-Khalil, smoother = ILU

$h\backslash m$	10^0	10^1	10^2	10^3	10^4	10^5	10^6	10^8	10^9	10^{11}	10^{13}
1/8	**22**, 0.371	**10**, 0.115	**10**, 0.116	**9**, 0.078	**9**, 0.056	**8**, 0.059	**8**, 0.045	**8**, 0.039	**8**, 0.039	**8**, 0.039	**8**, 0.039
1/16	**16**, 0.240	**13**, 0.199	**11**, 0.131	**9**, 0.098	**8**, 0.043	**7**, 0.043	**6**, 0.018	**6**, 0.007	**6**, 0.010	**5**, 0.010	**5**, 0.006
1/32	**20**, 0.329	**19**, 0.313	**14**, 0.192	**11**, 0.127	**9**, 0.093	**8**, 0.035	**7**, 0.041	**6**, 0.012	**6**, 0.008	**6**, 0.004	**5**, 0.008
1/64	**29**, 0.484	**26**, 0.435	**17**, 0.284	**12**, 0.161	**10**, 0.092	**8**, 0.061	**8**, 0.026	**6**, 0.016	**6**, 0.010	**6**, 0.006	**5**, 0.013

Table 2.8: Preconditioner = AGKS - V(1,1)-cycle, prolongation = Wesseling-Khalil, smoother = sGS

$h\backslash m$	10^0	10^1	10^2	10^3	10^4	10^5	10^6	10^8	10^9	10^{11}	10^{13}
1/8	**22**, 0.371	**10**, 0.115	**10**, 0.116	**9**, 0.078	**9**, 0.056	**8**, 0.059	**8**, 0.045	**8**, 0.039	**8**, 0.039	**8**, 0.039	**8**, 0.039
1/16	**16**, 0.268	**13**, 0.201	**11**, 0.131	**9**, 0.098	**8**, 0.043	**7**, 0.043	**6**, 0.017	**6**, 0.007	**6**, 0.004	**5**, 0.010	**5**, 0.005
1/32	**20**, 0.350	**19**, 0.317	**14**, 0.192	**11**, 0.127	**9**, 0.093	**8**, 0.035	**7**, 0.041	**6**, 0.010	**6**, 0.007	**6**, 0.008	**5**, 0.008
1/64	**29**, 0.483	**26**, 0.436	**17**, 0.283	**12**, 0.162	**10**, 0.092	**8**, 0.061	**8**, 0.030	**6**, 0.017	**6**, 0.011	**6**, 0.005	**5**, 0.013

Table 2.9: Preconditioner = AGKS - V(1,1)-cycle, prolongation = bi-linear, smoother = ILU

$h\backslash m$	10^0	10^1	10^2	10^3	10^4	10^5	10^6	10^8	10^9	10^{11}	10^{13}
1/8	**22**, 0.371	**10**, 0.115	**10**, 0.116	**9**, 0.078	**9**, 0.056	**8**, 0.059	**8**, 0.045	**8**, 0.039	**8**, 0.039	**8**, 0.039	**8**, 0.039
1/16	**16**, 0.237	**13**, 0.197	**11**, 0.131	**9**, 0.098	**8**, 0.043	**7**, 0.043	**6**, 0.018	**6**, 0.007	**6**, 0.011	**5**, 0.010	**5**, 0.006
1/32	**20**, 0.348	**19**, 0.312	**14**, 0.192	**11**, 0.126	**9**, 0.093	**8**, 0.035	**7**, 0.041	**6**, 0.010	**6**, 0.006	**6**, 0.021	**5**, 0.008
1/64	**29**, 0.483	**26**, 0.431	**17**, 0.283	**12**, 0.161	**10**, 0.092	**8**, 0.062	**8**, 0.026	**6**, 0.015	**6**, 0.010	**6**, 0.006	**5**, 0.013

Table 2.10: Preconditioner = AGKS - V(1,1)-cycle, prolongation = bi-linear, smoother = sGS

$h\backslash m$	10^0	10^1	10^2	10^3	10^4	10^5	10^6	10^8	10^9	10^{11}	10^{13}
1/8	**22**, 0.371	**10**, 0.115	**10**, 0.116	**9**, 0.078	**9**, 0.056	**8**, 0.059	**8**, 0.045	**8**, 0.039	**8**, 0.039	**8**, 0.039	**8**, 0.039
1/16	**16**, 0.256	**13**, 0.197	**11**, 0.131	**9**, 0.098	**8**, 0.043	**7**, 0.043	**6**, 0.017	**6**, 0.007	**6**, 0.004	**5**, 0.010	**5**, 0.004
1/32	**20**, 0.352	**19**, 0.317	**14**, 0.192	**11**, 0.127	**9**, 0.093	**8**, 0.035	**7**, 0.041	**6**, 0.010	**6**, 0.007	**6**, 0.020	**5**, 0.009
1/64	**29**, 0.481	**26**, 0.438	**17**, 0.281	**12**, 0.161	**10**, 0.092	**8**, 0.061	**8**, 0.026	**6**, 0.018	**6**, 0.012	**6**, 0.008	**5**, 0.014

$$P = \begin{bmatrix} P_{HH} & P_{HL} \\ P_{LH} & P_{LL} \end{bmatrix}. \tag{2.51}$$

The superior performance of AGKS preconditioner is partially due to employing these two distinct multilevel hierarchies, which is very much in spirit of the aforementioned decoupling in Section 2.6. In fact, due to decoupling, AGKS technology allows the usage of any ordinary prolongation operator. This operator does not have to be constructed in a sophisticated manner as in the case of Wesseling and Khalil [92] or Kwak [53].

As emphasized in [6], AGKS can be used purely as an algebraic preconditioner. Therefore, the standard multigrid preconditioner constraint that the coarsest level mesh resolves the boundary of the island is automatically eliminated. However, for a fair comparison, we enforce the coarsest level mesh to have that property.

When the discretization matrix is scaled by $1/m$, we observe a significant reduction in the iteration count for the AGKS preconditioner, while, CCMG suffers from inconsistent convergence behaviour. That is why, we only report the unscaled case for CCMG. Moreover, for the CCMG preconditioner, we use lexicographic ordering. On the other hand, for AGKS, we follow the standard way of ordering the highly-diffusive after the lowly-diffusive DOF as used in [6].

Note that as the diffusion coefficient m increases, the CCMG method becomes less effective. For sufficiently large m, it even diverges. CCMG shows this adverse behaviour for all types of transfer operators, and smoother types for almost all levels; see Tables 2.2–2.5. The CCMG preconditioner is more effective than the AGKS preconditioner for $m < 10^3$. However, for those m values, the AGKS preconditioner still manages to converge in less than 30 iterations.

The main issue addressed in our study is the robustness for large values of m. We observe that the CCMG preconditioner becomes ineffective, even diverges for $m \geq 10^6$ under both types of smoothers; see the corresponding columns in Tables 2.2–2.5. On the other hand,

the AGKS preconditioner becomes more effective with increasing m. Furthermore, as seen in Tables 2.7–2.10, AGKS preconditioner demonstrates consistently similar iteration counts and contraction numbers for all types of transfer operators and smoothers. Therefore, AGKS performance is independent of the utilized prolongation operators and smoothers.

We observe an interesting cut-off m value for performances of preconditioners. While in general, the CCMG performance starts to deteriorate at around $m > 10^5$, the AGKS preconditioner reaches its peak performance and maintains an optimal iteration count for $m \geq 10^5$. We reveal several observations. The CCMG preconditioner with sGS smoothing shows an adverse convergence behaviour for all prolongation types. On the other hand, the CCMG preconditioner with ILU smoothing shows a higher performance with Wesseling-Khalil prolongation type. The iteration counts for the CCMG method jumps to 60 at around $m = 10^5$ and $m = 10^6$ for sGS and ILU smoothing cases, respectively.

The CCMG preconditioner has been of type V-cycle so far. After observing convergence complications, we decided to try W(1,1)-cycle as an alternative; see the W(1,1)-cycle convergence history in Table 2.6. W(1,1)-cycle does not show a consistent convergence with respect to the contrast size. For instance, we observe a jump in the iteration count at around $m = 10^4$ and $m = 10^6$ for levels 3 and 4, respectively. Therefore, the performance of the CCMG preconditioners gets worse for $m > 10^5$ independently from the cycle type. Consequently, this observation indicates that CCMG fails to be robust with respect to the contrast size whereas AGKS maintains its robustness.

CCMG performance heavily depends on the smoother choice. It is well-known that pattern relaxations would not improve CCMG performance [55, p. 112]. In addition, since there is no anisotropy, the line smoothers also do not improve CCMG performance compared to sGS and ILU smoothers; see Llorente and Melson [55, p. 112] for other ordering related smoother complications. Hence, we used neither pattern relaxations nor line smoothers in our experiments. As pointed out by Mohr and Wienands [66], CCMG may need a sophisticated

smoother like ILU. The behaviour of ILU was extensively studied by Wittum [93, 94], also see [91, pp. 98 and 134]. In our experiments, the specific ILU choice is set to be no-fill-in.

We conclude the numerical experiments by reporting the cost of each preconditioner. For variational conditions, the decoupling of $K_{HH}(m)$ and S^{∞} in (2.47) causes the AGKS preconditioner to be cheaper than CCMG because it only employs P_{HH} and P_{LL} blocks in (2.51) whereas CCMG employs the whole P matrix; see the flop counts in Figure 2.4. When the size of the highly-diffusive island grows, the enforcement of the variational conditions of the AGKS preconditioner becomes even less costly than that of the CCMG preconditioner.

Finally, we report the cost per iteration for AGKS and CCMG V(1,1)-cycle preconditioners. AGKS preconditioner in (2.47) requires inversions of two blocks: $K_{HH}(m)$ and S^{∞} corresponding to highly- and lowly-diffusive regions, respectively. Therefore, for each iteration of $AGKS$ preconditioner, we utilize a full CCMG method for each block separately. This is exactly the setup that CCMG methods are known to be highly effective because each block corresponds to a discretization of the Laplace equation with homogeneous coefficients. Therefore, one iteration of the AGKS preconditioner is roughly 10 times more costly than that of the CCMG preconditioner; see the flop counts in Figure 2.4. This additional cost is worthy because AGKS preconditioner results in convergence in a few iterations for large values of m, whereas, the CCMG preconditioner results in a consistent failure.

2.8 Appendix

2.8.1 The technical part of the spectral analysis for the diagonally scaled matrix

Let $\{1, \ldots, s\}$ denote the index of islands in the domain. Let $N_k,\ k = 1, \ldots, s$ be the FV discretization matrix of $-\Delta$ on the k-th island Ω_k with respect to $\mathcal{T}_i$ with homogeneous pure Neumann boundary condition. Let $\mathcal{C}$ denote the set of all DOF in Ω.

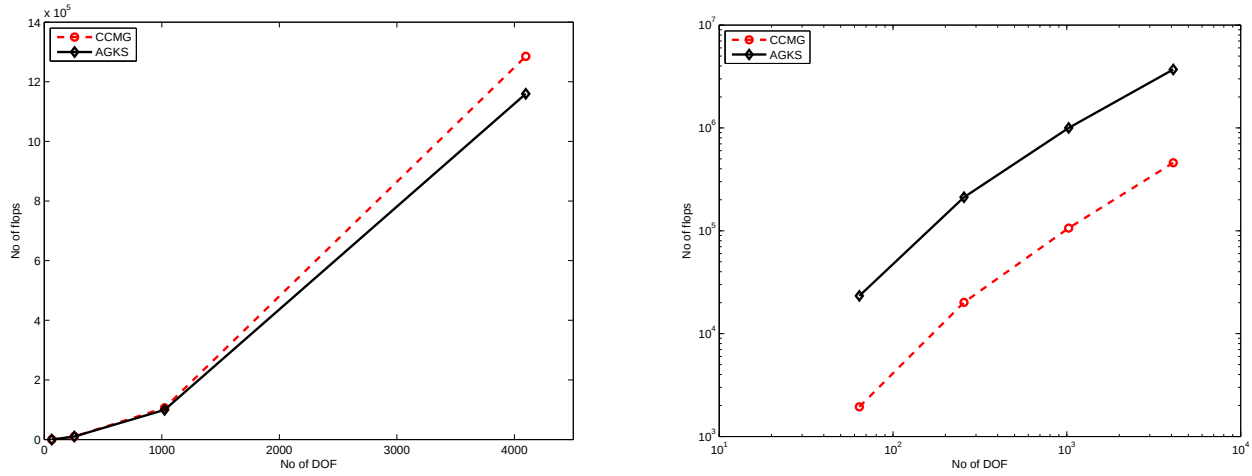

Figure 2.4: (Left) Flop counts for the enforcement of variational conditions. (Right) Flop counts for a single iteration of the preconditioners.

We start by examining the dependence of the (p, q)-th entry of $K(m)$ on m, for each $p \in \mathcal{C}$. Let Ω_{s+1} denote the outer region of islands, i.e.,

$$\Omega_{s+1} = \Omega \setminus \bigcup_{k=1,\ldots,s} \overline{\Omega}_k.$$

We denote the cell-centers that are adjacent to Ω_{s+1} and the ones that are interior to $\Omega_k,\ k = 1, \ldots, s$ by Γ_{Ω_k} and I_{Ω_k}, respectively. On the other hand, the cell-centers in the outer region Ω_{s+1} that are adjacent to the islands $\Omega_k, k = 1, \ldots, s$ are denoted by $\Gamma_{\Omega_{s+1}}$.

We define the following index set for $p, q \in \mathcal{C}$ with $p \neq q$:

$$\mathcal{I}(p \wedge q) := \begin{cases} k, & p \text{ and } q \in \Omega_k,\ k = 1, \ldots, s \\ s+1, & p \text{ or } q \in \Omega_{s+1}, \end{cases}$$

$$\mathcal{I}(p) := \begin{cases} k, & p \in I_{\Omega_k},\ k = 1, \ldots, s \\ s+1, k, & p \in \Gamma_{\Omega_k},\ k = 1, \ldots, s \\ s+1, & p \in \Omega_{s+1}. \end{cases}$$

Also, we define $\mathcal{I}(p \wedge p) = \mathcal{I}(p)$.

Note that the discretization matrix and its entries can be written as follows:

$$\begin{aligned} K(m) &= \sum_{k=1}^{s} mN_k(1) + N_{s+1}(m) \\ [K(m)]_{pq} &= \sum_{\ell \in \mathcal{I}(p \wedge q)} \alpha_\ell(m)[N_\ell]_{pq}, \end{aligned}$$

where

$$\alpha_\ell(m) = \begin{cases} m, & \ell = 1, \ldots, s \\ 1, & \ell = s+1, \end{cases} \tag{2.52}$$

and by abuse of notation, we have defined $N_\ell := N_\ell(1)$ for $\ell = 1, \ldots, s$ and $N_{s+1} := N_{s+1}(m)$. Then,

$$\begin{aligned} &[A(m)]_{pq} \\ &= [K(m)]_{pp}^{-1/2} \; [K(m)]_{pq} \; [K(m)]_{qq}^{-1/2}, \\ &= \left\{ \sum_{\ell \in \mathcal{I}(p)} \alpha_\ell(m)[N_\ell]_{pp} \right\}^{-1/2} \sum_{\ell \in \mathcal{I}(p \wedge q)} \alpha_\ell(m)[N_\ell]_{pq} \left\{ \sum_{\ell \in \mathcal{I}(q)} \alpha_\ell(m)[N_\ell]_{qq} \right\}^{-1/2}. \end{aligned}$$

For $p \in \mathcal{C}$, $[A(m)]_{pq} = 0$ if p, q are not adjacent cell-centers and $[A(m)]_{pp} = 1$. Furthermore note that, $[A(m)]_{pq}$ is m-dependent only if either p or $q \in \bigcup_{k=1,\ldots,s+1} \Gamma_{\Omega_k}$.

It is sufficient to study only the single island case because single island expression for

$$K(m) = mN_1 + N_2(m) \tag{2.53}$$

can be simply generalized to

$$K(m) = \sum_{k=1}^{s} mN_k + N_{s+1}(m).$$

2.8.1.1 Perturbation expansion analysis for the upper bound of the smallest eigenvalue

We devise a perturbation expansion analysis based on m, in order to study the m-dependent spectral behavior of $A(m)$. Hence, only the matrix entries $A(m)_{pq},\ p \neq q$, that have m-dependence are considered where cells p and q are adjacent. Combining (2.11) and (2.53), one can deduce that

$$N_2(m) = N_2^{\infty} + \mathcal{O}(m^{-1}). \tag{2.54}$$

We will use (2.54) in the below analysis. For clarity, we treat the perturbation expansion in full detail for the first case.

Case 1: $p \in \Gamma_{\Omega_1}$ and $q \in \Omega_2$,

$$\begin{aligned}
&[A(m)]_{pq} \\
&= \left\{m[N_1]_{pp} + [N_2(m)]_{pp}\right\}^{-1/2} [N_2(m)]_{pq} \left\{[N_2(m)]_{qq}\right\}^{-1/2} \\
&= m^{-1/2} \left\{[N_1]_{pp} + m^{-1}[N_2(m)]_{pp}\right\}^{-1/2} [N_2(m)]_{pq} \left\{[N_2(m)]_{qq}\right\}^{-1/2} \\
&= m^{-1/2} \left\{\ m^{-1}[N_1]_{pp}^{-1/2} - 1/2[N_1]_{pp}^{-3/2}\ [N_2(m)]_{pp} +\ \mathcal{O}(m^{-2})\right\}\ \ \{[N_2(m)]_{pq}\} \{[N_2(m)]_{qq}\}^{-1/2} \\
&= m^{-1} \left\{[N_1]_{pp}^{-1/2} + \mathcal{O}(m^{-1})\right\} \left\{[N_2^{\infty}]_{pq} + \mathcal{O}(m^{-1})\right\}\ \ \left\{m^{-1}[N_2^{\infty}]_{qq} + \mathcal{O}(m^{-2})\right\}^{-1/2} \\
&= \mathcal{O}(m^{-1/2})
\end{aligned}$$

Case 2: $p \in \Gamma_{\Omega_1}$ and $q \in \Gamma_{\Omega_1}$,

$$\begin{aligned}
&[A(m)]_{pq} \\
&= \left\{m[N_1]_{pp} + [N_2(m)]_{pp}\right\}^{-1/2} [mN_1]_{pq} \left\{m[N_1]_{qq} + [N_2(m)]_{qq}\right\}^{-1/2} \\
&= \left\{[N_1]_{pp} + m^{-1}[N_2(m)]_{pp}\right\}^{-1/2} [N_1]_{pq} \left\{[N_1]_{qq} + m^{-1}[N_2(m)]_{qq}\right\}^{-1/2} \\
&= [N_1]_{pp}^{-1/2}[N_1]_{pq}[N_1]_{qq}^{-1/2} + \mathcal{O}(m^{-1})
\end{aligned}$$

Case 3: $p \in \Gamma_{\Omega_1}$ and $q \in I_{\Omega_1}$,

$$\begin{aligned}
&[A(m)]_{pq} \\
&= \{m[N_1]_{pp} + [N_2(m)]_{pp}\}^{-1/2} [mN_1]_{pq} \{m[N_1]_{qq}\}^{-1/2} \\
&= \left\{[N_1]_{pp} + m^{-1}[N_2(m)]_{pp}\right\}^{-1/2} [N_1]_{pq} \{[N_1]_{qq}\}^{-1/2} \\
&= [N_1]_{pp}^{-1/2}[N_1]_{pq}[N_1]_{qq}^{-1/2} + \mathcal{O}(m^{-1})
\end{aligned}$$

Case 4: $p \in \Gamma_{\Omega_2}$ and $q \in \Omega_2$,

$$\begin{aligned}
&[A(m)]_{pq} \\
&= \{[N_2(m)]_{pp}\}^{-1/2} [N_2(m)]_{pq} \{[N_2(m)]_{qq}\}^{-1/2} \\
&= \left\{m^{-1}[N_2(m)]_{pp}\right\}^{-1/2} m^{-1}[N_2(m)]_{pq} \ \left\{m^{-1}[N_2(m)]_{qq}\right\}^{-1/2} \\
&= \left\{m^{-1}[N_2^{\infty}]_{pp} + \mathcal{O}(m^{-2})\right\}^{-1/2} \left\{m^{-1}[N_2^{\infty}]_{pq} + \mathcal{O}(m^{-2})\right\} \ \left\{m^{-1}[N_2^{\infty}]_{qq} + \mathcal{O}(m^{-2})\right\}^{-1/2} \\
&= [N_2^{\infty}]_{pp}^{-1/2}[N_2^{\infty}]_{pq}[N_2^{\infty}]_{qq}^{-1/2} + \mathcal{O}(m^{-1}).
\end{aligned}$$

We will use following modification of N_2 for our further analysis:

$$[\tilde{N_2}]_{pq} = \begin{cases} 0 & \text{if } p \in \Gamma_{\Omega_1} \\ [N_2^{\infty}]_{pq} & \text{otherwise.} \end{cases} \tag{2.55}$$

Consider the reduced version of (2.53)

$$\tilde{K}(m) = mN_1 + \tilde{N_2},$$

and let $\tilde{A}(m)$ denote the diagonally scaled version of $\tilde{K}(m)$. Then m-independent $\tilde{A}(m)$ has a single zero eigenvalue. Next, we proceed with the element-wise analysis of $A(m) - \tilde{A}(m)$.

Case 1: $p \in \Gamma_{\Omega_1}$ and $q \in \Omega_2$,

$$[A(m)]_{pq} = m^{-1/2}\ [N_1]_{pp}^{-1/2}\ [N_2^{\infty}]_{pq}\ [N_2^{\infty}]_{qq}^{-1/2} + \mathcal{O}(m^{-3/2})$$

and from (2.55) we get

$$[\tilde{A}(m)]_{pq} = 0.$$

Therefore,

$$[A(m)]_{pq} - [\tilde{A}(m)]_{pq} = \mathcal{O}(m^{-1/2}).$$

Case 2: $p \in \Gamma_{\Omega_1}$ and $q \in \Omega_1$,

$$[A(m)]_{pq} = [N_1]_{pp}^{-1/2}\ [N_1]_{pq}\ [N_1]_{qq}^{-1/2} + \mathcal{O}(m^{-1})$$

and from (2.55) we get

$$[\tilde{A}(m)]_{pq} = [N_1]_{pp}^{-1/2}\ [N_1]_{pq}[N_1]_{qq}^{-1/2}$$

Thus,

$$[A(m)]_{pq} - [\tilde{A}(m)]_{pq} = \mathcal{O}(m^{-1}).$$

Case 3: $p \in \Gamma_{\Omega_2}$(nodes of Ω_2),

$$[A(m)]_{pq} = [N_2^{\infty}]_{pp}^{-1/2}\ [N_2^{\infty}]_{pq}\ [N_2^{\infty}]_{qq}^{-1/2} + \mathcal{O}(m^{-1})$$

and from (2.55) we get

$$[\tilde{A}(m)]_{pq} = [N_2^{\infty}]_{pp}^{-1/2}\ [N_2^{\infty}]_{pq}\ [N_2^{\infty}]_{qq}^{-1/2}.$$

Thus,

$$[A(m)]_{pq} - [\tilde{A}(m)]_{pq} = \mathcal{O}(m^{-1}).$$

Case 4: Otherwise,

$$[A(m)]_{pq} - [\tilde{A}(m)]_{pq} = 0.$$

Therefore, $\lambda_{\max}(A(m) - \tilde{A}(m)) = \mathcal{O}(m^{-1/2})$.

LEMMA 3. *Let G and H be symmetric matrices of dimension $n \times n$. Then, for $k = 1, \ldots, n$, the following holds:*

$$\lambda_k(G) + \lambda_{\min}(H) \leq \lambda_k(G + H) \leq \lambda_k(G) + \lambda_{\max}(H).$$

Proof. The result follows from Courant-Fischer minimax Theorem; see [40, Corollary 8.1.3]. □

From Lemma 3, we have

$$\begin{aligned} \lambda_{\min}(A(m)) &\leq \lambda_{\min}(\tilde{A}(m)) + \lambda_{\max}(A(m) - \tilde{A}(m)) \\ &= \lambda_{\max}(A(m) - \tilde{A}(m)) \\ &= \mathcal{O}(m^{-1/2}) \end{aligned}$$

Moreover, we have for all $k \geq 1$,

$$\begin{aligned} \lambda_k(A(m)) &\geq \lambda_k(\tilde{A}(m)) + \lambda_{\min}(A(m) - \tilde{A}(m)) \\ &\geq \lambda_k(\tilde{A}(1)) - \mathcal{O}(m^{-1}) \geq C \end{aligned}$$

for some constant C independent of m, asymptotically. Thus, $A(m)$ has a single eigenvalue approaching to zero while the remaining eigenvalues are bounded away from 0.

2.8.1.2 Lower bound for the smallest eigenvalue

We aim to show the following lower bound for the smallest eigenvalue:

$$\lambda_{\min}(A(m)) \geq C\ m^{-1}. \tag{2.56}$$

For that, we will establish the below main estimates in the discussion to follow:

$$x^T K(m)x \geq x^T K(1)x \geq m^{-1} x^T K(m)x. \tag{2.57}$$

REMARK 3. *Establishing the estimate* (2.57) *is not as simple as in the FE discretization case due to m-dependence of* N_2 *in* (2.53)*. This requires further detailed matrix analysis.*

2.8.1.3 $x^T K(m)x \geq x^T K(1)x$ estimate

For the decomposition in (2.53), it is straightforward to see that $mN_1 \geq N_1$ for $m \geq 1$. Hence, in order to establish (2.57), we concentrate on the following auxiliary estimate:

$$x^T N_2(m)x \geq x^T N_2(1)x. \tag{2.58}$$

First, note that $N_2(m)$ has positive diagonal and negative off-diagonal entries. In addition, due to the discretization formula (2.9), it has a row sum equal to zero with the exception that the row sums corresponding to cell-centers that are adjacent to the boundary are positive. Hence, $N_2(m)$ is a diagonally dominant matrix. We further decompose $N_2(m)$ as follows:

$$N_2(m) = \bar{N}_2(m) + R_2, \tag{2.59}$$

where $\bar{N}_2(m)$ is a symmetric matrix with positive diagonal entries and a row sum equal to zero, and $R_2 := N_2(m) - \bar{N}_2(m)$ is the remainder matrix.

LEMMA 4. *Let* G *be a symmetric matrix and have a row sum equal to zero. In addition, let* $[G]_{pp} \geq 0$*, then* G *is symmetric positive semi-definite (SPSD).*

Proof. Let λ_p be the p-th eigenvalue of G. Using Gerschgorin's Theorem with the fact that G has a row sum equal to zero yields:

$$|\lambda_p - [G]_{pp}| \leq \sum_{q \neq p} |[G]_{pq}| = [G]_{pp}.$$

Then the result follows from

$$0 \leq \lambda_p \leq 2[G]_{pp}.$$

□

By Lemma 4, $\bar{N}_2(m)$ is immediately SPSD. In addition, R_2 is a diagonally dominant matrix with non-negative diagonal entries, again by Lemma 4, R_2 is SPSD. Now, we can conclude that $N_2(m)$ is SPSD.

From (2.11), one observes that $[K(m)]_{pp}$ is monotonically increasing in m. This important property implies that

$$[\bar{N}_2(m)]_{pp} \geq [\bar{N}_2(1)]_{pp}, \quad m \geq 1. \tag{2.60}$$

We need the following additional decomposition:

$$\bar{N}_2(m) = \bar{N}_2(1) + \bar{R}_2(m). \tag{2.61}$$

Combining (2.60) and (2.61), we obtain $[\bar{R}_2(m)]_{pp} \geq 0$. Hence, Lemma 4 implies that $\bar{R}_2(m)$ is SPSD. Using this, we now arrive at the auxiliary estimate (2.58) in the following:

$$\begin{aligned} x^T N_2(m) x &= x^T \bar{N}_2(1) x + x^T \bar{R}_2(m) x + x^T R_2 x \\ &\geq x^T \bar{N}_2(1) x + x^T R_2 x \\ &= x^T N_2(1) x. \end{aligned}$$

Consequently,

$$\begin{aligned} m x^T K(m) x &= m x^T N_1 x + x^T N_2(m) x \\ &\geq x^T N_1 x + x^T N_2(m) x \\ &\geq x^T N_1 x + x^T N_2(1) x \\ &= x^T K(1) x. \end{aligned}$$

2.8.1.4 $mx^T K(1)x \geq x^T K(m)x$ estimate

Combining (2.53) and (2.59), we obtain

$$K(m) = mN_1 + \bar{N}_2(m) + R_2,$$

where N_1 and R_2 are SPSD and independent of m, which yields the following for $m \geq 1$:

$$\begin{aligned} mx^T N_1 x &\geq x^T N_1 x, \\ mx^T R_2 x &\geq x^T R_2 x, \end{aligned}$$

Thus, in order to establish (2.57), it is sufficient to establish the auxiliary estimate

$$mx^T \bar{N}_2(1)x \geq x^T \bar{N}_2(m)x. \tag{2.62}$$

By using 2.11, one can also show that

$$m[\bar{N}_2(1)]_{pp} \geq [\bar{N}_2(m)]_{pp}. \tag{2.63}$$

We will use the following decomposition:

$$m\bar{N}_2(1) = \bar{N}_2(m) + \widehat{R}_2(m), \tag{2.64}$$

where $\widehat{R}_2(m)$ is the SPSD remainder matrix. Combining (2.63) and (2.64), we obtain $[\widehat{R}_2(m)]_{pp} \geq 0$, which leads us to the auxiliary estimate (2.62). Hence,

$$\begin{aligned} mx^T K(1)x &= mx^T N_1 x + mx^T N_2(1)x \\ &\geq mx^T N_1 x + x^T N_2(m)x \\ &= x^T K(m)x. \end{aligned}$$

In conclusion, we have obtained the two main estimates in (2.57). These yield similar estimates for diag $K(m)$.

$$\begin{aligned} x^T \text{diag } K(m)x &\geq x^T \text{diag } K(1)x \\ &\geq m^{-1} x^T \text{diag } K(m)x \end{aligned} \tag{2.65}$$

From (2.57) and (2.65), and letting $C_1 := \lambda_{\min}(A(1))$, we get:

$$\begin{aligned} x^T K(m)x &\geq x^T K(1)x \geq C_1 x^T \text{diag } K(1)x \\ &\geq C_1\ m^{-1} x^T \text{diag } K(m)x, \end{aligned}$$

yielding

$$C_1\ m^{-1} \leq \lambda_{\min}(A(m)) \leq C_2\ m^{-1/2}.$$

Chapter 3

The AGKS Preconditioner for High-contrast Stokes Problem

In this Chapter, we aim to bring the same rigorous preconditioning technology to *vector valued* problems such as the Stokes equation. The Stokes equation plays a fundamental role in the modeling of several problems in emerging geodynamics applications. Numerical solutions to the Stokes flow problems especially with high-contrast variations in viscosity is critically needed in the computational geodynamics community; see recent studies [37, 36, 59, 77]. The high-contrast viscosity corresponds to a small Reynolds number regime because the Reynolds number is inversely proportional to the viscosity value. One of the main applications of the high-contrast Stokes equation is the study of earth's mantle dynamics. The processes such as the long time scale dynamics of the earth's convecting mantle, the formation and subsequent evolution of plate tectonics can be satisfactorily modeled by the Stokes equation; see [37, 59, 67] for further details. Realistic simulation of mantle convection critically relies on the treatment of the two essential components of simulation: *the contrast size in viscosity* and *the mesh resolution*. Hence, our aim is to achieve robustness of the underlying preconditioner with respect to the contrast size and the mesh size simultaneously, which we call as m- and h-robustness, respectively.

We extend the usage of AGKS preconditioner to the solution of the stationary Stokes equation in a domain as in Figure 2.1.

$$\begin{aligned} -\nabla \cdot (\nu \nabla u) + \nabla p &= f \quad \text{in} \quad \Omega, \\ \nabla \cdot u &= 0 \quad \text{in} \quad \Omega, \end{aligned} \tag{3.1}$$

with piecewise constant high-contrast viscosity used in the slab subduction referred as the *Sinker* model by [59]:

$$\nu(x) = \begin{cases} m \gg 1, & x \in \Omega_H, \\ 1, & x \in \Omega_L. \end{cases} \tag{3.2}$$

Here, u, p, and f stand for the velocity, pressure, and body force, respectively.

The discretization of (3.1) gives rise to the following saddle point matrix:

$$\mathcal{A} \begin{bmatrix} u \\ p \end{bmatrix} = \begin{bmatrix} K(m) & B^t \\ B & 0 \end{bmatrix} \begin{bmatrix} u \\ p \end{bmatrix} = \begin{bmatrix} f \\ 0 \end{bmatrix}. \tag{3.3}$$

The velocity vector can be treated component-wise which allows the usage of a single finite element space for each component. The extension of AGKS preconditioner from diffusion to Stokes equation is accomplished by the following crucial block partitioning of (3.3); see [32, p. 226]:

$$\begin{bmatrix} K^x(m) & 0 & (B^x)^t \\ 0 & K^y(m) & (B^y)^t \\ B^x & B^y & 0 \end{bmatrix} \begin{bmatrix} u^x \\ u^y \\ p \end{bmatrix} = \begin{bmatrix} f^x \\ f^y \\ 0 \end{bmatrix}, \tag{3.4}$$

where $K^* = K^x = K^y$ are the scalar diffusion matrices, and B^x and B^y represent the weak derivatives in x and y directions, respectively. We apply the AGKS preconditioning idea to the K^x and K^y blocks by further decomposing each of them as the following 2×2 block system; see [11, Eqn. 11], [10, Eqn. 4], [6, Eqn. 3]:

$$K^*(m) = \begin{bmatrix} K^*_{HH}(m) & K^*_{HL} \\ K^*_{LH} & K^*_{LL} \end{bmatrix}, \tag{3.5}$$

where the DOF are identified as *high* and *low* based on the viscosity value in (3.2) and $K^*_{HH}, K^*_{HL}, K^*_{LH}$, and K^*_{LL} denote couplings between the high-high, high-low, low-high, and

low-low DOF, respectively. The exact inverse of K^* can be written as:

$$K^{*^{-1}} = \begin{bmatrix} I_{HH} & -K_{HH}^{*^{-1}}K_{HL}^* \\ 0 & I_{LL} \end{bmatrix} \begin{bmatrix} K_{HH}^{*^{-1}} & 0 \\ 0 & S^{*^{-1}} \end{bmatrix} \begin{bmatrix} I_{HH} & 0 \\ -K_{LH}^*K_{HH}^{*^{-1}} & I_{LL} \end{bmatrix}, \quad (3.6)$$

where I_{HH} and I_{LL} denote the identity matrices of the appropriate dimension and the Schur complement S^* is explicitly given by:

$$S^*(m) = K_{LL}^* - K_{LH}^*K_{HH}^{*^{-1}}(m)K_{HL}^*. \quad (3.7)$$

The AGKS preconditioner is defined as follows:

$$\hat{K}^{*^{-1}}(m) := \begin{bmatrix} I_{HH} & -K_{HH}^{\infty^\dagger}K_{HL}^* \\ 0 & I_{LL} \end{bmatrix} \begin{bmatrix} K_{HH}(m)^{*^{-1}} & 0 \\ 0 & S^{\infty^{-1}} \end{bmatrix} \begin{bmatrix} I_{HH} & 0 \\ -K_{LH}^*K_{HH}^{\infty^\dagger} & I_{LL} \end{bmatrix}, \quad (3.8)$$

where $K_{HH}^{\infty^\dagger}$ and S^∞ are the asymptotic values of $K_{HH}^{*^{-1}}$ and S^*, respectively; see [6, Lemma 1].

3.1 Literature review

There are many solution methods proposed for the system of equations in (3.3); see the excellent survey article by [18]. Based on where the emphasis is put in the design of a solution method, solving a saddle-point matrix system can be classified into two approaches: *preconditioning and solver*. The *preconditioning approach* aims to construct novel preconditioners for standard solver methods such as Uzawa, Minres, and the Schur complement reduction (SCR). A vast majority of the articles on the *preconditioning* approach focuses on the preconditioning of Schur complement matrix; see [50, 27, 52, 75, 71, 59, 77]. It is well known that the Schur complement matrix S is spectrally equivalent to the pressure mass matrix (PMM) for the steady Stokes equation; see [22]. For rigorous convergence analysis of Krylov solvers with PMM preconditioner, see [83, 89]. [28] established that scaled PMM lead to h-robustness for

the Stokes equation with large constant viscosity. Using a new inner product, [71] introduced a robust preconditioner for the Schur complement matrix $S = BK^{-1}B^t$ for discontinuous viscosity $0 < \nu \leq 1$ and showed that the preconditioned Uzawa (p-Uzawa) and Minres (p-Minres) became h-robust with this new PMM preconditioner. Further properties of this preconditioner such as clustering in the spectrum of preconditioned S system was shown by [45]. It was pointed out by [50] that [29] designed LSQR commutator (BFBt) preconditioner in order to overcome the m-robustness issues by using $\hat{S} = (BB^t)^{-1}BKB^t(BB^t)^{-1}$ preconditioner for S. [30, 27] further studied this preconditioner. Additionally, [59, 77, 36, 37] popularized the usage of variants of the BFBt preconditioner for the high-contrast Stokes equation with $\nu|_{\Omega_H} = m \gg 1$ in geodynamics applications. [59] established that this preconditioner was m-robust when used along with a p-SCR solver. [77] obtained h-robustness for this preconditioner when used with the Schur method and generalized conjugate residual method with block triangular preconditioners.

There have been studies focusing on different ways of preconditioning K for the Stokes equation restricted to constant viscosity case; see [26, 21, 84]. [32] observed that a single multigrid (MG) cycle with an appropriate smoother was usually a good preconditioner for K because MG is sufficiently effective as a preconditioner for the constant viscosity case. For discontinuous coefficient case, however, there has not been much study to analyze the performance of preconditioners for K in a Stokes solver framework. Since MG loses h-robustness, there is an imminent need for the robustness study of preconditioners for the case of discontinuous coefficients and we present the AGKS preconditioner to address this need.

The *solver method approach* aims to construct a solver by sticking with standard preconditioners such as MG for the K matrix and PMM or BFBt for the S matrix. The performance of the solver depends heavily on the choice of the inner preconditioner; see [26, 35, 14, 15]. The Uzawa solver is one of the most popular iterative methods for the saddle point problems in fluid dynamics; see [48, 35, 39]. Since this method requires the solution of K system in

each step, this leads to the utilization of an inexact Uzawa method involving an approximate evaluation of K^{-1}; see [17, 96]. This method involves an inner and outer iteration (in our context, S- and outer-solve, respectively), and the convergence of this method is studied extensively; see [17, 21, 26, 75].

[59] utilized p-SCR for the high-contrast viscosity Stokes equation and found that its performance highly depended on the underlying model and the discretization. They were able to obtain m-robustness of scaled BFBt preconditioner whereas they observed a poor performance for the scaled PMM preconditioner under p-SCR. The p-SCR is further studied by [36, 37] for three dimensional problems.

Another commonly used iterative method is Minres; see [74]. [34] suggested the block diagonal preconditioner for the p-Minres solver and [79] presented further results for this type of preconditioning. For constant viscosity case, there have been many studies for different choices of the preconditioners for K and S blocks; see [83, 18, 75, 89, 19]. For the discontinuous viscosity case, on the other hand, [70, 71] studied the performance of p-Minres with a new PMM preconditioner.

3.2 Solver methods

The LBB stability of Stokes discretizations has been extensively studied due to utilization of weak formulations to solve (2.1). We are interested in the LBB stability in the case of high-contrast coefficients. [70] proved the LBB stability restricted to $0 < \nu \leq 1$. Later, [71] eliminated this restriction and extended their results to cover general viscosity:

$$\sup_{u_h \in V_h} \frac{(\text{div } u_h, p_h)}{\|u_h\|_V} \geq c_{LBB} \|p_h\|_Q, \quad p_h \in Q_h. \tag{3.9}$$

The associated spaces and weighted norms are defined as follows:

$$
\begin{aligned}
V &:= [H_0^1(\Omega)]^d, \\
Q &:= \{p \in L^2(\Omega) : (\nu^{-1}p, 1) = 0\}, \\
\|u\|_V &:= (\nu\nabla u, \nabla v)^{\frac{1}{2}}, \quad u \in V, \\
\|p\|_Q &:= (\nu^{-1}p, p)^{\frac{1}{2}}, \quad p \in Q.
\end{aligned}
$$

The inequality in (3.9) immediately establishes the LBB stability of our discretization.

There are many solution methods for the indefinite saddle point problem (3.3). We concentrate on three different solver methods: the p-Uzawa, p-SCR, and p-Minres. We test the performance the AGKS preconditioner with these solver methods. First, we establish two spectral equivalences: between the velocity stiffness matrix K and the AGKS preconditioner and between the Schur complement matrix S and the scaled PMM. Note that the constant c_{LBB} in (3.9) is directly used for the spectral equivalence of S in the following.

LEMMA 5. *Let $\hat{K}$ and $\hat{S}$ denote the AGKS preconditioner and the scaled PMM. Then, for sufficiently large m, the following spectral equivalences hold:*

(a)

$$
(1 - cm^{-1/2})(\hat{K}u, u) \leq (Ku, u) \leq (1 + cm^{-1/2})(\hat{K}u, u), \tag{3.10}
$$

for some constant c independent of m.

(b)

$$
c_{LBB}^2(\hat{S}p, p)_Q \leq (Sp, p) \leq d(\hat{S}p, p)_Q, \tag{3.11}
$$

where c_{LBB} is the constant in (3.9) *which is independent of m and h.*

Proof. One can extract a symmetric positive semi-definite matrix $\mathcal{N}_{HH}^*$ with a rank one kernel from K_{HH}^* in (2.4). $\mathcal{N}_{HH}^*$ is the so-called Neumann matrix and the extraction leads to the following decomposition:

$$
K_{HH}^*(m) = m\mathcal{N}_{HH}^* + \Delta.
$$

Δ corresponds to the coupling between the DOF in Ω_L and on the boundary of Ω_H. Since $\ker(\mathcal{N}^*_{HH})$ has rank one, $\mathcal{N}^*_{HH}$ has a simple zero eigenvalue and the below spectral decomposition holds with $\lambda_i > 0, \quad i = 1, \ldots, n_H - 1$ where n_H denotes the order of $\mathcal{N}^*_{HH}$:

$$Z^t \mathcal{N}^*_{HH} Z = \mathrm{diag}(\lambda_1, \ldots, \lambda_{n_H - 1}, 0).$$

Although the eigenvectors in the columns of Z and the eigenvalues λ_i can change according to the underlying discretization, there is always one simple zero eigenvalue and its corresponding constant eigenvector independent of the discretization. This is a direct consequence of the diffusion operator corresponding to a Neumann problem. Therefore, the spectral equivalence established for the $P1$ finite element in [6, Thm. 1] extends to $Q2$ and $Q1$ discretizations, thereby, completing the proof of part (a) for K^*. The spectral equivalence of K easily follows from that of K^* because of the decomposition in (3.4).

The proof of (b) follows from [71, Thm. 6]. □

For the p-Uzawa and p-Minres solvers, we present convergence and conditioning results based on the above spectral equivalences.

3.2.1 The preconditioned Uzawa solver

The Uzawa algorithm is a classical solution method which involves block factorization with forward and backward substitution. Here, we use the preconditioned inexact Uzawa method described by [75] and [16]. The system (3.3) can be block factorized as follows:

$$\begin{bmatrix} K(m) & 0 \\ B & -I \end{bmatrix} \begin{bmatrix} I & K(m)^{-1} B^t \\ 0 & S(m) \end{bmatrix} \begin{bmatrix} u \\ p \end{bmatrix} = \begin{bmatrix} f \\ 0 \end{bmatrix}. \tag{3.12}$$

Let (u^k, p^k) be a given approximation of the solution (u, p). Using the block factorization (3.12) combined with a preconditioned Richardson iteration, one obtains:

$$\begin{bmatrix} u^{k+1} \\ p^{k+1} \end{bmatrix} = \begin{bmatrix} u^k \\ p^k \end{bmatrix} + \begin{bmatrix} I & -K^{-1}B^tS^{-1} \\ 0 & S^{-1} \end{bmatrix} \begin{bmatrix} K^{-1} & 0 \\ BK^{-1} & -I \end{bmatrix} \left(\begin{bmatrix} f \\ 0 \end{bmatrix} - \mathcal{A} \begin{bmatrix} u^k \\ p^k \end{bmatrix} \right). \tag{3.13}$$

This leads to the following iterative method:

$$u^{k+1} = u^k + w^k - \hat{K}^{-1}B^t z^k, \tag{3.14a}$$

$$p^{k+1} = p^k + z^k, \tag{3.14b}$$

where $w^k := \hat{K}^{-1} r_1^k$, $r_1^k := f - Ku^k - B^t p^k$, and $z^k := \hat{S}B(w^k + u^k)$. Computing z^k involves ℓ iterations of pCG. In this computation, since the assembly of S is prohibitively expensive, first we replace it by $\tilde{S}$. Then, we utilize the preconditioner $\hat{K}$ for K and $\hat{S}$ for $\tilde{S}$ where the explicit formula is given by:

$$\tilde{S} := B\hat{K}^{-1}B^t. \tag{3.15}$$

Thus, the total number of applications of $\hat{K}^{-1}$ in (3.14a) and (3.14b) becomes $\ell+2$. We refer the outer-solve (one Uzawa iteration) as steps (3.14a) and (3.14b) combined. In particular, we call the the computation of z^k as an S-solve. The stopping criterion of the S-solve plays an important for the efficiency of the Uzawa method and it is affected by the accuracy of $\hat{K}$; see the analysis in [75, Sec. 4]. In Section 3.2.2, we present the convergence analysis of p-Uzawa method when we use the AGKS preconditioner for velocity stiffness matrix. Following the results obtained from this analysis, we determine the stopping criterion of the S-solve as follows:

Let r_p^i be the residual of the S-solve at iteration i. Then, we abort the iteration when $\frac{\|r_p^i\|}{\|r_p^0\|} \leq \delta_{tol}$ where

- $\delta_{tol} = 0.5$ or

- maximum iteration reaches 4.

For the details about the choice of δ_{tol}, see Section 3.2.2.1.

3.2.2 Analysis of the preconditioned Uzawa solver

There have been many convergence analyses of the Uzawa solver in the literature. These studies mostly covered the continuous viscosity case, including the ones by [17] and [75]. To our knowledge, the convergence analysis for the discontinuous viscosity case has never been addressed before. The extension of the convergence analysis to the high-contrast viscosity is our novel contribution. The analysis by [75] lays the foundation of our convergence results. Unlike their case of interest, *i.e.*, a continuous (constant) viscosity $\nu \to 0$, we treat discontinuous (piecewise constant) $\nu|_{\Omega_H} \to \infty$. [75, 54] showed that the convergence of the p-Uzawa solver with MG preconditioner was independent of ν. This favorable property is due to the ν independent spectral equivalence between the velocity stiffness matrix and the MG preconditioner. For the case of discontinuous ν, we prove that the p-Uzawa solver with AGKS preconditioner depends on ν; see (3.10). Interestingly this dependence turns out to be an advantage for the high-contrast case [1] because it lays the foundation of the results in (a) and (b) below. By using (3.10), we establish three important results:

(a) We prove the convergence of the inexact p-Uzawa solver for large viscosity values $\nu|_{\Omega_H} = m$.

(b) We prove that the inexact p-Uzawa method converges to the exact one as $m \to \infty$.

(c) We quantify the convergence rate of the inexact p-Uzawa solver by the viscosity contrast m in (3.27) and (3.28) when the AGKS preconditioner is used for the approximation of velocity stiffness matrix.

We find that the p-Uzawa method is the most suitable solver for reflecting the effectiveness of a preconditioner designed for high-contrast problems. Since viscosity contrast m can be

[1] The design of the AGKS preconditioner is centered on asymptotically large values of $\nu|_{\Omega_H} = m$. When m is sufficiently large, the AGKS preconditioner becomes m-robust due to the spectral equivalence in (3.10).

directly incorporated to the convergence rate, a preconditioner that can use large m values to its advantage will be discerned most obviously under the p-Uzawa solver. In fact, we observe the superior performance of the AGKS preconditioner when it is used under the p-Uzawa method.

Our convergence analysis is based on the one given by [75]. We start by defining the following norms:

$$\begin{aligned} \|u\|_{\hat{K}} &:= (\hat{K}u, u)^{\frac{1}{2}} \qquad \text{for } \; u \in \mathbb{R}^d \\ \|p\|_{\tilde{S}} &:= (\tilde{S}p, p)^{\frac{1}{2}} \qquad \text{for } \; p \in e^{\perp_Q} \end{aligned}$$

Let $\begin{bmatrix} u \\ p \end{bmatrix}$ be the exact solution of (2.1) and e^k be the error in the k-th step of the p-Uzawa method:

$$e^k = \begin{bmatrix} e_u^k \\ e_p^k \end{bmatrix} := \begin{bmatrix} u \\ p \end{bmatrix} - \begin{bmatrix} u^k \\ p^k \end{bmatrix}.$$

Define $\delta_{tol} < 1$ to be the prescribed tolerance of the S-solve enforcing:

$$\frac{\|p - p^k\|_{\tilde{s}}}{\|p\|_{\tilde{s}}} \leq \delta_{tol}. \tag{3.16}$$

Utilizing the spectral equivalence (3.10), we have the following error estimates for sufficiently large m.

Lemma 6.

$$\|e_u^{k+1}\|_{\hat{K}} \leq c\, m^{-1/2}(2 + \delta_{tol})\|e_u^k\|_{\hat{K}} + \delta_{tol}\|e_p^k\|_{\tilde{S}} \tag{3.17}$$

$$\|e_p^{k+1}\|_{\tilde{S}} \leq c\, m^{-1/2}(1 + \delta_{tol})\|e_u^k\|_{\hat{K}} + \delta_{tol}\|e_p^k\|_{\tilde{S}}. \tag{3.18}$$

Proof. The error can be written component-wise as follows:

$$\begin{aligned} e_u^{k+1} &= u - u^{k+1} = u - u^k - \hat{K}^{-1}(Ke_u^k + B^t e_p^k - B^t z) = (I - \hat{K}^{-1}K)e_u^k - (\hat{K}^{-1}B^t)e_p^{k+1}, \\ e_p^{k+1} &= p - p^{k+1} = e_p^k + z = (e_p^k - \tilde{S}^{-1}Bw) + (\tilde{S}^{-1}Bw - z). \end{aligned}$$

Then it can be bounded as follows:

$$\|e_u^{k+1}\|_{\hat{K}}| \leq \|I - \hat{K}^{-1/2}K\hat{K}^{-1/2}\| \, \|e_u^k\|_{\hat{K}} - \|\hat{K}^{-1/2}B^t\tilde{S}^{-1/2}\| \, \|e_p^{k+1}\|_{\tilde{S}}, \tag{3.19}$$

$$\|e_p^{k+1}\|_{\tilde{S}} \leq \|e_p^k - \tilde{S}^{-1}Bw\| + \|\tilde{S}^{-1}Bw - z\|. \tag{3.20}$$

Note that the spectral equivalence in (3.10) leads to:

$$\|I - \hat{K}^{-1/2}K\hat{K}^{-1/2}\| \leq cm^{-1/2}. \tag{3.21}$$

By using the definition of $\tilde{S}$, we obtain the following:

$$\|\hat{K}^{-1/2}B^t\tilde{S}^{-1/2}\| = 1. \tag{3.22}$$

Using (3.19), (3.21), and (3.22), we arrive at:

$$\|e_u^{k+1}\|_{\hat{K}} \leq c\, m^{-1/2}\|e_u^k\|_{\hat{K}} + \|e_p^{k+1}\|_{\tilde{S}}. \tag{3.23}$$

We proceed with the e_p^{k+1} bound. First, note that one can prove:

$$(\tilde{S}^{-1}Bw, Bw)^{1/2} \leq c\, m^{-1/2}\|e_u^k\|_{\hat{K}} + \|e_p^k\|_{\tilde{S}}. \tag{3.24}$$

Then, using (3.16) and (3.24), respectively, we arrive at:

$$\|e_p^k - \tilde{S}^{-1}Bw\| \leq cm^{-1/2}\|e_u^k\|_{\hat{K}}, \tag{3.25}$$

$$\|\tilde{S}^{-1}Bw - z\| \leq \delta_{tol}(cm^{-1/2}\|e_u^k\|_{\hat{K}} + \|e_p^k\|_{\tilde{S}}). \tag{3.26}$$

Finally, (3.18) follows from (3.20), (3.25), and (3.26). (3.17) follows from (3.23) and (3.18).

□

THEOREM 2. *Let the spectral equivalences in* (3.10) *and* (3.11) *hold. Then, the error bound for the p-Uzawa solver is given by the following:*

$$\frac{\max\{\|e_u^{k+1}\|_{\hat{K}}, \|e_p^{k+1}\|_{\tilde{S}}\}}{\max\{\|e_u^k\|_{\hat{K}}, \|e_p^k\|_{\tilde{S}}\}} = \delta_{tol} + \mathcal{O}(m^{-1/2}) \tag{3.27}$$

$$\frac{\|e_u^k\|_{\hat{K}} + \|e_p^k\|_{\tilde{S}}}{\|e_u^0\|_{\hat{K}} + \|e_p^0\|_{\tilde{S}}} = \frac{5}{2}\delta_{tol}^k + \mathcal{O}(m^{-1/2}) \tag{3.28}$$

Proof. One can write (3.17) and (3.18) as follows:

$$\begin{bmatrix} \|e_u^{k+1}\|_{\hat{K}} \\ \|e_p^{k+1}\|_{\tilde{S}} \end{bmatrix} \leq C \begin{bmatrix} \|e_u^k\|_{\hat{K}} \\ \|e_p^k\|_{\tilde{S}} \end{bmatrix}$$

where the error iteration matrix C is given by:

$$C = \begin{bmatrix} cm^{-1/2}(2 + \delta_{tol}) & \delta_{tol} \\ cm^{-1/2}(1 + \delta_{tol}) & \delta_{tol} \end{bmatrix}. \tag{3.29}$$

The result in (3.27) follows from

$$\|C\|_\infty = cm^{-1/2}(2 + \delta_{tol}) + \delta_{tol} = \delta_{tol} + \mathcal{O}(m^{-1/2}).$$

(3.28) requires an upper bound for $\|C^k\|_1$. For that, we use the following spectral decompo-

sition of C:

$$C = VDV^{-1}.$$

The proof is completed by using $\|C^k\|_1 \leq \rho(C)^k \|V\|_1 \|V^{-1}\|_1$ and the following estimates:

$$\begin{aligned} \rho(C) &= \delta_{tol} + \mathcal{O}(m^{-1/2}) \\ \|V\|_1 &\leq \frac{5}{2} + \mathcal{O}(m^{-1/2}) \\ \|V^{-1}\|_1 &= 1. \end{aligned}$$

The details of the above spectral bounds are given in Section 3.4.1. □

REMARK 4. *For m sufficiently large, it follows from Theorem 2 that the p-Uzawa solver always converges when the preconditioner of choice is AGKS. In addition, the contraction factor for the inexact Uzawa method converges to that of the exact one; $\delta_{tol} + \mathcal{O}(m^{-1/2})$ and δ_{tol}, respectively. We can deduce that only one iteration of pCG with the AGKS preconditioner is enough for the accuracy of S-solve in the asymptotic regime* [2]*. We give the justification of this deduction in Section 3.2.2.1.*

3.2.2.1 The choice of optimal δ_{tol}

Let k and ℓ be the number of outer- and S-solve iterations of the p-Uzawa solver. Here we comment on the effect of the choice of δ_{tol} on the total number of iterations for varying m values. An optimal δ_{tol} is chosen so that the total number of p-Uzawa iterations is minimized. In other words, δ_{tol} guarantees not only the convergence, but also the efficiency of the p-Uzawa solver. Let $\epsilon < 1$ be the tolerance of the p-Uzawa solver and $\beta < 1$ be contraction factor of the S-solve. Using (3.28) and (3.16), we have:

$$\rho(C)^k \leq \epsilon, \quad \beta^\ell \leq \delta_{tol}.$$

[2] For the definition of asymptotic regime, see Section 3.3. Note that the asymptotic regime of the p-Uzawa solver is observed to be $m \geq 10^3$

In order to find the optimal δ_{tol}, we minimize the total number of p-Uzawa iterations given by $k\ell$:

$$\begin{aligned} k\ell &\leq \frac{\ln(\epsilon)}{\ln(\rho(C))}\frac{\ln(\delta_{tol})}{\ln(\beta)} \\ &= \frac{\ln(\epsilon)}{\ln(\beta)}\frac{\ln(\delta_{tol})}{\ln(\rho(C))} \\ &=: iter_{exact}\, R_{inexact/exact}. \end{aligned}$$

Here $R_{inexact/exact}$ represents the ratio of the number of iterations of the p-Uzawa and exact Uzawa solvers. It suffices to minimize $R_{inexact/exact}$ to figure out the range for optimal δ_{tol}. We present the plot of $R_{inexact/exact}$ for a generic constant $c = 1$ [3] in Figure 3.1. As m value gets larger, specifically for $m \geq 10^3$, we observe that $R_{inexact/exact}$ reaches its minimum value for almost all δ_{tol}. As m gets larger, the fact that the smallest value of $R_{inexact/exact} \to 1$ indicates that the total number of p-Uzawa iterations goes to that of the exact one. Since it was pointed out by [75] that $\delta_{tol} = 0.5$ is an optimal value for the MG preconditioner, we choose the same δ_{tol} in p-Uzawa in order to make a fair comparison between AGKS and MG.

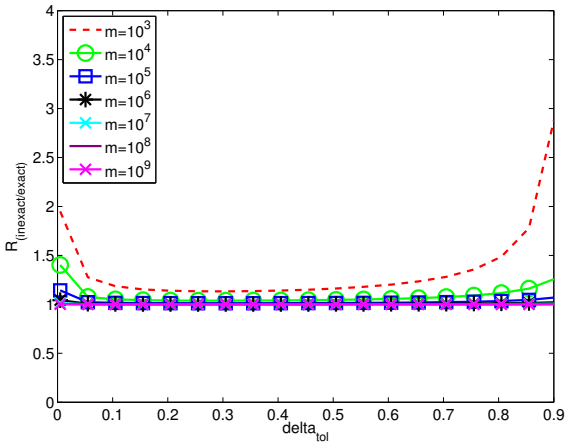

Figure 3.1: The plot of $R_{inexact/exact}$ for fixed $\beta = 0.8$, and $m \geq 10^3$.

[3] The constant c is from the explicit expression of $\mathcal{O}(m^{-1/2})$ in (3.10). A numerical study reveals that $R_{inexact/exact}|_{c=1}$ is an upper bound for $R_{inexact/exact}$.

3.2.3 The preconditioned Schur complement reduction solver

The preconditioned Schur complement reduction (p-SCR) solver is a direct method which decouples the velocity and pressure equations. This method involves the following block Gaussian eliminated system:

$$\begin{bmatrix} K(m) & B^t \\ 0 & S(m) \end{bmatrix} \begin{bmatrix} u \\ p \end{bmatrix} = \begin{bmatrix} f \\ f^p \end{bmatrix}, \tag{3.30}$$

where $f^p = BK^{-1}f$. Applying backward substitution, one obtains the following decoupled system of equations:

$$\text{Solvefor } p: \qquad Sp = f^p, \tag{3.31}$$

$$\text{Solvefor } u: \qquad Ku = f - B^t p. \tag{3.32}$$

The systems in (3.31) and (3.32) are solved by preconditioned Krylov solvers. Since the explicit construction of S is required in each step of these subspace methods, we replace the system in (3.31) by the following equation:

$$\tilde{S}p = f^p, \tag{3.33}$$

where $\tilde{S}$ is the approximation of S by $B\hat{K}^{-1}B^t$ as in (3.15), and $\hat{K}$ is the preconditioner for K. The methods applied to solve (3.31) and (3.32) are referred as the S-solve and the K-solve, respectively; see Section 3.3. Since the p-SCR solver is a direct method, the convergence of the S-solve highly depends on the accuracy of the K^{-1} approximation used in each step. Therefore, instead of one application of $\hat{K}^{-1}$ (as in the case of p-Uzawa solver), we use an accurate approximation of K^{-1} in each step of the S-solve. This is the main distinction between the usage of p-SCR and p-Uzawa solvers.

3.2.4 The preconditioned Minres solver

The p-Minres is a popular iterative method applied to the system (3.3). Let $v := \begin{bmatrix} u \\ p \end{bmatrix}$. With the given initial guess $v^0 := \begin{bmatrix} u^0 \\ p^0 \end{bmatrix}$ where $p^0 \in e^{\perp_Q}$ and with the corresponding error $r^0 := v - v^0$, the p-Minres solver computes:

$$v^k = \underset{v \in v^0 + \mathcal{K}^k(\mathcal{B}^{-1}\mathcal{A}, \tilde{r}^0)}{\operatorname{argmin}} \| \mathcal{B}^{-1} \left(\begin{bmatrix} f \\ 0 \end{bmatrix} - \mathcal{A}\, v \right) \|.$$

Here, $\tilde{r}^0 = \mathcal{B}^{-1} r^0$ and $\mathcal{K}^k = span\{\tilde{r}^0, \mathcal{B}^{-1}\mathcal{A}\tilde{r}^0, \ldots (\mathcal{B}^{-1}\mathcal{A})^k \tilde{r}^0\}$, and the preconditioner has the following block diagonal structure:

$$\mathcal{B} = \begin{bmatrix} \hat{K} & 0 \\ 0 & \hat{S} \end{bmatrix}, \tag{3.34}$$

where $\hat{K}$ and $\hat{S}$ are the preconditioners for K and S, respectively. In each step of the p-Minres solver the above preconditioner is applied in the following fashion: for the K-block one application of $\hat{K}$ and for the S-block several applications of pCG to the $\tilde{S}$-system with $\hat{S}$ as the preconditioner. Here, $\tilde{S} = B\hat{K}^{-1}B^t$ stands for the approximation of S. Since S is replaced by $\tilde{S}$, this turns the p-Minres algorithm to an inexact one; see the inexactness discussion in Section 3.3.3. The p-Minres iterations are called outer-solve whereas the pCG solve for the $\tilde{S}$-system is called inner-solve.

The convergence rate of the p-Minres method depends on the condition number of the preconditioned matrix, $\mathcal{B}^{-1}\mathcal{A}$. Combining the spectral equivalences given in (3.10) and (3.11) with the well-known condition number estimate in the book by [12], we obtain:

$$\kappa_{\mathcal{B}}(\mathcal{B}^{-1}\mathcal{A}) \leq \frac{\max\{(1 + cm^{-1/2}), d\}}{\min\{(1 - cm^{-1/2}), c_{LBB}^2\}}$$

It immediately follows that the convergence rate of the p-Minres method is independent of m asymptotically.

3.3 Numerical experiments

The goal of the numerical experiments is to compare the performance of the AGKS and MG preconditioners by using three different solvers: p-Uzawa, p-SCR and p-Minres. We use a four-level hierarchy in which the numbers of DOF, N_1, N_2, N_3, and N_4, are $659, 2467, 9539$, and 37507 from coarsest to finest level. We consider cavity flow with enclosed boundary conditions with right hand side functions $f = 1$ and $g = 0$ on a 2D domain $[-1, 1] \times [-1, 1]$.

For discretization, we use the Q_2-Q_1 (the so-called Taylor-Hood) stable finite elements and stabilized Q_1-Q_1 finite elements for the velocity-pressure pair. We consider the case of a single island (viscous inclusion) located at the region $[-1/4, 1/4]\times[-3/4, 3/4]$. For an extension, we also consider the cases of L-shaped island and two disconnected islands; see Figure 3.2. The observation about these cases are given in Section 3.3.4. The implementation of discretization is based on ifiss3.1 software provided by [82]; also see [31]. The AGKS preconditioner implementation is based on our implementation in [6, 10, 11]. The implementation of the MG preconditioner is derived from the one by [5]. We employ a V(1,1)-cycle, with point Gauss-Seidel (GS) smoother. A direct solver is used for the coarsest level. For each level of refinement, we present the number of iteration corresponding to each solve (outer-solve and S-solve; S-solve and K-solve, outer-solve and inner-solve for p-Uzawa, p-SCR, and p-Minres iterations, respectively). In the tables, N, N_S, and N_{K^*} stand for the number of DOF in $\mathcal{A}, S$, and K^* systems, respectively. We enforce an iteration bound of 200. If the method seems to converge slightly beyond this bound, we denote it by $*$. A zero initial guess is used. The numerical experiments were performed on a dual core Macbook Pro, running at 2.4 GHz with 4GB RAM.

In analyzing m-robustness, we observe a special feature. The iteration count remains fixed when m becomes larger than a certain threshold value. We define the notion *asymptotic*

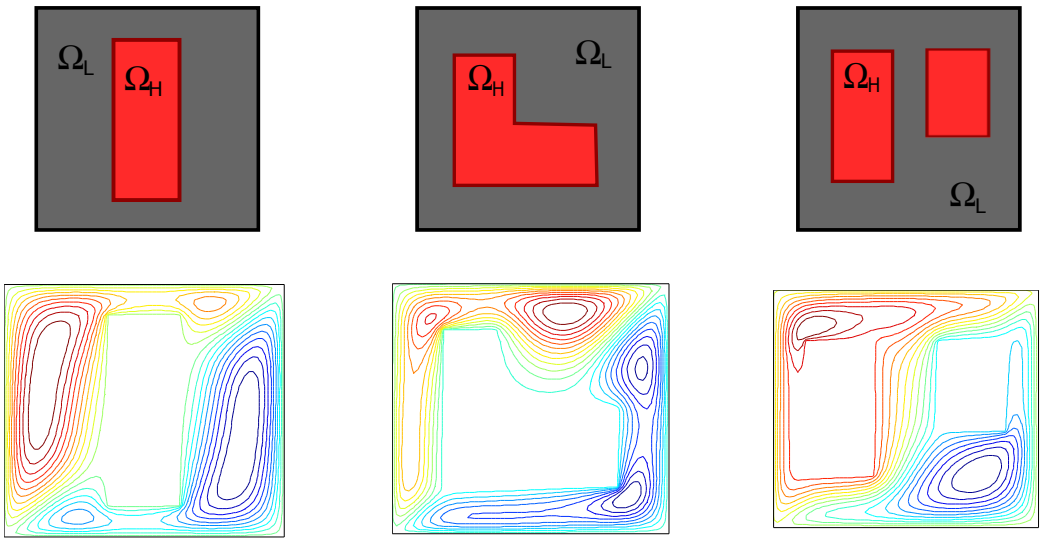

Figure 3.2: The streamline plot of the high-contrast Stokes equation for three different high-viscosity island configurations; (left) rectangular, (middle) L-shaped, and (right) two disconnected islands.

regime to indicate m values bigger than this threshold. Identifying an asymptotic regime is desirable because it immediately indicates m-robustness.

3.3.1 The preconditioned Uzawa solver

We use pCG solver with scaled PMM as a preconditioner, 0.5 as tolerance and 4 as maximum number of iterations, for the S-system in each iteration of p-Uzawa. The tolerance for the outer-solve is set to be 5×10^{-6}. We report the performance of the p-Uzawa solver applied to a rectangular mesh with Q_2-Q_1 discretization. We observe that the p-Uzawa method is m-robust as long as the optimal stopping criterion is used for the S-solve; see Table 3.1. This stopping criterion is chosen according to the convergence analysis in Section 3.2.2.

The performances of the AGKS and MG preconditioners are observed as follows. When the MG preconditioner is used, the p-Uzawa solver loses m- and h-robustness; see Table 3.1. Especially for viscosity values larger than 10^5, we further observe that the iteration number of pCG method for the S-solve, denoted by ℓ, reaches the maximum iteration count 4. Since the MG preconditioner is applied $\ell+2$ times at each iteration of the outer solve, we illustrate how this results in an unreasonable number of applications of the MG preconditioner; see

Table 3.1: Number of iterations for p-Uzawa, $Q2$-$Q1$, rectangular mesh. (top) MG, (bottom) AGKS

$N\backslash m$	$\mathbf{10^0}$	$\mathbf{10^1}$	$\mathbf{10^2}$	$\mathbf{10^3}$	$\mathbf{10^4}$	$\mathbf{10^5}$	$\mathbf{10^6}$	$\mathbf{10^7}$	$\mathbf{10^8}$	$\mathbf{10^9}$
	outer − solve									
659	13	15	15	17	19	19	19	19	22	22
2467	13	17	17	18	20	21	21	21	21	21
9539	18	20	20	23	25	26	27	28	31	32
37507	13	23	23	26	27	38	35	40	48	50
659	24	15	14	14	14	14	14	14	14	14
2467	38	21	18	19	18	18	18	18	18	18
9539	47	31	16	16	15	15	15	15	15	15
37507	70	50	17	16	15	15	15	15	15	15

$N_S\backslash m$	$\mathbf{10^0}$	$\mathbf{10^1}$	$\mathbf{10^2}$	$\mathbf{10^3}$	$\mathbf{10^4}$	$\mathbf{10^5}$	$\mathbf{10^6}$	$\mathbf{10^7}$	$\mathbf{10^8}$	$\mathbf{10^9}$
	$S-$solve									
81	2	3	2	2	3	3	3	3	2	2
289	4	4	4	4	4	4	4	4	4	4
1089	1	2	3	4	4	4	4	3	3	3
4225	1	1	1	1	3	2	4	3	4	3
81	3	2	3	3	3	3	3	3	3	3
289	3	3	3	3	3	3	3	3	3	3
1089	1	1	3	1	1	1	1	1	1	1
4225	1	1	3	1	1	1	1	1	1	1

Figure 3.3. For instance in Table 3.1, for the case of $m = 10^8$, we have $\ell = 4$. Therefore, in each outer-iteration, we apply the MG preconditioner $\ell + 2 = 6$ times as explained in Section 3.2.2. At level = 4, since the total number of MG application is the product of the outer-solve count with $\ell + 2$, it becomes $48 \times 6 = 288$. The iteration increases even more rapidly as we refine the mesh. Therefore, the loss of h-robustness sets a major drawback as larger size problems are considered.

On the other hand, the AGKS preconditioner maintains m- and h-robustness simultaneously. Asymptotically, only one iteration of pCG is sufficient to obtain an accurate S-solve; see Table 3.1. When we do the above calculation, we find that the total number of AGKS applications is $15 \times (1 + 2) = 45$. Since this application count remains fixed as the mesh is refined, we infer the h-robustness of the AGKS preconditioner; see Figure 3.3. Hence, the AGKS preconditioner will acceleratedly outperform the MG preconditioner as more mesh refinements are introduced.

3.3.2 The preconditioned Schur complement reduction solver

Since p-SCR is a direct method, the solution to the saddle point system is obtained by separate solutions for the K and S systems (with an accuracy of 5×10^{-6}.) These solution processes are called K- and S-solve, respectively. For the K-solve, we apply the pCG method with either AGKS or MG preconditioner. For the S-solve, we apply the pCG method with scaled PMM preconditioner. In each iteration of the S-solve, an accurate approximation of K^{-1} is needed due to the definition of S. Hence, a K-solve is done in each step of S-solve. Since an accurate K-system solution is required for both the K-solve and S-solve, the p-SCR method plays a critical role in revealing the effectiveness of the AGKS and MG as standalone preconditioners.

Typically a sophisticated preconditioner such as BFBt is suggested to handle the S system due to complications arising from high-contrast viscosity; see [59, 77]. We overcome these complications by focusing on an accurate K-solve in each iteration of the S-solve. Therefore,

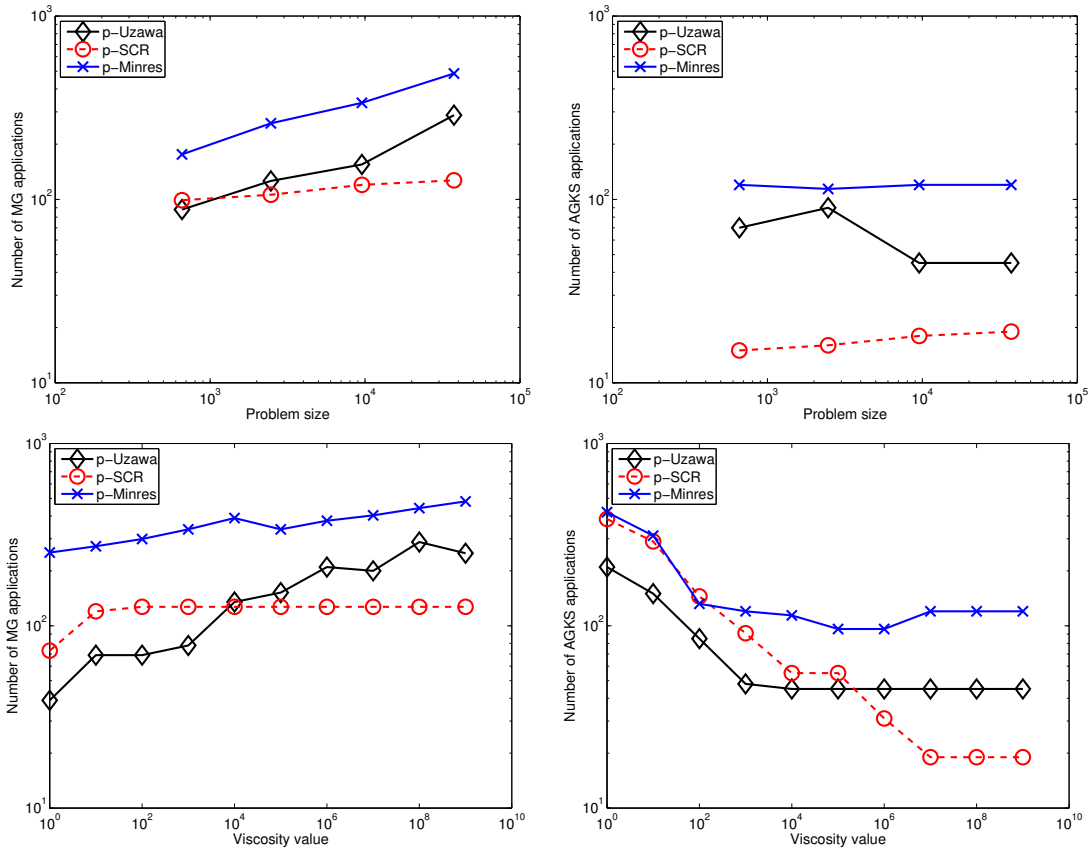

Figure 3.3: The plot of the number of (top-left) MG applications versus problem size for fixed viscosity value $m = 10^8$, (top-right) MG applications versus viscosity value for fixed level = 4 (bottom-left) AGKS applications vs problem size for fixed viscosity value $m = 10^8$, (bottom-right) AGKS applications versus viscosity value for fixed level 4.

even a simple preconditioner such as scaled PMM maintains m-robustness resulting in a good performance of pCG for the S-solve. But h-robustness was lost; see Table 3.2. It is in agreement with the p-SCR behaviour (even) with BFBt preconditioner observed by [59].

As long as the K solve is accurate, the preconditioner choice (whether AGKS or MG) does not affect the performance of pCG in S-solve. However, this performance heavily depends on the mesh aspect ratio and the choice of discretization. We obtain the fastest convergence when $Q2$-$Q1$ discretization is used on a rectangular mesh; see Table 3.2. In this case, one iteration of AGKS is enough to obtain an accurate solution to the K-system. When the aspect ratio deteriorates, S-solve is affected only with an increase in the iteration count, whereas the K-solve is adversely affected by the loss of robustness. Specifically, for the $Q2$-

Table 3.2: Number of iterations for p-SCR, $Q2$-$Q1$, rectangular mesh. (top) MG, (bottom) AGKS.

$N_S \backslash m$	$\mathbf{10^0}$	$\mathbf{10^1}$	$\mathbf{10^2}$	$\mathbf{10^3}$	$\mathbf{10^4}$	$\mathbf{10^5}$	$\mathbf{10^6}$	$\mathbf{10^7}$	$\mathbf{10^8}$	$\mathbf{10^9}$
					$S-$solve					
81	10	14	14	14	14	14	14	14	14	14
289	10	15	15	15	15	15	15	15	15	15
1089	11	16	17	17	17	17	17	17	17	17
4225	12	17	18	18	18	18	18	18	18	18

$N_S \backslash m$	$\mathbf{10^0}$	$\mathbf{10^1}$	$\mathbf{10^2}$	$\mathbf{10^3}$	$\mathbf{10^4}$	$\mathbf{10^5}$	$\mathbf{10^6}$	$\mathbf{10^7}$	$\mathbf{10^8}$	$\mathbf{10^9}$
81	10	14	14	14	14	14	14	14	14	14
289	10	15	15	15	15	15	15	15	15	15
1089	11	16	17	17	17	17	17	17	17	17
4225	12	17	18	18	18	18	18	18	18	18

$N_{K^*} \backslash m$	$\mathbf{10^0}$	$\mathbf{10^1}$	$\mathbf{10^2}$	$\mathbf{10^3}$	$\mathbf{10^4}$	$\mathbf{10^5}$	$\mathbf{10^6}$	$\mathbf{10^7}$	$\mathbf{10^8}$	$\mathbf{10^9}$
					$K-$solve					
289	7	7	7	7	7	7	7	7	7	7
1089	6	7	7	7	7	7	7	7	7	7
4225	6	7	7	7	7	7	7	7	7	7
16641	6	7	7	7	7	7	7	7	7	7

$N_{K^*} \backslash m$	$\mathbf{10^0}$	$\mathbf{10^1}$	$\mathbf{10^2}$	$\mathbf{10^3}$	$\mathbf{10^4}$	$\mathbf{10^5}$	$\mathbf{10^6}$	$\mathbf{10^7}$	$\mathbf{10^8}$	$\mathbf{10^9}$
289	12	8	5	3	3	3	1	1	1	1
1089	17	10	6	4	3	3	2	1	1	1
4225	24	14	7	5	3	3	1	1	1	1
16641	32	17	8	5	3	3	2	1	1	1

$Q1$ discretization, aspect ratio deterioration spoils the h-robustness of the MG preconditioner whereas it spoils the m-robustness of the AGKS preconditioner; see Tables 3.3 and 3.5.

We observe that the performance of p-SCR method is very poor for the $Q1$-$Q1$ discretization due to the rapid increase in iteration count of the S-solve. With this discretization, the AGKS preconditioner maintains the m- and h- robustness even when the aspect ratio is poor. But high iteration counts in the S-solver (see Tables 3.4–3.5) causes the $Q1$-$Q1$ discretization to be an inappropriate choice for the p-SCR solver.

3.3.3 The preconditioned Minres solver

We notice that the p-Minres has not been the solver of choice for high-contrast problems due to its unfavorable performance with PMM for the S-system; see [70]. We have taken a novel approach for the S system. First, we replace S by $\tilde{S} = B\hat{K}^{-1}B^t$ where $\hat{K}^{-1}$ step is one application of the AGKS preconditioner. This makes the solver method *inexact*. Then, we solve $\tilde{S}$ system by using a pCG solver with scaled PMM preconditioner with tolerance 0.05 with a maximum of 20 iterations. The pCG and p-Minres solution steps are called the inner- and outer-solve, respectively. Our approach for the S-system is similar to the one we take in the p-Uzawa solver. But, notice that now the inner solver requires more accuracy in order to guarantee a convergent p-Minres solver.

As in the p-Uzawa case, the effectiveness of the AGKS preconditioner has been confirmed as it maintains both the m- and h-robustness whereas MG suffers from the loss of both; see Table 3.6. Furthermore, we observe that the choice of $\hat{K}^{-1}$–an application of either MG or AGKS–in the inner-solve dramatically affects the performance inner-solve. Specifically, the scaled PMM preconditioner is m-robust, but not h-robust for the inner-solve with MG, whereas it is both m- and h-robust for inner-solve with AGKS.

3.3.4 Remarks on the AGKS performance for different solvers

Here we compare the performance of the AGKS preconditioner under three different solvers. For p-Uzawa and p-Minres solvers, we report numerical results for only $Q2$-$Q1$ discretization

Table 3.3: Number of iterations for p-SCR, $Q2$-$Q1$, skewed mesh ($\frac{\pi}{4}$). (top) MG, (bottom) AGKS.

$N_S \backslash m$	$\mathbf{10^0}$	$\mathbf{10^1}$	$\mathbf{10^2}$	$\mathbf{10^3}$	$\mathbf{10^4}$	$\mathbf{10^5}$	$\mathbf{10^6}$	$\mathbf{10^7}$	$\mathbf{10^8}$	$\mathbf{10^9}$
	$S-$solve									
81	17	23	27	31	32	32	32	32	32	32
289	20	28	33	38	39	38	38	38	38	38
1089	22	34	38	43	45	45	44	44	44	44
4225	25	41	43	47	49	49	49	49	49	49
81	16	22	25	30	30	31	31	31	31	31
289	18	26	31	38	38	38	37	37	37	37
1089	20	32	36	41	44	44	43	43	43	43
4225	22	40	41	45	48	48	48	48	48	48

$N_{K^*} \backslash m$	$\mathbf{10^0}$	$\mathbf{10^1}$	$\mathbf{10^2}$	$\mathbf{10^3}$	$\mathbf{10^4}$	$\mathbf{10^5}$	$\mathbf{10^6}$	$\mathbf{10^7}$	$\mathbf{10^8}$	$\mathbf{10^9}$
	$K-$solve									
289	8	9	9	9	9	9	9	9	9	9
1089	8	9	10	11	12	12	12	12	12	12
4225	8	9	11	13	13	13	13	13	13	13
16641	8	9	12	15	15	15	15	15	15	15
289	16	13	12	12	12	12	14	15	15	16
1089	22	15	14	13	13	14	14	16	16	18
4225	22	15	14	13	13	14	14	16	16	18
16641	22	15	14	13	13	14	14	16	16	18

Table 3.4: Number of iterations for p-SCR, $Q1$-$Q1$, rectangular mesh, (top) MG, (bottom) AGKS.

$N_S \backslash m$	$\mathbf{10^0}$	$\mathbf{10^1}$	$\mathbf{10^2}$	$\mathbf{10^3}$	$\mathbf{10^4}$	$\mathbf{10^5}$	$\mathbf{10^6}$	$\mathbf{10^7}$	$\mathbf{10^8}$	$\mathbf{10^9}$
					$S-$solve					
81	14	28	47	65	73	84	95	107	125	150
289	17	42	118	*	*	*	*	*	*	*
1089	18	55	180	*	*	*	*	*	*	*
4225	20	60	189	*	*	*	*	*	*	*

$N_{K^*} \backslash m$	$\mathbf{10^0}$	$\mathbf{10^1}$	$\mathbf{10^2}$	$\mathbf{10^3}$	$\mathbf{10^4}$	$\mathbf{10^5}$	$\mathbf{10^6}$	$\mathbf{10^7}$	$\mathbf{10^8}$	$\mathbf{10^9}$
					$K-$solve					
289	7	7	7	7	7	7	7	7	7	7
1089	6	7	7	7	7	7	7	7	7	7
4225	6	7	7	7	7	7	7	7	7	7
16641	6	7	7	7	7	7	7	7	7	7

81	9	25	52	80	96	110	135	158	180	190
289	15	32	90	171	*	*	*	*	*	*
1089	17	48	178	*	*	*	*	*	*	*
4225	19	60	193	*	*	*	*	*	*	*

289	12	8	6	4	4	4	2	2	2	2
1089	17	10	7	5	4	4	2	2	2	2
4225	24	13	8	6	4	4	3	2	2	2
16641	24	13	9	6	4	4	3	2	2	2

Table 3.5: Number of iterations for p-SCR, $Q1$-$Q1$, skewed mesh ($\frac{\pi}{4}$). (top) MG, (bottom) AGKS.

$N_S \backslash m$	$\mathbf{10^0}$	$\mathbf{10^1}$	$\mathbf{10^2}$	$\mathbf{10^3}$	$\mathbf{10^4}$	$\mathbf{10^5}$	$\mathbf{10^6}$	$\mathbf{10^7}$	$\mathbf{10^8}$	$\mathbf{10^9}$
					$S-$solve					
81	14	28	47	65	73	84	95	107	125	150
289	17	42	118	*	*	*	*	*	*	*
1089	18	55	180	*	*	*	*	*	*	*
4225	20	60	189	*	*	*	*	*	*	*

$N_{K^*} \backslash m$	$\mathbf{10^0}$	$\mathbf{10^1}$	$\mathbf{10^2}$	$\mathbf{10^3}$	$\mathbf{10^4}$	$\mathbf{10^5}$	$\mathbf{10^6}$	$\mathbf{10^7}$	$\mathbf{10^8}$	$\mathbf{10^9}$
					$K-$solve					
289	7	8	9	11	11	11	11	11	11	11
1089	8	8	11	13	13	13	13	13	13	13
4225	8	9	12	14	15	15	15	15	15	15
16641	8	9	13	15	17	17	17	17	17	17

81	9	25	52	80	96	110	135	158	180	190
289	15	32	90	171	*	*	*	*	*	*
1089	17	48	178	*	*	*	*	*	*	*
4225	19	60	193	*	*	*	*	*	*	*

289	15	11	9	8	7	6	6	6	6	7
1089	21	14	10	8	8	7	6	7	7	7
4225	30	17	11	9	8	8	7	7	7	10
16641	35	21	15	9	8	7	6	7	7	9

Table 3.6: Number of iterations for p-Minres, $Q2$-$Q1$, rectangular mesh, (top) MG, (bottom) AGKS.

$N\backslash m$	$\mathbf{10^0}$	$\mathbf{10^1}$	$\mathbf{10^2}$	$\mathbf{10^3}$	$\mathbf{10^4}$	$\mathbf{10^5}$	$\mathbf{10^6}$	$\mathbf{10^7}$	$\mathbf{10^8}$	$\mathbf{10^9}$
	outer − solve									
659	15	15	18	19	19	19	20	20	23	24
2467	20	19	21	24	23	24	25	28	29	30
9539	21	19	24	24	24	24	25	26	28	32
37507	21	21	23	26	30	26	29	31	34	36
659	29	23	18	16	18	16	16	18	20	20
2467	40	30	17	17	16	16	16	19	19	19
9539	50	45	20	20	19	16	16	20	20	20
37507	70	52	22	20	19	16	16	20	20	20

$N_{K^*}\backslash m$	$\mathbf{10^0}$	$\mathbf{10^1}$	$\mathbf{10^2}$	$\mathbf{10^3}$	$\mathbf{10^4}$	$\mathbf{10^5}$	$\mathbf{10^6}$	$\mathbf{10^7}$	$\mathbf{10^8}$	$\mathbf{10^9}$
	inner − solve									
81	6	7	7	7	7	7	7	7	7	7
289	8	9	9	9	9	9	9	9	9	9
1089	9	11	11	11	11	11	11	11	11	11
4225	12	13	13	13	13	13	13	13	13	13
81	20	20	5	5	5	5	5	5	5	5
289	20	20	5	5	5	5	5	5	5	5
1089	20	20	5	5	5	5	5	5	5	5
4225	20	20	5	5	5	5	5	5	5	5

on a rectangular mesh with a single island. However, we have performed experiments for other discretizations with L-shaped and two disconnected island cases with both rectangular and skewed mesh. Since we see similar behaviour, we report only our observations rather than giving the iteration tables.

The p-Uzawa solver turns out to be the best choice since AGKS preserves both m- and h-robustness regardless of the discretization type, deterioration in the aspect ratio of the mesh, or the island configuration. The change in one of the above only causes increase in the number of iterations, but qualitatively m- and h-robustness are maintained. Moreover, we observe that the asymptotic regime of the p-Uzawa solver starts with the m value 10^3; see left-bottom in Figure 3.3.

p-SCR solver, on the other hand, becomes the fastest for the problem in consideration with Q_2-Q_1 discretization in a rectangular mesh. However, the AGKS under the p-SCR solver is not h-robust; see the left column of Table 3.2. As island configuration changes, the number of iterations of both K- and S-solve increases. In addition to that, as the discretization changes, the m-robustness of PMM for S-solve is lost. Therefore, as the problem gets larger or island configuration becomes more complicated, the p-SCR solver becomes less desirable than p-Uzawa; see bottom-left and top-left in Figure 3.3. The asymptotic regime of the p-Uzawa solver is $m \geq 10^7$.

The AGKS preconditioner under the p-Minres solver also maintains both m- and h-robustness as the discretization, the aspect ratio of the mesh, or the island configuration change. However, the number of iterations in the p-Minres solver increases dramatically when the island is L-shaped. Compared to p-Uzawa, one needs a more accurate inner-solve for a convergent p-Minres. In addition, the asymptotic regime of p-Minres solver is $m \geq 10^7$. Combining these three features, p-Minres becomes less desirable compared to p-Uzawa; see bottom-left and top-left in Figure 3.3. We observe that p-Minres method has the poorest performance among p-Uzawa and p-SCR methods in terms of number of AGKS and MG

applications. However, this solver is potentially useful for large size problems as the AGKS preconditioner maintains h-robustness.

3.4 Appendix

3.4.1 Proof of Theorem 2

Here we give the details of the algebraic operations in the proof of Theorem 2.

LEMMA 7. *Let t be given by $t := \sqrt{c^2(\delta_{tol}+2)^2 + 2c\delta_{tol}^2 m^{1/2} + \delta_{tol}^2 m}$. Then*

$$t = \delta_{tol}\, m^{1/2} + 2c\delta_{tol} + \mathcal{O}(m^{-1/2}). \tag{3.35}$$

Proof.

$$\begin{aligned} t = \frac{t^2}{t} &\leq \frac{c^2(\delta_{tol}+2)^2 + 2c\delta_{tol}^2 m^{1/2} + \delta_{tol}^2 m}{\delta_{tol} m^{1/2}} \\ &= \delta_{tol} m^{1/2} + 2c\delta_{tol} + \frac{c^2(\delta_{tol}+2)^2}{\delta_{tol} m^{1/2}} \\ &= \delta_{tol} m^{1/2} + 2c\delta_{tol} + \mathcal{O}(m^{-1/2}). \end{aligned}$$

□

The error iteration matrix C was given in (3.29). Its spectral radius $\rho(C)$ in (3.36) and 1-norm of its eigenvector matrix in (3.37) were obtain by using symbolic computation.

LEMMA 8.

$$\rho(C) = \delta_{tol} + \mathcal{O}(m^{-1/2}).$$

Proof. Using the spectral radius of the matrix C in (3.29) and Lemma 7, we get the following:

$$\begin{aligned} \rho(C) &= \frac{c(\delta_{tol}+2) + \delta_{tol} m^{1/2} + t}{2m^{1/2}} \\ &= \frac{c(\delta_{tol}+2) + \delta_{tol} m^{1/2} + \delta_{tol} m^{1/2} + 2c\delta_{tol} + \mathcal{O}(m^{-1/2})}{2m^{1/2}} \\ &= \delta_{tol} + \mathcal{O}(m^{-1/2}). \end{aligned} \tag{3.36}$$

□

LEMMA 9.

$$\|V\|_1 = \frac{5}{2} + \mathcal{O}(m^{-1/2}).$$

Proof. Using the eigenvectors of C and Lemma 7, we obtain the following bound:

$$\begin{aligned} \|V\|_1 &= \frac{4c + 3c\delta_{tol} - \delta_{tol} m^{1/2} + t}{2c(1+\delta_{tol})} \\ &= \frac{4c + 5c\delta_{tol} + \mathcal{O}(m^{-1/2})}{2c(1+\delta_{tol})} \\ &= \frac{5}{2} + \mathcal{O}(m^{-1/2}). \end{aligned} \tag{3.37}$$

□

The contraction factor of the p-Uzawa method in (3.28) follows from Lemma 8 and Lemma 9.

Chapter 4

The AGKS Preconditioner for the High-contrast Biharmonic Plate Equation

In this Chapter, we extend the applicability of the AGKS preconditioner even further and show that the very same preconditioner can be used for a wider family of elliptic partial differential equations (PDEs). The broadness of the applicability of the AGKS preconditioner has been achieved by singular perturbation analysis (SPA) as it provides valuable insight into qualitative nature of the underlying PDE and its discretization. The devised SPA is utilized to explain the properties of the submatrices related to $K(m)$. In particular, SPA of highly-bending block $K_{HH}(m)$, as modulus of bending $m \to \infty$, has important implications for the behaviour of the Schur complement $S(m)$ of $K_{HH}(m)$ in $K(m)$. Namely,

$$S(m) := K_{LL} - K_{LH}K_{HH}^{-1}(m)K_{HL} = S_\infty + \mathcal{O}(m^{-1}) \ , \tag{4.1}$$

where S_∞ is a LRP of K_{LL}.

The rank of the perturbation depends on the number of disconnected components comprising the highly-bending region. This special limiting form of $S(m)$ allows us to build a robust approximation of $S(m)^{-1}$ by merely using solvers for K_{LL} by the help of the Sherman-Morrison-Woodbury formula.

Preconditioning for the biharmonic equation was extensively studied in the domain decomposition setting [63, 95] and multigrid, BPX, and hierarchical basis settings [20, 47, 62, 56, 72, 73]. Other solution strategies were also developed such as fast Poisson solvers [60, 61] and iterative methods [25]. However, there is only limited preconditioning literature available for discontinuous coefficients. Domain decomposition preconditioners have been studied

[58] for the mortar type discretization of the biharmonic equation with large jumps in the coefficients.

The high-contrast in material properties is ubiquitous in composite materials. Hence, the modeling of composite materials is an immediate application of the biharmonic plate equation with high-contrast coefficients. Since the usage of composite materials is steadily increasing, the simulation and modeling of composite has become essential. We witness that the utilization of composites has become an industry standard. For instance, light weight composite materials are now being used in modern aircrafts by Airbus and Boeing. There is imminent need for robust preconditioning technology in the computational material science community as the modeling and simulation capability of composites evolve.

In [88], the Euler-Bernoulli equation with discontinuous coefficients was studied for the kinematics of composite beams. In the beam setting, the physical meaning of the PDE coefficient corresponds to the product of Young's modulus and moment of inertia [76, p. 103], [88]. In the biharmonic plate equation setting, the PDE coefficient represents the plate modulus of bending [76, p. 406]. Nonhomogeneous elastic plates have been considered in [57] with varying modulus of elasticity.

Our model problem is limited to the biharmonic equation which captures only the *isotropic* materials. The extension of our analysis to a more generalized 4-th order PDE is widely open. Such PDEs have an important role in structural mechanics as they are used in modeling *anisotropic* materials. Plane deformations of anisotropic materials were studied in [64], but extension to simultaneously heterogeneous and anisotropic case needs to be further explored. Grossi [46] has studied the existence of the weak solutions of anisotropic plates. The coercivity of the bilinear forms has also been established which may lay the foundations for our future work related to LRPs.

The reduction of the *analysis of the two-dimensional problem in the classical theory of elasticity* to the solution of biharmonic equation is due to Airy, who used the calculations in the design of a structural support system for an astronomical telescope.

The study of 3D problems in the mathematical theory of elasticity also touches upon formulations which involve the biharmonic operator. These developments essentially lay the foundation to the study of the mathematical theory of elasticity which forms an important aspect of the mechanics of deformable media.

The solutions developed for slow viscous flow problems including flow of molten metals, flow particulate suspensions and in the modeling of bio-fluid dynamics.

Relevant field equations are used to develop the biharmonic equations governing plane problems in elasticity theory and slow viscous flow. In addition, biharmonic equation is governing equation in flexure of thin plates, described by the Germain-Poisson-Kirchoff this plate theory.

4.1 The underlying PDE and the linear system

We study the following high-contrast biharmonic equation for the clamped plate problem:

$$\begin{aligned} \nabla^2 (\alpha \nabla^2 u) &= f \quad \text{in} \quad \Omega \subset \mathbb{R}^2, \\ u = \partial_n u &= 0 \quad \text{on} \quad \partial\Omega. \end{aligned} \tag{4.2}$$

We restrict the plate bending process to a *binary regime* (see Figure 2.1) in which the coefficient α is a piecewise constant function with the following values:

$$\alpha(x) = \begin{cases} m \gg 1, & x \in \Omega_H, \\ 1, & x \in \Omega_L. \end{cases} \tag{4.3}$$

It is quite common to idealize the discontinuous PDE coefficient α by a piecewise constant function [13, 51]. In the case of high-contrast diffusion equation, Aksoylu and Beyer [4] showed that the idealization of diffusivity by piecewise constant coefficients is meaningful by showing a continuous dependence of the solutions on the diffusivity; also see [3]. A similar justification can be extended to the high-contrast biharmonic plate equation.

4.1.1 Bilinear forms for the biharmonic equation

In the theory of elasticity, potential energy is defined by using *rotationally invariant* functions. For plates, the potential energy is given by [23, p. 30]:

$$J(v) := \frac{1}{2}\int_\Omega \alpha\ \left[\{\text{trace}\, Hess\}^2 + 2(\sigma-1)\det Hess\right]\ dx - \int_\Omega fv\ dx, \tag{4.4}$$

where $Hess$ is the Hessian,

$$Hess = \begin{bmatrix} \partial_{11}v & \partial_{12}v \\ \partial_{21}v & \partial_{22}v \end{bmatrix}.$$

The bilinear form corresponding to energy minimization in (4.4) is given by:

$$a(u,v) := \int_\Omega \alpha\ \left[\nabla^2 u\,\nabla^2 v + (1-\sigma)\{2\partial_{12}u\,\partial_{12}v - \partial_{11}u\,\partial_{22}v - \partial_{22}u\,\partial_{11}v\}\right]\ dx, \tag{4.5}$$

where $0 < \sigma < 1/2$ is the Poisson's ratio. Note that the straightforward bilinear form associated to (4.2) is obtained by using Green's formula:

$$\int_\Omega \nabla^2\left(\alpha\,\nabla^2 u\right) v\ dx = \int_\Omega \alpha\,\nabla^2 u\,\nabla^2 v\ dx + \int_{\partial\Omega} \alpha\,\partial_n\nabla^2 u\, v\ d\gamma - \int_{\partial\Omega} \alpha\,\nabla^2 u\,\partial_n v\ d\gamma. \tag{4.6}$$

We see that both (4.5) and (4.6) contain the so-called *canonical* bilinear form, $\tilde{a}(u,v)$, associated to the biharmonic equation (4.2):

$$\tilde{a}(u,v) := \int_\Omega \alpha\,\nabla^2 u\,\nabla^2 v\ dx. \tag{4.7}$$

When $u, v \in H_0^2(\Omega)$, both bilinear forms $a(u,v)$ and $\tilde{a}(u,v)$ correspond to the strong formulation (4.2) due to second Green's formula and the zero contribution of the below term:

$$\int_\Omega (1-\sigma)\{2\partial_{12}u\,\partial_{12}v - \partial_{11}u\,\partial_{22}v - \partial_{22}u\,\partial_{11}v\}\ dx. \tag{4.8}$$

4.1.2 Effects of high-contrast on the spectrum

Roughness of PDE coefficients causes loss of robustness of preconditioners. This is mainly due to clusters of eigenvalues with varying magnitude. Although diagonal scaling has no effect on the asymptotic behaviour of the condition number, it leads to an improved clustering in the spectrum. The spectrum of diagonally scaled stiffness matrix, A, is bounded from above and below except three eigenvalues in the case of a single isolated highly-bending island. On the other hand, the spectrum of K contains eigenvalues approaching infinity with cardinality depending on the number of degrees of freedom (DOF) contained within highly-bending island. For the case of $m = 10^9$, we depict the spectra of K and A and their subblocks in Figure 4.1. Clustering provided by diagonal scaling can be advantageous for faster convergence of Krylov subspace solvers especially when deflation methods designed for small eigenvalues are used; for further discussion see [7].

Utilizing the matrix entry based analysis by Graham and Hagger [41] for linear finite elements (FE), in [10], we extended the spectral analysis to cell-centered finite volume discretization and obtained an identical spectral result for A. Namely, the number of small eigenvalues of A depends on the number of isolated islands comprising the highly-bending region. We observe a similar behaviour for the biharmonic plate equation where the only difference is that for each island we observe three small eigenvalues rather than one. The three dimensional kernel of the Neumann matrix is responsible for that difference; see §4.2. A similar matrix entry based analysis can be applied to this problem, but this analysis is more involved for the HCT discretization than that for linear FE.

4.2 Discretization and low-rank perturbations

We consider an H^2-conformal Galerkin finite element discretization with Hsieh-Clough-Tocher (HCT) element. HCT element is constructed by subdividing the triangle element into three subtriangles by connecting its vertices to its centroid. Then, a C^1 function consisting of piecewise cubic polynomials defined on each subtriangle is built. The function

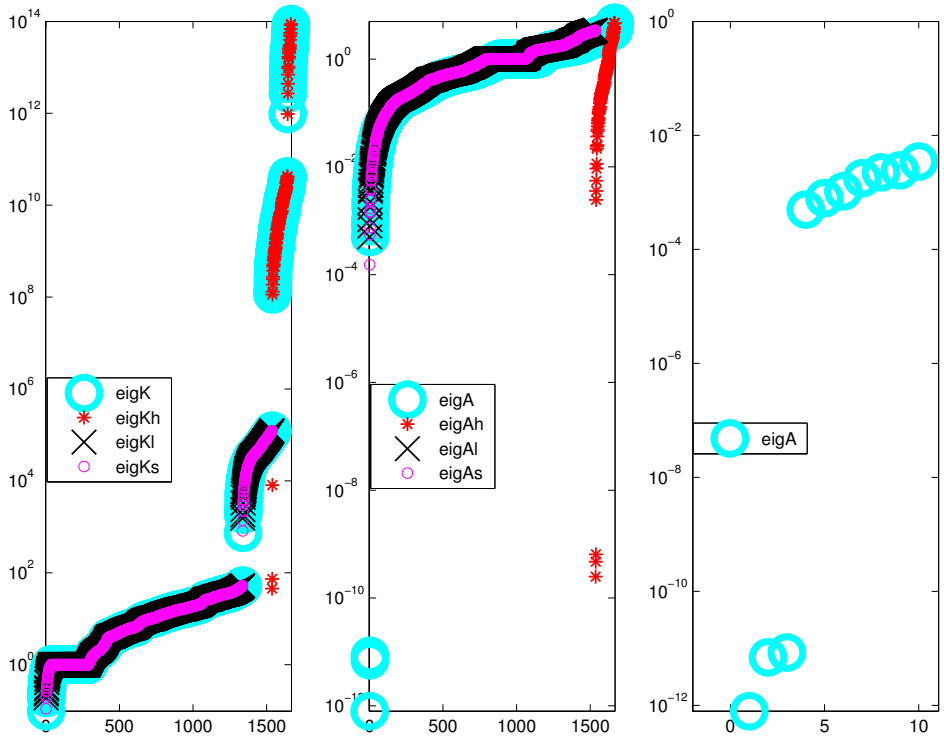

Figure 4.1: The HCT discretization of the biharmonic equation with $m = 10^9$. (Left) The spectrum of the stiffness matrix K. (Middle) Spectrum of the diagonally scaled stiffness matrix. (Right) The zoomed out version of the three smallest eigenvalue of diagonally scaled matrix.

value and its first derivatives are specified on the vertices of the original triangle, and the normal derivative of the function is specified on the midpoint of each sides of the triangle; see Figure 4.2. HCT element is conforming but nonnested, and consists of 12 degrees of freedom. For more detailed definition of HCT element, see [24].

Let the linear system arising from the discretization be denoted by:

$$K(m)\ x = b. \tag{4.9}$$

Ω is decomposed with respect to magnitude of the coefficient value as

$$\Omega = \overline{\Omega}_H \cup \Omega_L, \tag{4.10}$$

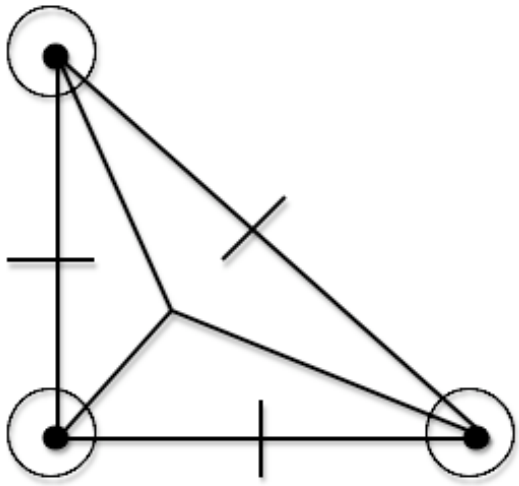

Figure 4.2: The Hsieh-Clough-Tocher element

where Ω_H and Ω_L denote the highly- and lowly-bending regions, respectively. DOF that lie on the interface, $\Gamma := \overline{\Omega}_H \cap \overline{\Omega}_L$, between the two regions are included in Ω_H. When m-dependence is explicitly stated and the discretization system (4.9) is decomposed with respect to (4.10), i.e., the magnitude of the coefficient values, we arrive at the following 2×2 block system:

$$\begin{bmatrix} K_{HH}(m) & K_{HL} \\ K_{LH} & K_{LL} \end{bmatrix} \begin{bmatrix} x_H \\ x_L \end{bmatrix} = \begin{bmatrix} b_H \\ b_L \end{bmatrix}. \tag{4.11}$$

There are important properties associated to the K_{HH} block in (4.11): It is the only block that has m-dependence, and furthermore, a matrix with low-rank kernel can be extracted from it. Our preconditioner construction is based on LRPs from this extraction. Next, we explain how to extract the so-called *Neumann matrix* and why $a(u, v)$ is the suitable bilinear form for that purpose. By rewriting (4.5) as the following

$$a(u,v) = \int_\Omega \alpha \, \left[\sigma \, \nabla^2 u \, \nabla^2 v + (1-\sigma)\{\partial_{11} u \, \partial_{11} v + \partial_{22} u \, \partial_{22} v + 2 \, \partial_{12} u \, \partial_{12} v\}\right] \, dx, \tag{4.12}$$

we see that

$$\begin{aligned} a(v,v) &= \alpha \, \sigma \, \|\nabla^2 v\|^2_{L_2(\Omega)} + \alpha \, (1-\sigma) |v|^2_{H^2(\Omega)} \\ &\geq \alpha \, (1-\sigma) |v|^2_{H^2(\Omega)}. \end{aligned} \tag{4.13}$$

The inequality (4.13) has important implications. Namely, $a(v,v)$ is $V_{\mathcal{P}_1}(\Omega)$-coercive where $V_{\mathcal{P}_1}(\Omega) \subset H^2(\Omega)$ is a closed subspace such that $V_{\mathcal{P}_1}(\Omega) \cap \mathcal{P}_1 = \emptyset$ and $\mathcal{P}_1$ denotes the set of polynomials of degree at most 1. Furthermore, (4.13) immediately implies that $a(v,v)$ is $H_0^2(\Omega)$-coercive.

Let $\mathcal{T}^h$ be the triangulation of Ω and $V^h(\Omega)$ be the associated discrete space. Let $V^h(\overline{\Omega}_H)$ be the restriction of $V^h(\Omega)$ onto $\overline{\Omega}_H$ based on the decomposition in (4.10). We define the *Neumann matrix* $\mathcal{N}_{HH}$ as follows:

$$\langle \mathcal{N}_{HH} \underline{\phi}_H^h, \underline{\psi}_H^h \rangle := a(\phi_H^h, \psi_H^h),$$

where $\phi_H^h, \psi_H^h \in V^h(\overline{\Omega}_H)$ are the basis functions whose values of DOF are denoted by $\underline{\phi}_H^h$ and $\underline{\psi}_H^h$, respectively. Since $a(\cdot,\cdot)$ is $V_{\mathcal{P}_1}(\Omega)$-coercive, this implies by (4.13) that

$$\ker \mathcal{N}_{HH} = \mathcal{P}_1^h|_{\overline{\Omega}_H} = \ \mathrm{span}\{\underline{1}_H, \underline{x}_H, \underline{y}_H\}. \tag{4.14}$$

Hence, with m defined in (4.3), K_{HH} in (4.11) has the following decomposition:

$$K_{HH}(m) = m\mathcal{N}_{HH} + R, \tag{4.15}$$

where R is the coupling matrix corresponding to DOF on the interface Γ.

Now, we are in a position to reveal the resulting main numerical linear algebra implication. As $m \to \infty$, the limiting Schur complement S_∞ in (4.1) becomes a rank-3 perturbation of K_{LL}. This result relies on the fact that the inverse of the limiting K_{HH} is of rank-3; see (4.17). This is due to the fact that $\mathcal{N}_{HH}$ has a rank 3 kernel whose (normalized) discretization is given by:

$$e_H := [\underline{1}_H, \underline{x}_H, \underline{y}_H]. \tag{4.16}$$

4.3 Main singular perturbation analysis results

LEMMA 10. *The asymptotic behaviour of the submatrices in* (2.5) *is given by the following:*

$$K_{HH}(m)^{-1} = e_H \eta^{-1} e_H^t + \mathcal{O}(m^{-1}), \tag{4.17}$$

$$S(m) = K_{LL} - (K_{LL} e_H)\eta^{-1}(e_H^t K_{LL}) + \mathcal{O}(m^{-1}), \tag{4.18}$$

$$K_{LH} K_{HH}(m)^{-1} = (K_{LL} e_H)\eta^{-1} e_H^t + \mathcal{O}(m^{-1}), \tag{4.19}$$

where

$$\eta := e_H^t \, K_{HH} \, e_H. \tag{4.20}$$

Proof. Since $\mathcal{N}_{HH}$ is symmetric positive semidefinite, using (4.14) we have the following spectral decomposition where n_H denotes the cardinality of DOF in $\overline{\Omega}_H$:

$$Z^t \mathcal{N}_{HH} Z = \operatorname{diag}(\lambda_1, \ldots, \lambda_{n_H-3}, 0, 0, 0), \tag{4.21}$$

where $\{\lambda_i : \ i = 1, \ldots, n_H\}$ is a non-increasing sequence of eigenvalues of $\mathcal{N}_{HH}$ and Z is orthogonal. Since, the eigenvectors corresponding to the zero eigenvalues are discretization of the polynomials $1, x$, and y, we can write $Z = \left[\tilde{Z} \mid e_H\right]$ where e_H is defined in (4.16). Using (4.15), we have:

$$\begin{aligned} Z^t K_{HH}(m) Z \ &= \ \begin{bmatrix} m \operatorname{diag}(\lambda_1, \ldots, \lambda_{n_H-3}) + \tilde{Z}^t R \tilde{Z} & \tilde{Z}^t R e_H \\ e_H^t R \tilde{Z} & e_H^t R e_H \end{bmatrix} \\ &=: \ \begin{bmatrix} \tilde{\Lambda}(m) & \tilde{\delta} \\ \tilde{\delta}^T & \eta \end{bmatrix}. \end{aligned} \tag{4.22}$$

To find the limiting form of $K_{HH}(m)^{-1}$ note that

$$\begin{aligned}\tilde{\Lambda}(m) &= m \text{ diag}(\lambda_1, \ldots, \lambda_{n_H-3}) + \tilde{Z}^t R \tilde{Z} \\ &= m \text{ diag}(\lambda_1, \ldots, \lambda_{n_H-3}) \left(\tilde{I} + m^{-1} \text{ diag}(\lambda_1^{-1}, \ldots, \lambda_{n_H-3}^{-1}) \tilde{Z}^t R \tilde{Z} \right).\end{aligned}$$

Then,

$$\|\tilde{\Lambda}(m)^{-1}\|_2 \leq \frac{m^{-1} \max_{i \leq n_H-3} \lambda_i^{-1}}{1 - m^{-1} \max_{i \leq n_H-3} \lambda_i^{-1} \|\tilde{Z}^t R \tilde{Z}\|_2},$$

for sufficiently large m, we can conclude the following:

$$\tilde{\Lambda}(m)^{-1} = \mathcal{O}(m^{-1}). \tag{4.23}$$

We proceed with the following inversion:

$$\begin{bmatrix} \tilde{\Lambda}(m) & \tilde{\delta} \\ \tilde{\delta}^t & \eta \end{bmatrix}^{-1} = U(m) \; V(m) \; U(m)^t,$$

where

$$U(m) := \begin{bmatrix} \tilde{I} & -\tilde{\Lambda}(m)^{-1} \tilde{\delta} \\ 0^t & 1 \end{bmatrix},$$

$$V(m) := \begin{bmatrix} \tilde{\Lambda}(m)^{-1} & 0 \\ 0^t & \left(\eta - \tilde{\delta}^t \tilde{\Lambda}(m)^{-1} \tilde{\delta} \right)^{-1} \end{bmatrix}.$$

Then, (4.23) implies that

$$\begin{aligned} U(m) &= I + \mathcal{O}(m^{-1}), \\ V(m) &= \begin{bmatrix} O & 0 \\ 0^t & \eta^{-1} \end{bmatrix} + \mathcal{O}(m^{-1}). \end{aligned}$$

Combining the above results, we arrive at

$$\begin{bmatrix} \tilde{\Lambda}(m) & \tilde{\delta} \\ \tilde{\delta}^t & \eta \end{bmatrix}^{-1} = \begin{bmatrix} O & 0 \\ 0^t & \eta^{-1} \end{bmatrix} + \mathcal{O}(m^{-1}) ,$$

and, by (4.22), we have

$$\begin{aligned} K_{HH}(m)^{-1} &= Z \begin{bmatrix} O & 0 \\ 0^t & \eta^{-1} \end{bmatrix} Z^t + \mathcal{O}(m^{-1}) \\ &=: e_H \eta^{-1} e_H^t + \mathcal{O}(m^{-1}) , \end{aligned} \tag{4.24}$$

which proves (4.17) of the Lemma.

Parts (4.18) and (4.19) follow from simple substitution and using (2.6).

□

REMARK 5. *If we further decompose DOF associated with $\overline{\Omega}_H$ into a set of interior DOF associated with index I and interface DOF with index Γ, we obtain the following block representation of K_{HH}:*

$$K_{HH}(m) = \begin{bmatrix} K_{II}(m) & K_{I\Gamma}(m) \\ K_{\Gamma I}(m) & K_{\Gamma\Gamma}(m) \end{bmatrix}. \tag{4.25}$$

The entries in the block $K_{\Gamma\Gamma}(m)$ are assembled from contributions both from finite elements in Ω_H and Ω_L, i.e. $K_{\Gamma\Gamma}(m) = A^{(H)}_{\Gamma\Gamma}(m) + A^{(L)}_{\Gamma\Gamma}$.

We further write e_H in block form; $e_H = (e_I^t \ , \ e_\Gamma^t)^t$. Finally we note that the off-diagonal

blocks have the decomposition:

$$K_{LH} \;=\; \begin{bmatrix} 0 \; K_{L\Gamma} \end{bmatrix} \;=\; K_{HL}^t. \tag{4.26}$$

Therefore, the results of Lemma 10 can be rewritten as the following:

$$\begin{aligned} K_{HH}(m)^{-1} &= e_H \left(e_\Gamma^t K_{\Gamma\Gamma}^{(L)} e_\Gamma \right)^{-1} e_H^t + \mathcal{O}(m^{-1}), \\ S(m) &= K_{LL} - (K_{L\Gamma} e_\Gamma) \left(e_\Gamma^t K_{\Gamma\Gamma}^{(L)} e_\Gamma \right)^{-1} (e_\Gamma^t K_{\Gamma L}) + \mathcal{O}(m^{-1}), \\ K_{LH} K_{HH}(m)^{-1} &= (K_{L\Gamma} e_\Gamma) \left(e_\Gamma^t K_{\Gamma\Gamma}^{(L)} e_\Gamma \right)^{-1} e_H^t + \mathcal{O}(m^{-1}). \end{aligned}$$

We will use the following limit values of the block matrices (in Lemma 10) in the definition of the preconditioner in (4.30):

$$K_{HH}^{\infty\dagger} := e_H \eta^{-1} e_H^t, \tag{4.27}$$

$$S_\infty := K_{LL} - K_{LH} K_{HH}^{\infty\dagger} K_{HL}. \tag{4.28}$$

4.3.1 Qualitative nature of the solution

We advocate the usage of SPA because it is a very effective tool in gaining qualitative insight about the asymptotic behavior of the solution of the underlying PDE. Through SPA, in Lemma 10, we were able to fully reveal the asymptotic behaviour of the submatrices of K in (2.5). This information leads to a characterization of the limit of the underlying discretized inverse operator. We now prove that *the solution over the highly-bending island converges to a linear polynomial*. In other words, $x_H^\infty \in \text{span } e_H$. This is probably the most fundamental qualitative feature of the solution of the high-contrast biharmonic plate equation.

LEMMA 11. *Let e_H as in* (4.16). *Then,*

$$x_H(m) = e_H \; c_H \;+\; \mathcal{O}(m^{-1}), \tag{4.29}$$

where c_H is a 3×1 vector determined by the solution in the lowly-bending region.

Proof. We prove the result by providing an explicit quantification of the limiting process based on Lemma 10:

$$\begin{aligned} x_L(m) &= S^{-1}(m)\ \{b_L - K_{LH}\, K_{HH}^{-1}(m) b_H\} \\ &= S_\infty^{-1}\{b_L - K_{LH}\,(e_H \eta^{-1} e_H^t)\, b_H\} + \mathcal{O}(m^{-1}) \\ &=: x_L^\infty + \mathcal{O}(m^{-1}), \\ x_H(m) &= K_{HH}^{-1}(m)\ \{b_H - K_{HL}\, x_L(m)\} \\ &= e_H \eta^{-1} e_H^t \{b_H - K_{HL}\, x_L^\infty\} + \mathcal{O}(m^{-1}) \\ &=: e_H\ c_H\ +\ \mathcal{O}(m^{-1}). \end{aligned}$$

□

4.4 Construction of the preconditioner

Let the limit in (4.17) be denoted by $K_{HH}^{\infty\dagger} := e_H \eta^{-1} e_H^t$. Based on the above perturbation analysis, our proposed preconditioner is defined as follows:

$$B_{AGKS}(m) := \begin{bmatrix} I_{HH} & -K_{HH}^{\infty\dagger} K_{HL} \\ 0 & I_{LL} \end{bmatrix} \begin{bmatrix} K_{HH}(m)^{-1} & 0 \\ 0 & S_\infty^{-1} \end{bmatrix} \begin{bmatrix} I_{HH} & 0 \\ -K_{LH} K_{HH}^{\infty\dagger} & I_{LL} \end{bmatrix}, \tag{4.30}$$

where $K_{HH}^{\infty\dagger}$ and S_∞ are defined in (4.27) and (4.28), respectively.

We need the following auxiliary result to be used in the proof of Theorem 3 which characterizes the spectral behaviour of the preconditioned system.

LEMMA 12. *For sufficiently large m, we have*

$$K_{HH}^{-1/2} = e_H \eta^{-1/2} e_H^t + \mathcal{O}(m^{-1/2}), \tag{4.31}$$

where η is this time 3×3 SPD matrix independent of m defined in (4.20).

Proof. We start by writing down the spectral decomposition of $K_{HH}(m)$

$$Q(m)^t K_{HH}(m) Q(m) \;=\; \mathrm{diag}(\mu_1(m), \ldots, \mu_{n_H-3}(m), \mu_{n_H-2}(m), \mu_{n_H-1}(m), \mu_{n_H}(m)),$$

where $\{\mu_i(m) : \; i = 1, \ldots, n_H\}$ denotes a non-increasing ordering of the eigenvalues of $K_{HH}(m)$. Since $K_{HH}(m)$ is SPD, we have $\mu_i(m) > 0$ for all $i \leq n_H$. We use the main fact that eigenvalues and eigenvectors of a symmetric matrix are Lipschitz continuous functions of the matrix entries [49, 90].

By (4.21) and (4.24) in Lemma 10, we give the following spectral decomposition:

$$K_{HH}^{-1}(m) = z_1\, 0\, z_1^t + \ldots + z_{n_H-3}\, 0\, z_{n_H-3}^t + e_H\, \eta^{-1}\, e_H^t + \mathcal{O}(m^{-1}). \tag{4.32}$$

Note that η in (4.22) is a 3×3 symmetric, and hence, diagonalizable matrix. We proceed towards a fully diagonalized form of the limiting $K_{HH}^{-1}(m)$. For that, we use the diagonalization of η^{-1}:

$$\eta^{-1} = \hat{z}_{H_1}\, \mu_{H_1}^{-1}\, \hat{z}_{H_1}^t + \hat{z}_{H_x}\, \mu_{H_x}^{-1}\, \hat{z}_{H_x}^t + \hat{z}_{H_y}\, \mu_{H_y}^{-1}\, \hat{z}_{H_y}^t.$$

Therefore, we have the following expression for the last term in (4.32):

$$e_H \eta^{-1} e_H^t = [z_{H_1}\, z_{H_x}\, z_{H_y}]\, \mathrm{diag}(\mu_{H_1}^{-1}, \mu_{H_x}^{-1}, \mu_{H_y}^{-1})\, [z_{H_1}\, z_{H_x}\, z_{H_y}]^t, \tag{4.33}$$

where

$$\begin{aligned} \left[z_{H_1}\, z_{H_x}\, z_{H_y}\right] &:= \left[e_{H_1}\, e_{H_x}\, e_{H_y}\right], \left[\hat{z}_{H_1}\, \hat{z}_{H_x}\, \hat{z}_{H_y}\right] \\ \left[e_{H_1}, e_{H_x}, e_{H_y}\right] &:= e_H. \end{aligned}$$

Now by substituting (4.33) in (4.32), we have the following spectral decomposition which corresponds to the fully diagonalized version:

$$K_{HH}^{-1}(m) = z_1\, 0\, z_1^t + \ldots + z_{n_H-3}\, 0\, z_{n_H-3}^t + z_{H_1}\, \mu_{H_1}\, z_{H_1}^t + z_{H_x}\, \mu_{H_x}\, z_{H_x}^t + z_{H_y}\, \mu_{H_y}\, z_{H_y}^t + \mathcal{O}(m^{-1})$$
$$=: Z_\infty \,\mathrm{diag}(0, \ldots, 0, \mu_{H_1}^{-1}, \mu_{H_x}^{-1}, \mu_{H_y}^{-1})\, Z_\infty^t + \mathcal{O}(m^{-1}). \tag{4.34}$$

The expression in (4.34) also implies the convergence of the eigenvectors of $K_{HH}(m)$:

$$Q(m) = Z_\infty + \mathcal{O}(m^{-1}). \tag{4.35}$$

Note that Z_∞ differs from Z in (4.21) only in the last three columns due to diagonalization of η.

From (4.34), we obtain a characterization of the largest three eigenvalues of $K_{HH}(m)^{-1}$:

$$\mu_{n_H-2}(m)^{-1} = \mu_{H_1}^{-1} + \mathcal{O}(m^{-1}) \tag{4.36a}$$
$$\mu_{n_H-1}(m)^{-1} = \mu_{H_x}^{-1} + \mathcal{O}(m^{-1}) \tag{4.36b}$$
$$\mu_{n_H}(m)^{-1} = \mu_{H_y}^{-1} + \mathcal{O}(m^{-1})\ . \tag{4.36c}$$

Using (4.34) and (4.36), we arrive at the following:

$$\mathrm{diag}(\mu_1(m)^{-1/2}, \ldots, \mu_{n_H-3}(m)^{-1/2}, \mu_{n_H-2}(m)^{-1/2}, \mu_{n_H-1}(m)^{-1/2}, \mu_{n_H}(m)^{-1/2})$$
$$= \mathrm{diag}(0, \ldots, 0, \mu_{H_1}^{-1/2}, \mu_{H_x}^{-1/2}, \mu_{H_y}^{-1/2}) + \mathcal{O}(m^{-1/2}). \tag{4.37}$$

By using (4.37) and (4.35), we arrive at the desired result:

$$\begin{aligned} K_{HH}(m)^{-1/2} &= Q(m)\,\mathrm{diag}(\mu_1(m)^{-1/2}, \ldots, \mu_{n_H}(m)^{-1/2}) Q(m)^t \\ &= Z_\infty \,\mathrm{diag}(0, \ldots, 0, \mu_{H_1}^{-1/2}, \mu_{H_x}^{-1/2}, \mu_{H_y}^{-1/2})\, Z_\infty^t + \mathcal{O}(m^{-1/2}) \\ &= [z_{H_1}\, z_{H_x}\, z_{H_y}]\,\mathrm{diag}(\mu_{H_1}^{-1/2}, \mu_{H_x}^{-1/2}, \mu_{H_y}^{-1/2})\,[z_{H_1}\, z_{H_x}\, z_{H_y}]^t + \mathcal{O}(m^{-1/2}) \\ &= e_H\, \eta^{-1/2}\, e_H^t + \mathcal{O}(m^{-1/2}). \end{aligned}$$

□

Now, we can prove the main theorem that shows the AGKS preconditioner is an effective preconditioner for the solution of biharmonic-plate equation for $m \gg 1$.

THEOREM 3. *For sufficiently large m, we have*

$$\sigma(B_{AGKS}(m)\ K(m)) \ \subset\ [1 - cm^{-1/2}, 1 + cm^{-1/2}]$$

for some constant c independent of m, and therefore

$$\kappa(B_{AGKS}(m)\ K(m)) \ =\ 1 \ +\ \mathcal{O}(m^{-1/2}).$$

Proof. The proof follows from the proof of Theorem 1.

□

4.5 Numerical experiments

The goal of the numerical experiments is to compare the performance of the two preconditioners: AGKS and MG. The domain is a unit square whose coarsest level triangulation consists of 32 triangles. We consider the case of a single highly-bending island located at the region $[1/4, 2/4] \times [1/4, 2/4]$ consisting of 2 coarsest level triangles. For an extension, we also consider the cases of L shaped island and two disconnected islands. The implementation of HCT discretization is based on Pozrikidis' software provided in [76]. For these experiments, the problem sizes are 131, 451, 1667, 6403 for levels $1, 2, 3$ and 4.

We denote the norm of the relative residual at iteration i by $rr^{(i)}$:

$$rr^{(i)} := \frac{\|r^{(i)}\|_2}{\|r^{(0)}\|_2},$$

where $r^{(i)}$ denotes the residual at iteration i with a stopping criterion of $rr^{(i)} \leq 10^{-7}$. In Tables 4.1–4.5, preconditioned conjugate gradient iteration count and the average reduction factor are reported for combinations of preconditioner, smoother types, and number of

smoothing iterations. The average reduction factor of the residual is defined as:

$$\left(rr^{(i)}\right)^{1/i}.$$

We enforce an iteration bound of 60. If the method seems to converge slightly beyond this bound, we denote it by 60^{+}, whereas, stalling is denoted by ∞.

We use Galerkin variational approach to construct the coarser level algebraic systems. The multigrid preconditioner MG is derived from the implementation by Aksoylu, Bond, and Holst [5]. We employ a V(s,s)-cycle, $s = 1, 5, 10$, with point symmetric Gauss-Seidel (sGS) and point Gauss-Seidel (GS) smoothers. A direct solver is used for the coarsest level.

Due to Shermann-Morrison-Woodbury formula, the inversion of S_∞ and $S(m)$ require the inversions of 3×3 and $n_H \times n_H$ matrices. [1] Therefore, the low-rank perturbation clearly yields a computational advantage. By exploiting the fact that S_∞ in (4.1) is only a LRP of K_{LL}, we can build robust preconditioners for S_∞ in (4.30) via standard multigrid preconditioners. (4.1) implies that

$$S_\infty = K_{LL} - v\eta^{-1}v^T,$$

where $v := K_{LH}e_H$. M_{HH} and M_{LL} denote the standard multigrid V(s,s)-cycles for K_{HH} and K_{LL}, respectively. We can construct an efficient and robust preconditioner $\tilde{S}^{-1}$ for S_∞ using the Sherman-Morrison-Woodbury formula, i.e.

$$\tilde{S}^{-1} \;:=\; M_{LL} \;+\; M_{LL}v\,(\eta - v^T M_{LL} v)^{-1}\, v^T M_{LL}. \tag{4.38}$$

[1] Let $T_\infty := \eta - v^t K_{LL}^{-1} v$ and $T(m) := K_{HH} - K_{LH}^t K_{LL}^{-1} K_{LH}$. The inversions yield the following operations respectively:

$$S_\infty^{-1} = K_{LL}^{-1} + K_{LL}^{-1}\, v\; T_\infty^{-1}\; v^t\, K_{LL}^{-1}$$
$$S(m)^{-1} = K_{LL}^{-1} + K_{LL}^{-1}\, K_{LH}\; T(m)^{-1}\; K_{LH}^t\, K_{LL}^{-1}.$$

T_∞ is of size 3×3 (in the case of a single island), independent of n_H and m, whereas $T(m)$ is of size $n_H \times n_H$, dense, and depends on m.

Table 4.1: Single island case: AGKS + HCT + sGS + smooth number 1-5-10

$N\backslash m$	10^0	10^1	10^2	10^3	10^4	10^5	10^7	10^9	10^{10}
smooth number $= 1$									
131	**24**, 0.485	**20**, 0.447	**18**, 0.407	**17**, 0.371	**17**, 0.381	**16**, 0.337	**18**, 0.371	**16**, 0.362	**17**, 0.384
451	**52**, 0.730	**38**, 0.650	**21**, 0.452	**13**, 0.286	**12**, 0.249	**12**, 0.256	**13**, 0.279	**12**, 0.253	**11**, 0.213
1667	**60**$^+$, 0.857	**60**$^+$, 0.768	**33**, 0.610	**20**, 0.426	**18**, 0.401	**19**, 0.410	**21**, 0.447	**19**, 0.420	**19**, 0.417
6403	$\boldsymbol{\infty}$, 0.972	**60**$^+$, 0.930	**60**$^+$, 0.839	**45**, 0.692	**37**, 0.637	**36**, 0.636	**36**, 0.638	**36**, 0.635	**39**, 0.661
smooth number $= 5$									
131	**24**, 0.485	**20**, 0.447	**18**, 0.407	**17**, 0.371	**17**, 0.381	**16**, 0.337	**18**, 0.371	**16**, 0.362	**17**, 0.384
451	**40**, 0.664	**28**, 0.547	**15**, 0.330	**8**, 0.131	**6**, 0.054	**6**, 0.023	**4**, 0.014	**4**, 0.016	**4**, 0.012
1667	**60**$^+$, 0.786	**48**, 0.706	**24**, 0.490	**12**, 0.258	**8**, 0.091	**6**, 0.058	**5**, 0.035	**5**, 0.026	**5**, 0.024
6403	**60**$^+$, 0.947	**60**$^+$, 0.862	**43**, 0.682	**21**, 0.427	**12**, 0.223	**8**, 0.091	**6**, 0.051	**6**, 0.052	**6**, 0.062
smooth number $= 10$									
131	**24**, 0.485	**20**, 0.447	**18**, 0.407	**17**, 0.371	**17**, 0.381	**16**, 0.337	**18**, 0.371	**16**, 0.362	**17**, 0.384
451	**37**, 0.634	**26**, 0.528	**15**, 0.330	**8**, 0.131	**6**, 0.050	**6**, 0.017	**4**, 0.010	**3**, 0.004	**3**, 0.003
1667	**60**$^+$, 0.785	**43**, 0.680	**20**, 0.442	**12**, 0.213	**8**, 0.080	**6**, 0.030	**4**, 0.004	**4**, 0.002	**4**, 0.008
6403	**60**$^+$, 0.943	**60**$^+$, 0.861	**38**, 0.653	**20**, 0.410	**10**, 0.177	**8**, 0.090	**5**, 0.028	**5**, 0.015	**5**, 0.023

Table 4.2: Single island case: MG + HCT + sGS + smooth number 1-5-10

$N\backslash m$	10^0	10^1	10^2	10^4	10^5	10^6	10^7	10^8	10^9
				smooth	**number**	$= 1$			
131	$\mathbf{60}^+, 0.885$	$\mathbf{60}^+, 0.898$	$\mathbf{60}^+, 0.932$	$\infty, 0.988$	$\infty, 0.997$	$\infty, 1.075$	$\infty, 1.089$	$\infty, 1.065$	$\infty, 1.137$
451	$\infty, 0.963$	$\infty, 0.987$	$\infty 1.014$	$\infty, 1.050$	$\infty, 1.086$	$\infty, 1.106$	$\infty, 1.172$	$\infty, 1.081$	$\infty, 1.091$
1667	$\infty, 0.985$	$\infty, 1.015$	$\infty, 1.044$	$\infty, 1.062$	$\infty, 1.122$	$\infty, 1.109$	$\infty, 1.142$	$\infty, 1.170$	$\infty, 1.124$
6403	$\infty, 1.025$	$\infty, 1.040$	$\infty, 1.057$	$\infty, 1.125$	$\infty, 1.145$	$\infty, 1.130$	$\infty, 1.171$	$\infty, 1.112$	$\infty, 1.187$
				smooth	**number**	$= 5$			
131	$\mathbf{60}^+, 0.885$	$\mathbf{60}^+, 0.898$	$\mathbf{60}^+, 0.932$	$\infty, 0.988$	$\infty, 0.997$	$\infty, 1.075$	$\infty, 1.089$	$\infty, 1.065$	$\infty, 1.137$
451	$\mathbf{60}^+, 0.761$	$\mathbf{60}^+, 0.829$	$\mathbf{60}^+, 0.920$	$\infty, 1.070$	$\infty, 1.084$	$\infty, 1.120$	$\infty, 1.174$	$\infty, 1.118$	$\infty, 1.166$
1667	$\mathbf{60}^+, 0.854$	$\mathbf{60}^+, 0.923$	$\infty, 0.999$	$\infty, 1.038$	$\infty, 1.0037$	$\infty, 1.0085$	$\infty, 1.134$	$\infty, 1.154$	$\infty, 1.208$
6403	$\mathbf{60}^+, 0.931$	$\infty, 0.979$	$\infty, 0.998$	$\infty, 1.012$	$\infty, 1.023$	$\infty, 1.058$	$\infty, 1.041$	$\infty, 1.063$	$\infty, 1.099$
				smooth	**number**	$= 10$			
131	$\mathbf{60}^+, 0.885$	$\mathbf{60}^+, 0.898$	$\mathbf{60}^+, 0.932$	$\infty, 0.988$	$\infty, 0.997$	$\infty, 1.075$	$\infty, 1.089$	$\infty, 1.065$	$\infty, 1.137$
451	$\mathbf{48}, 0.660$	$\mathbf{53}, 0.701$	$\mathbf{60}^+, 0.825$	$\infty, 0.955$	$\infty, 1.032$	$\infty, 1.115$	$\infty, 1.179$	$\infty, 1.200$	$\infty, 1.196$
1667	$\mathbf{40}, 0.624$	$\mathbf{49}, 0.680$	$\mathbf{60}^+, 0.797$	$\infty, 1.001$	$\infty, 1.088$	$\infty, 1.035$	$\infty, 1.064$	$\infty, 1.052$	$\infty, 1.095$
6403	$\mathbf{60}^+, 0.890$	$\mathbf{60}^+, 0.929$	$\infty, 0.972$	$\infty, 1.049$	$\infty, 1.017$	$\infty, 1.052$	$\infty, 1.051$	$\infty, 1.134$	$\infty, 1.170$

Table 4.3: L-shaped island case: AGKS + HCT + sGS + smooth number 1-5-10

$N\backslash m$	10^0	10^1	10^2	10^3	10^4	10^5	10^7	10^9	10^{10}
smooth number $=$ 1									
131	**23**, 0.515	**20**, 0.4878	**15**, 0.378	**12**, 0.310	**10**, 0.247	**9**, 0.148	**9**, 0.168	$\boldsymbol{\infty}$, 1.055	$\boldsymbol{\infty}$, 1.132
451	$\mathbf{60}^+$, 0.801	**49**, 0.745	**35**, 0.657	**25**, 0.544	**21**, 0.491	**21**, 0.421	**22**, 0.529	**25**, 0.570	**25**, 0.573
1667	$\boldsymbol{\infty}$, 0.961	$\mathbf{60}^+$, 0.893	$\mathbf{60}^+$, 0.818	**50**, 0.735	**47**, 0.730	**49**, 0.742	**37**, 0.727	**40**, 0.830	**47**, 0.819
smooth number $=$ 5									
131	**23**, 0.515	**20**, 0.4878	**15**, 0.378	**12**, 0.310	**10**, 0.247	**9**, 0.148	**9**, 0.168	$\boldsymbol{\infty}$, 1.055	$\boldsymbol{\infty}$, 1.132
451	**54**, 0.770	**44**, 0.709	**27**, 0.579	**17**, 0.443	**13**, 0.321	**11**, 0.254	**9**, 0.112	**9**, 0.149	**9**, 0.233
1667	$\boldsymbol{\infty}$, 0.964	$\mathbf{60}^+$, 0.893	**44**, 0.730	**25**, 0.559	**18**, 0.406	**14**, 0.367	**11**, 0.289	**10**, 0.292	**19**, 0.379
smooth number $=$ 10									
131	**23**, 0.515	**20**, 0.4878	**15**, 0.378	**12**, 0.310	**10**, 0.247	**9**, 0.148	**9**, 0.168	$\boldsymbol{\infty}$, 1.055	$\boldsymbol{\infty}$, 1.132
451	**54**, 0.771	**44**, 0.709	**27**, 0.571	**18**, 0.441	**14**, 0.313	**11**, 0.244	**9**, 0.157	**9**, 0.147	**9**, 0.268
1667	$\boldsymbol{\infty}$, 0.964	$\mathbf{60}^+$, 0.893	**44**, 0.708	**25**, 0.564	**17**, 0.400	**13**, 0.280	**11**, 0.250	**10**, 0.278	**18**, 0.412

Table 4.4: L-shaped island case: MG + HCT + sGS + smooth number 1-5-10

$N\backslash m$	10^0	10^1	10^2	10^4	10^5	10^6	10^7	10^8	10^9
smooth number $= 1$									
131	$\mathbf{60}^+, 0.885$	$\mathbf{60}^+, 0.917$	$\infty, 1.004$	$\infty, 1.109$	$\infty, 1.093$	$\infty, 1.099$	$\infty, 1.141$	$\infty, 1.149$	$\infty, 1.032$
451	$\infty, 0.968$	$\infty, 1.004$	$\infty 1.041$	$\infty, 1.097$	$\infty, 1.098$	$\infty, 1.111$	$\infty, 1.095$	$\infty, 1.136$	$\infty, 1.179$
1667	$\infty, 0.992$	$\infty, 1.029$	$\infty, 1.055$	$\infty, 1.078$	$\infty, 1.135$	$\infty, 1.107$	$\infty, 1.143$	$\infty, 1.134$	$\infty, 1.179$
smooth number $= 5$									
131	$\mathbf{60}^+, 0.885$	$\mathbf{60}^+, 0.917$	$\infty, 1.004$	$\infty, 1.109$	$\infty, 1.093$	$\infty, 1.099$	$\infty, 1.141$	$\infty, 1.149$	$\infty, 1.032$
451	$\mathbf{60}^+, 0.761$	$\mathbf{60}^+, 0.868$	$\mathbf{60}^+, 0.970$	$\infty, 1.098$	$\infty, 1.137$	$\infty, 1.119$	$\infty, 1.128$	$\infty, 1.169$	$\infty, 1.195$
1667	$\mathbf{60}^+, 0.855$	$\infty, 0.952$	$\infty, 1.029$	$\infty, 1.039$	$\infty, 1.079$	$\infty, 1.120$	$\infty, 1.182$	$\infty, 1.183$	$\infty, 1.191$
smooth number $= 10$									
131	$\mathbf{60}^+, 0.885$	$\mathbf{60}^+, 0.917$	$\infty, 1.004$	$\infty, 1.109$	$\infty, 1.093$	$\infty, 1.099$	$\infty, 1.141$	$\infty, 1.149$	$\infty, 1.032$
451	$\mathbf{41}, 0.671$	$\mathbf{60}^+, 0.775$	$\mathbf{60}^+, 0.900$	$\infty, 1.060$	$\infty, 1.141$	$\infty, 1.141$	$\infty, 1.144$	$\infty, 1.178$	$\infty, 1.194$
1667	$\mathbf{38}, 0.648$	$\mathbf{60}^+, 0.767$	$\mathbf{60}^+, 0.913$	$\infty, 1.055$	$\infty, 1.030$	$\infty, 1.098$	$\infty, 1.117$	$\infty, 1.171$	$\infty, 1.218$

Table 4.5: Two islands case: AGKS + HCT + sGS + smooth number 1-5-10

$N\backslash m$	10^0	10^1	10^2	10^3	10^4	10^5	10^7	10^9	10^{10}
smooth number $=$ 1									
131	**21**, 0.495	**18**, 0.455	**12**, 0.266	**8**, 0.144	**6**, 0.046	**4**, 0.016	**3**, 0.009	**3**, 0.002	**3**, 0.001
451	**49**, 0.754	**36**, 0.674	**19**, 0.478	**11**, 0.261	**8**, 0.165	**8**, 0.166	**9**, 0.209	**8**, 0.160	**8**, 0.162
1667	**60**$^+$, 0.890	**60**$^+$, 0.841	**36**, 0.680	**18**, 0.459	**13**, 0.315	**13**, 0.336	**13**, 0.315	**13**, 0.314	**13**, 0.316
smooth number $=$ 5									
131	**21**, 0.495	**18**, 0.455	**12**, 0.266	**8**, 0.144	**6**, 0.046	**4**, 0.016	**3**, 0.009	**3**, 0.002	**3**, 0.001
451	**42**, 0.717	**32**, 0.625	**17**, 0.436	**10**, 0.215	**6**, 0.074	**5**, 0.057	**4**, 0.004	**4**, 0.001	**3**, 0.003
1667	**60**$^+$, 0.867	**54**, 0.772	**26**, 0.577	**14**, 0.311	**8**, 0.133	**6**, 0.050	**4**, 0.018	**4**, 0.010	**4**, 0.011
smooth number $=$ 10									
131	**21**, 0.495	**18**, 0.455	**12**, 0.266	**8**, 0.144	**6**, 0.046	**4**, 0.016	**3**, 0.009	**3**, 0.002	**3**, 0.001
451	**42**, 0.717	**32**, 0.625	**17**, 0.436	**10**, 0.215	**6**, 0.074	**5**, 0.057	**4**, 0.004	**4**, 0.001	**3**, 0.003
1667	**60**$^+$, 0.866	**54**, 0.769	**26**, 0.576	**14**, 0.311	**8**, 0.133	**6**, 0.041	**4**, 0.007	**4**, 0.004	**4**, 0.006

Note also that we can precompute and store $M_{LL}v$ during the setup phase. This means that we only need to apply the multigrid V(s,s)-cycle M_{LL} once per iteration. Therefore, the following practical version of preconditioner (4.30) is used in the implementation:

$$\tilde{B}_{AGKS} := \begin{bmatrix} I_{HH} & -K_{HH}^{\infty\dagger}K_{HL} \\ 0 & I_{LL} \end{bmatrix} \begin{bmatrix} M_{HH} & 0 \\ 0 & \tilde{S}^{-1} \end{bmatrix} \begin{bmatrix} I_{HH} & 0 \\ -K_{LH}K_{HH}^{\infty\dagger} & I_{LL} \end{bmatrix}. \tag{4.39}$$

We construct two different multilevel hierarchies for multigrid preconditioners M_{HH} in (4.39) and M_{LL} in (4.38) for DOF corresponding to Ω_H and Ω_L, respectively. For prolongation, linear interpolation is used as in [20]. The prolongation matrices P_{HH} and P_{LL} are extracted from the prolongation matrix for whole domain Ω in the fashion following (4.11):

$$P = \begin{bmatrix} P_{HH} & P_{HL} \\ P_{LH} & P_{LL} \end{bmatrix}.$$

As emphasized in [6], AGKS can be used purely as an algebraic preconditioner. Therefore, the standard multigrid preconditioner constraint that the coarsest level mesh resolves the boundary of the island is automatically eliminated. However, for a fair comparison, we enforce the coarsest level mesh to have that property.

We do not observe convergence improvement when a subdomain deflation strategy based on the smallest eigenvalues is used as in the diffusion equation case [10]. The eigenvectors of the Neumann matrix, e_H in (4.16), cannot approximate the eigenvectors corresponding to the smallest eigenvalues of K_{HH} which are of $\mathcal{O}(1)$ (see Figure 4.1) since the remainder matrix R in (4.15) is of $\mathcal{O}(10^4)$. Therefore, a deflation strategy utilizing e_H will not necessarily guarantee deflation of the smallest eigenvalues of K_{HH} in the biharmonic case.

We have studied three experiment cases: a square island, an L-shaped island, and two islands (two triangle islands with different coefficient values). With these experiments, we obtain the following results regarding the effect of number of smoothing iterations on the

convergence behavior. We do not show the results of MG performance for the two-island case. This is because there is a contrast between the coefficients always, and MG fails to converge for any m. For the other two cases, the convergence of MG heavily depends on m and the number of smoothing iterations, i.e., for small m, the more the smoothing iteration, the faster the convergence; see Tables 4.2 and 4.4. However, if the coefficient m is bigger than 10^1, the MG method fails to converge independent of the smoothing number.

Throughout the AGKS experiments, we observe different behaviors of convergence. First of all, for the single square island case, AGKS requires more than one smoothing iteration for convergence; see Table 4.1. The choice of 5 smoothing iterations is sufficient for AGKS to reach h-robustness and its peak performance for $m > 10^5$. For the L-shaped island case, m-robustness is obtained for smoothing number 1. When the smoothing number is increased to 10, h- and m-robustness are obtained simultaneously; see Table 4.3.

To test the performance of the AGKS preconditioner for the third case, i.e., the case of two islands with different coefficients, we fix the coefficient of one of the islands to 10^9, and devise a coefficient parameter for the second island. We observe that AGKS preconditioner enjoys m robustness even when the smoothing number is one. Moreover, when we set the smoothing number to 5 we obtain that AGKS preconditioner converges in a few iterations for large m and is h robust. In fact, as it can be seen from Table 4.5, for the same problem size, AGKS preconditioner demonstrates the best performance for the 2 islands case.

Hence, when smoothing number is set to be greater than 10, we can conclude that the AGKS preconditioner clearly enjoys h-robustness for sufficiently large m values independently of the shape or the number of the islands. In contrast, MG is not h-robust regardless of the m value and the smoothing number. MG is totally ineffective as the problem size increases.

Finally, we report the m-robustness results. The loss of m-robustness of MG can be observed consistently for all m values while the AGKS preconditioner becomes more effective with increasing m and reaches its peak performance by maintaining an optimal iteration

count for all $m \geq 10^5$. This indicates that $m \geq 10^5$ corresponds to the asymptotic regime. Even increasing the m value from 10^2 to 10^3 reduces the iteration count significantly, a clear sign of close proximity to the asymptotic regime. In addition, the AGKS outperforms MG even for $m = 1$. Consequently, we infer that AGKS is m-robust.

We conclude the numerical experiments by reporting the cost of each preconditioner. For variational conditions, the decoupling of $K_{HH}(m)$ and S^{∞} in (4.30) causes the AGKS preconditioner to be cheaper than MG see the flop counts in Figure 4.3. When the size of the highly-bending region grows, the enforcement of the variational conditions of the AGKS preconditioner becomes even less costly than that of the MG preconditioner.

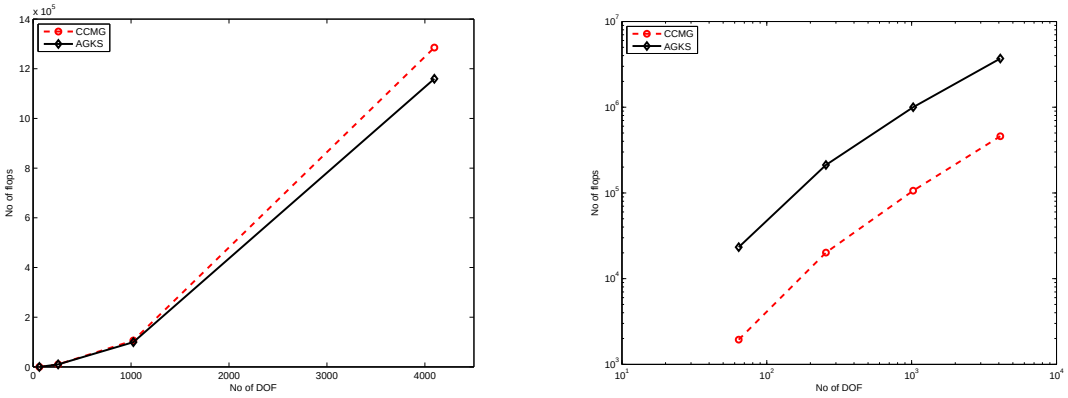

Figure 4.3: (Left) Flop counts for the enforcement of variational conditions. (Right) Flop counts for a single iteration of the preconditioners.

Finally, we report the cost per iteration for AGKS and MG V(1,1)-cycle preconditioners. The AGKS preconditioner in (4.30) requires inversions of two blocks: $K_{HH}(m)$ and S^{∞} corresponding to highly- and lowly-bending regions, respectively. Therefore, for each iteration of $AGKS$ preconditioner, we utilize a full MG method for each block separately. This is exactly the setup that MG methods are known to be highly effective because each block corresponds to a discretization of the Laplace equation with homogeneous coefficients. Therefore, one iteration of the AGKS preconditioner is roughly 20 times more costly than that of the MG preconditioner; see the flop counts in Figure 4.3. This additional cost is worthy because after smoothing number set to be 5, the AGKS preconditioner results in convergence in a few iterations for large values of m, whereas, no matter what the smoothing number is, the

MG preconditioner results in a consistent failure.

4.6 Generalization to elliptic PDEs of order $2k$

In essence, the biharmonic plate equation preconditioner is an extension of the construction for the diffusion equation. It is possible to generalize this construction to a family of elliptic PDEs of order $2k, k > 2$. We present how to obtain LRPs from associated bilinear forms. We choose a different perspective than the one in Section 4.2. We start with a canonical bilinear form and show the modification it needs to go through in order to construct LRPs.

Let the generalized problem be stated as follows: Find $u \in H_0^k(\Omega)$ such that

$$T_k u := (-1)^k \nabla^k \left(\alpha_k \nabla^k u\right) = f \qquad \text{in } \Omega. \tag{4.40}$$

The straightforward bilinear form associated to (4.40) is obtained by application of Green's formula k times:

$$\int_\Omega \nabla^k \left(\alpha_k \nabla^k u\right) v \; dx = \int_\Omega \alpha_k \nabla^k u \nabla^k v \; dx + \text{ boundary terms.} \tag{4.41}$$

Then, we define a bilinear form corresponding to (4.40) which can be seen as a *generalization* of the *canonical* bilinear form in (4.7):

$$\tilde{a}_k(u, v) := \int_\Omega \alpha_k \nabla^k u \nabla^k v \; dx. \tag{4.42}$$

Without modification, $\tilde{a}_k(\cdot, \cdot)$ cannot lead to LRPs because $\tilde{a}_k(v, v)$ is not $H_0^k(\Omega)$-coercive. This is due to the fact that $\tilde{a}_k(v, v) = 0$ for $v \in \mathcal{P}_{k-1} \cap H_0^k(\Omega)$. Hence, the stiffness matrix induced by (4.42) has a large kernel involving elements from $\mathcal{P}_{k-1}^h \cap V^h$ which indicates that extraction of a Neumann matrix with a low-dimensional kernel is impossible. In order to

overcome this complication, we utilize a modified bilinear form:

$$a_k(u,v) = \tilde{a}_k(u,v) + (1-\sigma_k)\,\hat{a}_k(u,v).$$

The bilinear form should maintain the following essential properties:

1. $H_0^k(\Omega)$-coercive.

2. $V_{\mathcal{P}_{k-1}(\Omega)}$-coercive.

3. Corresponds to a strong formulation giving $T_k u$ in (4.40) precisely,

where $V_{\mathcal{P}_{k-1}(\Omega)}$ is a closed subspace such that $V_{\mathcal{P}_{k-1}}(\Omega) \cap \mathcal{P}_{k-1} = \emptyset$ and $\mathcal{P}_{k-1}$ denotes the set of polynomials of degree at most $k-1$.

The above properties (1) and (2) will be immediately satisfied if the generalization of (4.13) holds for the modified bilinear form:

$$a_k(v,v) \geq c_k\,|v|^2_{H^k(\Omega)}. \tag{4.43}$$

A similar construction of the *Neumann* matrix can be immediately generalized as follows:

$$\langle \mathcal{N}^{(k)}_{HH} \underline{\phi}^h, \underline{\psi}^h \rangle := a_k(\phi^h_H, \psi^h_H).$$

The low-rank perturbations arise from the following decomposition of $K^{(k)}_{HH}(m)$:

$$K^{(k)}_{HH}(m) = m\,\mathcal{N}^{(k)}_{HH} + R^{(k)}, \quad \left(K^{(k)}_{HH}(m)\right)^{-1} = e^{(k)}_H \eta^{(k)^{-1}} e^{(k)^t}_H + \mathcal{O}(m^{-1}),$$

where $\eta^{(k)} := e^{(k)^t}_H K^{(k)}_{HH} e^{(k)}_H$. LRP is produced by $e^{(k)}_H \in \mathcal{P}^h_{k-1}$ because the rank is equal to the cardinality of the basis polynomials in $\mathcal{P}^h_{k-1}$.

$$\ker \mathcal{N}^{(k)}_{HH} = \mathcal{P}^h_{k-1}|_{\overline{\Omega}_H}.$$

Due to (4.8), $a_2(\cdot,\cdot)$ in (4.5) corresponds to the strong formulation T_2 exactly. Let us denote the strong formulation to which $a_k(\cdot,\cdot)$ corresponds by $\hat{T}_k$. We have $\hat{T}_k = T_k,\ k = 1, 2$ for the high-contrast diffusion and biharmonic plate equations, respectively:

$$a_1(v,v) := (\nabla v, \alpha_1 \nabla v),$$
$$a_2(v,v) := \sigma_2 \left(\nabla^2 v, \alpha_2 \nabla^2 v\right) + \alpha_2 (1-\sigma_2)|v|^2_{H^2(\Omega)}.$$

However, for general k, $a_k(\cdot,\cdot)$ may not correspond to T_k. In addition, one may need more general boundary conditions if similar zero contributions in (4.8) can be obtained for general k. Further research is needed to see if such boundary conditions are physical. Currently, it is also unclear for which applications such general PDEs can be used. However, there are interesting invariance theory implications when one employs bilinear forms corresponding to rotationally invariant functions compatible to energy definition in (4.4). This allows a generalization of the energy notion and may be the subject for future research. For further information, we list the relevant bilinear forms that are composed of rotationally invariant functions derived by the utilization of invariance theory.

$$a_3(v,v) := \sigma_3 \left(\nabla^3 v, \alpha_3 \nabla^3 v\right) + \alpha_3 (1-\sigma_3)|v|^2_{H^3(\Omega)},$$
$$a_4(v,v) := \sigma_4 \left(\nabla^4 v, \alpha_4 \nabla^4 v\right) + \alpha_4 (1-\sigma_4)|v|^2_{H^4(\Omega)} + \alpha_4 \gamma_4 |\nabla^2 v|^2_{H^2(\Omega)}.$$

Note that the above bilinear forms satisfy (4.43).

Chapter 5

Conclusion

The focus of this thesis is on the robust preconditioning for the solution of various high-contrast elliptic partial differential equations. The AGKS preconditioner was originally designed for the high-contrast diffusion equation under finite element discretization. In Chapter 2 we extended the AGKS preconditioner from finite element discretization to cell-centered finite volume discretization. Hence, we have shown that the same preconditioner could be used for different discretizations with minimal modification. Furthermore, in Chapter 3, we extended the usage of AGKS preconditioner to the solution of the stationary Stokes equation, and we have reached the conclusion that the same preconditioning technology can be used for the *vector valued* problems, and the AGKS preconditioner can be coupled with other preconditioners for the preconditioning of the saddle point problems. Finally, in Chapter 4 we applied the same family of preconditioners to high-contrast biharmonic plate equation, and demonstrated that the AGKS preconditioner can be used for higher order problems only with minimal modifications. Therefore, we have accomplished a desirable preconditioning design goal by using the same family of preconditioners to solve the elliptic family of high-contrast PDEs with varying discretizations for which we numerically accomplish the contrast size and mesh size robustness simultaneously. This is mainly due similarities in low-rank perturbation properties of the underlying PDEs and their discretizations. Once this striking property is established, we would immediately be able to extend the use of the AGKS preconditioner to a significantly larger group of PDEs.

Bibliography

[1] Aarnes, J.E.: Modelling of multiscale structures in flow simulations for petroleum reservoirs. In: Geometric Modelling, Numerical Simulation, and Optimization Applied Mathematics at SINTEF, pp. 307–360. Springer Verlag (2007)

[2] Aarnes, J.E., Hou, T.: Multiscale domain decomposition methods for elliptic problems with high aspect ratios. Acta Mathematicae Applicatae Sinica **18**(1), 63–76 (2002)

[3] Aksoylu, B., Beyer, H.R.: On the characterization of the asymptotic cases of the diffusion equation with rough coefficients and applications to preconditioning. Numer. Funct. Anal. Optim. **30**, 405–420 (2009)

[4] Aksoylu, B., Beyer, H.R.: Results on the diffusion equation with rough coefficients. SIAM J. Math. Anal. **42**(1), 406–426 (2010)

[5] Aksoylu, B., Bond, S., Holst, M.: An odyssey into local refinement and multilevel preconditioning III: Implementation and numerical experiments. SIAM J. Sci. Comput. **25**(2), 478–498 (2003)

[6] Aksoylu, B., Graham, I.G., Klie, H., Scheichl, R.: Towards a rigorously justified algebraic preconditioner for high-contrast diffusion problems. Comput. Vis. Sci. **11**, 319–331 (2008)

[7] Aksoylu, B., Klie, H.: A family of physics-based preconditioners for solving elliptic equations on highly heterogeneous media. Appl. Num. Math. **59**, 1159–1186 (2009)

[8] Aksoylu, B., Unlu, Z.: Numerical study of the high-contrast stokes equation and its robust preconditioning. In: G.A. Anastassiou, O. Duman (eds.) Advances in Applied Mathematics and Approximation Theory, *Springer Proceedings in Mathematics & Statistics*, vol. 41, pp. 237–262. Springer New York (2013). DOI 10.1007/978-1-4614-6393-1_15. URL `http://dx.doi.org/10.1007/978-1-4614-6393-1_15`

[9] Aksoylu, B., Unlu, Z.: Robust preconditioners for the high-contrast stokes equation. Journal of Computational and Applied Mathematics **259, Part B**(0), 944–954 (2014). DOI http://dx.doi.org/10.1016/j.cam.2013.10.016. URL `http://www.sciencedirect.com/science/article/pii/S0377042713005608`. Recent Advances in Applied and Computational Mathematics: ICACM-IAM-METU On the occasion of 10th anniversary of the foundation of Institute of Applied Mathematics, Middle East Technical University, Ankara, Turkey

[10] Aksoylu, B., Yeter, Z.: Robust multigrid preconditioners for cell-centered finite volume discretization of the high-contrast diffusion equation. Comput. Vis. Sci. **13**, 229–245 (2010). DOI 10.1007/s00791-010-0140-6

[11] Aksoylu, B., Yeter, Z.: Robust multigrid preconditioners for the high-contrast biharmonic plate equation. Numer. Linear Algeb. Appl. **18**, 733–750 (2011). DOI 10.1002/nla.761

[12] Axelsson, O.: Iterative solution methods. Cambridge University Press, Cambridge (1994)

[13] Bakhvalov, N.S., Knyazev, A.V.: A new iterative algorithm for solving problems of the fictitious flow method for elliptic equations. Soviet Math. Dokl. **41**, 481–485 (1990)

[14] Bakhvalov, N.S., Knyazev, A.V., Parashkevov, R.R.: An efficient iterative method for Stokes and Lame equations for nearly incompressible media with highly discontinuous coefficients (1997). Tech. Report

[15] Bakhvalov, N.S., Knyazev, A.V., Parashkevov, R.R.: Extension theorems for Stokes and Lame equations for nearly incompressible media and their applications to numerical solution of problems with highly discontinuous coefficients. Numer. Linear Algebra Appl. **9**, 115–139 (2002)

[16] Bank, R.E., Welfert, B.D.: A posteriori error estimates for the stokes equations: a comparison. Comput. Methods Appl. Mech. Eng. **82**(1-3), 323–340 (1990). DOI http://dx.doi.org/10.1016/0045-7825(90)90170-Q

[17] Bank, R.E., Welfert, B.D., Yserentant, H.: A class of iterative methods for solving mixed finite element equations. Numerische Mathematik **56**, 645–666 (1990)

[18] Benzi, M., Golub, G.H., Liesen, J.: Numerical solution of saddle point problems. Acta Numerica **14**, 1–137 (2005)

[19] Benzi, M., Wathen, A.J.: Some preconditioning techniques for saddle point problems. In: W. Schilders, H.A. van der Vorst, J. Rommes (eds.) Model Order Reduction: Theory, Research Aspects and Applications, Mathematics in Industry, pp. 195–211. Springer-Verlag (2008)

[20] Braess, D., Peisker, P.: A conjugate gradient method and a multigrid algorithm for morley's finite element approximation of the biharmonic equation. Numerische Mathematik **50**, 567–586 (1987)

[21] Bramble, A., Pasciak, J., Vassilev, A.: Analysis of the inexact uzawa algorithm for saddle point-problems. SIAM Journal on Numerical Analysis (1997)

[22] Brezzi, F., Fortin, M.: Mixed and hybrid finite element methods. Springer-Verlag (1991)

[23] Ciarlet, P.G.: The Finite Element Method for Elliptic Problems. Classics in applied mathematics. SIAM, Philadelphia, PA (2002)

[24] Clough, R.W., Tocher, J.L.: Finite element stiffness matrices for analysis of plates in bending. In: Proceedings of the conference on matrix methods in structural mechanics (1965)

[25] Dang, Q.A.: Iterative method for solving the Neumann boundary value problem for biharmonic type equation. J. Comput. Appl. Math **196**, 643–643 (2006)

[26] Elman, H., Golub, G.: Inexact and preconditioned uzawa algorithms for saddle point problems. SIAM Journal on Numerical Analysis (1994)

[27] Elman, H., Howle, V.E., Shadid, J., Shuttleworth, R., Tuminaro, R.: Block preconditioners based on approximate commutators. SIAM Journal on Scientific Computing **27**(5), 1651–1668 (2006). DOI 10.1137/040608817. URL `http://link.aip.org/link/?SCE/27/1651/1`

[28] Elman, H., Silvester, D.: Fast nonsymmetric iterations and preconditioning for navier-stokes equations. SIAM J. Sci. Comput **17**, 33–46 (1996)

[29] Elman, H.C.: Preconditioning for the steady-state navier stokes equations with low viscosity. SIAM J. Sci. Comput **20**, 1299–1316 (1999)

[30] Elman, H.C., Howle, V.E., Shadid, J.N., Tuminaro, R.S.: a parallel block multi-level preconditioner for the 3d incompressible navier-stokes equations. Journal of Computational Physics **187**, 504–523 (2003)

[31] Elman, H.C., Ramage, A., Silvester, D.J.: Algorithm 866: IFISS, a Matlab toolbox for modelling incompressible flow. ACM Transactions on Mathematical Software **33**(2), 14 (2007). URL `http://doi.acm.org/10.1145/1236463.1236469`. Article 14, 18 pages

[32] Elman, H.C., Silvester, D.J., Wathen, A.J.: Finite elements and fast iterative solvers: with applications in incompressible fluid dynamics. Numerical Mathematics and Scientific Computation. Oxford University Press, New York (2005)

[33] Eymard, R., Gallouet, T., Herbin, R.: The finite volume method. In: P.G. Ciarlet, J. Lions (eds.) Handbook for Numerical Analysis, pp. 715–1022. North Holland (2000)

[34] Fortin, M.: Some iterative methods for incompressible flow problems. Comput. Phys. Comm. **53**, 393–399 (1989)

[35] Fortin, M., Glowinski, R.: Augmented Lagrangian Methods: Application to the numerical solution of boundary value problems. North-Holland, Amsterdam (1983)

[36] Furuichi, M.: Numerical modeling of three dimensional self-gravitating Stokes flow problem with free surface. Procedia Computer Science **4**, 1506–1515 (2011)

[37] Furuichi, M., May, D.A., Tackley, P.J.: Development of a Stokes flow solver robust to large viscosity jumps using a schur complement approach with mixed precision arithmetic. J. Comput. Phys. **230**, 8835–8851 (2011)

[38] Gerritsen, M., Durlofsky, L.: Modeling fluid flow in oil reservoirs. Annu. Rev. Fluid Mech **37**, 211–238 (2005)

[39] Glowinski, R.: Numerical methods for nonlinear variational problems. Springer-Verlag, New York (1984)

[40] Golub, G.H., Van Loan, C.F.: Matrix computations, third edn. Johns Hopkins Studies in the Mathematical Sciences. Johns Hopkins University Press, Baltimore, MD (1996)

[41] Graham, I.G., Hagger, M.J.: Unstructured additive Schwarz-conjugate gradient method for elliptic problems with highly discontinuous coefficients. SIAM J. Sci. Comp. **20**(6), 2041–2066 (1999)

[42] Graham, I.G., Lechner, P., Scheichl, R.: Domain decomposition for multiscale pdes. Bath Institute for Complex Systems **Preprint 11**, 1–32 (2006)

[43] Graham, I.G., Lechner, P.O., Scheichl, R.: Domain decomposition for multiscale PDEs. Numer. Math. **106**, 589–626 (2007). DOI 10.1007/s00211-007-0074-1

[44] Graham, I.G., Scheichl, R.: Robust domain decomposition algorithms for multiscale PDEs. Numer. Methods Partial Differential Equations pp. 859–878 (2007). DOI 10.1002/num.20254

[45] Grinevich, P.P., Olshanskii, M.A.: An iterative method for the stokes-type problem with variable viscosity. SIAM J. Sci. Comput **31**, 3959–3978 (2009)

[46] Grossi, R.O.: On the existence of weak solutions in the study of anisotropic plates. J. Sound Vibration **242**, 542–552 (2001)

[47] Hanisch, M.R.: Multigrid preconditioning for the biharmonic Dirichlet problem. SIAM Journal on Numerical Analysis **30**, 184–214 (1993)

[48] K. J. Arrow, L.H., Uzawa, H.: Studies in linear and non-linear programming. Stanford University Press, Stanford, CA (1958)

[49] Kato, T.: A short introduction to perturbation theory for linear operators. Springer, Berlin (1982)

[50] Kay, D., Loghin, D., Wathen, A.: Preconditioner for the steady-state navier-stokes equations. SIAM Journal on Scientific Computing **24**(1), 237–256 (2002)

[51] Knyazev, A., Widlund, O.: Lavrentiev regularization + Ritz approximation = uniform finite element error estimates for differential equations with rough coefficients. Math. Comp. **72**(241), 17–40 (2003)

[52] Kobelkov, G.M., Olshanskii, M.A.: Effective preconditioning of uzawa type schemes for a generalized stokes problem. Numerische Mathematik **86**, 443–470 (2000). URL `http://dx.doi.org/10.1007/s002110000160`. 10.1007/s002110000160

[53] Kwak, D.Y.: V-cycle multigrid for cell-centered finite differences. SIAM J. Sci. Comput. **21**(2), 552–564 (1999)

[54] Larin, M., Reusken, A.: A comparative study of efficient iterative solvers for generalized stokes equations. Numerical Linear Algebra with Applications (2007)

[55] Llorente, I.M., Melson, N.D.: Behavior of plane relaxation methods as multigrid smoothers. Elect. Trans. Numer. Anal. **10**, 92–114 (2000)

[56] Maes, J., Bultheel, A.: A hierarchical basis preconditioner for the biharmonic equation on the sphere. IMA J. Numer. Anal. **26**(3), 563–583 (2006)

[57] Manolis, G.D., Rangelov, T.V., Shaw, R.P.: The non-homogeneous biharmonic plate equation: fundamental solutions. Internat. J. Solids Structures **40**, 5753–5767 (2003)

[58] Marcinkowski, L.: An additive Schwarz method for mortar finite element discretizations of the 4th order elliptic problem in 2D. Electron. Trans. Numer. Anal. **26**, 34–54 (2007)

[59] May, D.A., Moresi, L.: Preconditioned iterative methods for Stokes flow problems arising in computational geodynamics. Physics of the Earth and Planetary Interiors **171**, 33–47 (2008)

[60] Mayo, A.: The fast solution of Poisson's and the biharmonic equations on irregular regions. SIAM J. Numer. Anal. **21**(2), 285–299 (1984)

[61] Mayo, A., Greenbaum, A.: Fast parallel iterative solution of Poisson's and the biharmonic equations on irregular regions. SIAM J. Sci. Statist. Comput. **13**(1), 101–118 (1992)

[62] Mihajlovic, M., Silvester, D.: A black-box multigrid preconditioner for the biharmonic equation. BIT **44**, 151–163 (2004)

[63] Mihajlović, M., Silvester, D.: Efficient parallel solvers for the biharmonic equation. Parallel Computing **30**(1), 35–55 (2004)

[64] Miller, K.L., Horgan, C.O.: End effects for plane deformations of an elastic anisotropic semi-infinite strip. J. Elasticity **38**, 261–316 (1995)

[65] Ming, P., Ye, X.: Numerical methods for multiscale elliptic problems. J. Comp. Phys. **214**, 421–445 (2006)

[66] Mohr, M., Wienands, R.: Cell-centered multigrid revisited. Comput. Vis. Sci. **7**, 129–140 (2004)

[67] Moresi, L.N., Solomatov, V.S.: Numerical investigation of 2D convection with extremely large viscosity variations. Physics of Fluids **7**, 2154–2162 (1995)

[68] Nicolaides, R.: Deflation of conjugate gradients with applications to boundary value problems. SIAM J. Numer. Anal. **24**, 355–365 (1987)

[69] Nœtinger, B., Artus, V., Zargar, G.: The future of stochastic and upscaling methods in hydrogeology. Hydrogeology Journal **13**, 184–201 (2005)

[70] Olshanskii, M.A., Reusken, A.: A stokes interface problem: stability, finite element analysis and a robust solver. European congress on computational methods in applied sciences and engineering (2004)

[71] Olshanskii, M.A., Reusken, A.: Analysis of a stokes interface problem. Numer. Math. **103**(1), 129–149 (2006). URL `http://springerlink.metapress.com/openurl.asp?genre=article&id=doi:10.1007/s00211-005-0646-x`

[72] Oswald, P.: Hierarchical conforming finite element methods for the biharmonic equation. SIAM J. Numerical Analysis **29**(6), 1610–1625 (1992)

[73] Oswald, P.: Multilevel preconditioners for discretizations of the biharmonic equation by rectangular finite elements. Numer. Lin. Alg. Appl. **2**, 487–505 (1995)

[74] Paige, C., Saunders, M.A.: Solution of sparse indefinite systems of linear equations. SIAM J. Numer. Anal. **12**, 617–629 (1975)

[75] Peters, J., Reichelt, V., Reusken, A.: Fast iterative solvers for discrete Stokes equations. SIAM J. Sci. Comput. **27**(2), 646–666 (2005)

[76] Pozrikidis, C.: Introduction to Finite and Spectral Element Methods using MATLAB. Chapman & Hall/CRC, Boca Raton, FL (2005)

[77] ur Rehman, M., Geenen, T., Vuik, C., Segal, G., MacLachlan, S.: On iterative methods for the incompressible Stokes problem. International Journal for Numerical methods in fluids (2010). DOI 10.1002/fld.2235

[78] Ruge, J.W., Stüben, K.: Algebraic multigrid (AMG). In: S.F. McCormick (ed.) Multigrid Methods, *Frontiers in Applied Mathematics*, vol. 3, pp. 73–130. SIAM, Philadelphia, PA (1987)

[79] Rusten, T., Winther, R.: A Preconditioned Iterative Method for Saddlepoint Problems. SIAM Journal on Matrix Analysis and Applications **13**, 887 (1992)

[80] Scheichl, R., Vainikko, E.: Additive schwarz and aggregation-based coarsening for elliptic problems with highly variable coefficients. Tech. Rep. Preprint 9/06, Bath Institute For Complex Systems, University of Bath, UK (2006). Available at http://www.bath.ac.uk/math-sci/BICS, to appear in Computing

[81] Scheichl, R., Vainikko, E.: Additive schwarz and aggregation-based coarsening for elliptic problems with highly variable coefficients. Computing **80**(4), 319–343 (2007)

[82] Silvester, D., Elman, H., Ramage, A.: Incompressible Flow and Iterative Solver Software (IFISS) version 3.1 (2011). `http://www.manchester.ac.uk/ifiss/`

[83] Silvester, D., Wathen, A.: Fast iterative solution of stabilised Stokes systems part II: using general block preconditioners. SIAM Journal on Numerical Analysis **31**, 1352–1367 (1994)

[84] Stoll, M., Wathen, A.: The Bramble-Pasciak$^+$ preconditioner for sadlle point problems. Tech. rep., Oxford University Computing Laboratory, Technical report, Report no. 07/13, Oxford, UK (2007)

[85] Vuik, C., Segal, A., Meijerink, J.: An efficient preconditioned CG method for the solution of a class of layered problems with extreme contrasts of coefficients. J. Comp. Phys. **152**, 385–403 (1999)

[86] Vuik, C., Segal, A., Meijerink, J.: An efficient preconditioned CG method for the solution of a classof layered problems with extreme contrasts of coefficients. J. Comp. Phys. **152**, 385–403 (1999)

[87] Vuik, C., Segal, A., Meijerink, J., Wijma, G.: The construction of projection vectors for a ICCG method applied to problems with extreme contrasts in the coefficients. J. Comp. Phys. **172**, 426–450 (2001)

[88] Wang, T.S.: A Hermite cubic immersed finite element space for beam design problems (2005). Master thesis, Department of Mathematics, Virginia Polytechnic Institute and State University

[89] Wathen, A., Silvester, D.: Fast iterative solution of stabilised stokes systems. part i: Using simple diagonal preconditioners. SIAM Journal on Numerical Analysis **30**(3), 630–649 (1993). DOI 10.1137/0730031. URL `http://link.aip.org/link/?SNA/30/630/1`

[90] Watkins, D.S.: Fundamentals of Matrix Computations. Wiley-Interscience; second edition, New York (2002)

[91] Wesseling, P.: Cell-centered multigrid for interface problems. J. Comput. Phys. **79**, 85–91 (1988)

[92] Wesseling, P., Khalil, M.: Vertex-centered and cell-centered multigrid for interface problems. Journal of Computational Physics **98**, 1–10 (1992)

[93] Wittum, G.: Linear iterations as smoothers in multigrid methods: Theory with applications to incomplete decompositions. Impact Comput. Sci. Eng. **1**, 180–215 (1989)

[94] Wittum, G.: On the robustness of ILU–smoothing. SIAM J. Sci. Stat. Comput. **10**, 699–717 (1989)

[95] Zhang, X.: Multilevel schwarz methods for the biharmonic dirichlet problem. SIAM Journal on Scientific Computing **15**(3), 621–644 (1994). DOI 10.1137/0915041. URL `http://link.aip.org/link/?SCE/15/621/1`

[96] Zulehner, W.: Analysis of iterative methods for saddle point problems: a unified approach. Math. Comp. **71**, 479–505 (2002)

Appendix: Permission to Use

The main results of this thesis appeared in the previously published journal articles

- B. Aksoylu and Z. Unlu, Robust preconditioners for the high-contrast Stokes equation, *Journal of Computational and Applied Mathematics*, Contributions from ICACM - International Conference on Applied and Computational Mathematics, (2013).

- With kind permission from Springer Science and Business Media: [B. Aksoylu and Z. Unlu, Numerical study of the high-contrast Stokes equation and its robust preconditioning, *Advances in Applied Mathematics and Approximation Theory*, Contributions from AMAT 2012, Springer Proceedings in Mathematics & Statistics, Anastassiou, George A.; Duman, Oktay (Eds.). 41 (2013), pp. 237–262, doi: 10.1007/978-1-4614-6393-1.]

- With kind permission from Springer Science and Business Media: [B. Aksoylu and Z.Yeter, Robust multigrid preconditioners for the high-contrast biharmonic plate equation. *Numerical Linear Algebra with Applications*. 18 (2010), pp. 733-750, doi: 10.1002/nla.761.]

- With kind permission from Springer Science and Business Media:[B. Aksoylu and Z.Yeter, Robust multigrid preconditioners for cell-centered finite volume discretization of the high-contrast diffusion equation. *Computing and Visualization in Science*. 13 (2010), pp. 229-245, doi:10.1007/s00791-010-0140-6.]

For the first article mensioned above, I used the following permission: According to Elsevier Inc[1] "Author's publishing in Elsevier journals have wide rights to use their works for teaching and scholarly purposes without needing to seek permission". These rights include

[1]http://www.elsevier.com/journal-authors/author-rights-and-responsibilities

- "Inclusion in a thesis or dissertation"
- "Voluntary posting on open web sites operated by author or authors institution for scholarly purposes"

For more information, please see www.elsevier.com/journal-authors/author-rights-and-responsibilities.

For the remaining three articles above, a License Agreement between the author and Springer was provided by Copyright Clearance Center ("CCC").

Vita

Zuhal Unlu was born in 1985 in Afyonkarahisar, Turkey. In June 2007, she earned her Bachelor of Science degree in Mathematics at Middle East Technical University in Ankara, Turkey. Unlu began her graduate studies at Louisiana State University in August 2007 and earned a Master of Science degree in December, 2009. Currently she is a candidate for the degree of Doctor of Philosophy in Mathematics, which will be awarded in August 2014.